



U.S. Army Corps
of Engineers

COMPUTER-AIDED STRUCTURAL ENGINEERING (CASE) PROJECT

TECHNICAL REPORT ITL-92-2



FINITE ELEMENT MODELING OF WELDED THICK PLATES FOR BONNEVILLE NAVIGATION LOCK

AD-A251 501



by

John J. Jaeger

Information Technology Laboratory

DEPARTMENT OF THE ARMY

Waterways Experiment Station, Corps of Engineers
3909 Halls Ferry Road, Vicksburg, Mississippi 39180-6199

and

Zhili Feng, Dong S. Kim, Sung G. Lee
James C. Papritan, Yong L. Shim, Chon L. Tsai

Department of Welding Engineering

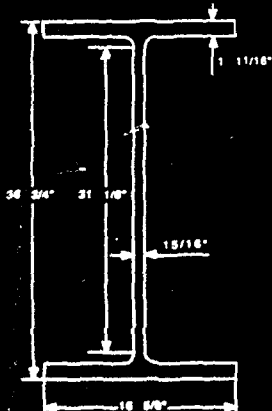
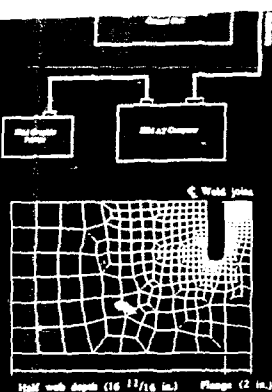
Ohio State University
190 W. 19th Avenue
Columbus, Ohio 43210-1366



May 1992

Final Report

Approved For Public Release; Distribution is Unlimited



*Original contains color
plates: All DTIC reproductions
will be in black and
white*

DTIC
ELECTE
JUN 12 1992
S B D

Prepared for DEPARTMENT OF THE ARMY
US Army Corps of Engineers

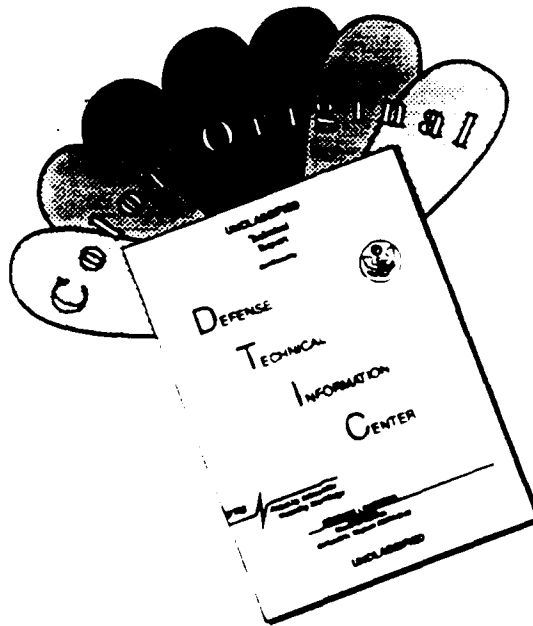
**Best
Available
Copy**

Destroy this report when no longer needed. Do not return
it to the originator.

The findings in this report are not to be construed as an official
Department of the Army position unless so designated
by other authorized documents.

The contents of this report are not to be used for
advertising, publication, or promotional purposes.
Citation of trade names does not constitute an
official endorsement or approval of the use of
such commercial products.

DISCLAIMER NOTICE



THIS DOCUMENT IS BEST QUALITY AVAILABLE. THE COPY FURNISHED TO DTIC CONTAINED A SIGNIFICANT NUMBER OF COLOR PAGES WHICH DO NOT REPRODUCE LEGIBLY ON BLACK AND WHITE MICROFICHE.

REPORT DOCUMENTATION PAGE			Form Approved OMB No. 0704-0188	
Public reporting burden for this collection of information is estimated to average 1 hour per response, including the time for reviewing instructions, searching existing data sources, gathering and maintaining the data needed, and completing and reviewing the collection of information. Send comments regarding this burden estimate or any other aspect of this collection of information, including suggestions for reducing this burden, to Washington Headquarters Services, Directorate for Information Operations and Reports, 1215 Jefferson Davis Highway, Suite 1204, Arlington, VA 22202-4302, and to the Office of Management and Budget, Paperwork Reduction Project (0704-0188), Washington, DC 20503.				
1. AGENCY USE ONLY (Leave blank)		2. REPORT DATE May 1992		3. REPORT TYPE AND DATES COVERED Final report
4. TITLE AND SUBTITLE Finite Element Modeling of Welded Thick Plates for Bonneville Navigation Lock			5. FUNDING NUMBERS DACW 39-89-L-0006	
6. AUTHOR(S) John J. Jaeger; Zhili Feng; Dong S. Kim; Sung G. Lee; James C. Papritan; Yong L. Shim; Chon L. Tsai				
7. PERFORMING ORGANIZATION NAME(S) AND ADDRESS(ES) *Original contains color plates: All DTIC reproductions will be in black and white. See reverse.			8. PERFORMING ORGANIZATION REPORT NUMBER Technical Report ITL-92-2	
9. SPONSORING/MONITORING AGENCY NAME(S) AND ADDRESS(ES) US Army Corps of Engineers Washington, DC 20314-1000			10. SPONSORING/MONITORING AGENCY REPORT NUMBER	
11. SUPPLEMENTARY NOTES Available from National Technical Information Service, 5285 Port Royal Road, Springfield, VA 22161				
12a. DISTRIBUTION/AVAILABILITY STATEMENT Approved for public release; distribution is unlimited			12b. DISTRIBUTION CODE	
13. ABSTRACT (Maximum 200 words) The primary objective for this research was to investigate what influence welding parameters and joint geometry have on the magnitude and distribution of residual stress on thick-section butt joints. Failure initiating at the web flange intersection of weld access holes has previously occurred on thick-section steel-rolled shapes. Contributing factors to failure include high tensile residual stress from welding, low base metal toughness, and high stress concentration from the weld access hole geometry. A thermal mechanical finite element model was developed to predict temperature and stress history in the steel-rolled shapes studied. Comparisons were made between the numerical model and experimental results. Several joint geometries and weld sequences were considered. The finite element model developed by this research can be used to evaluate the influence of welding parameters and joint geometry on welding-induced residual stresses.				
14. SUBJECT TERMS See reverse.			15. NUMBER OF PAGES 95	
			16. PRICE CODE	
17. SECURITY CLASSIFICATION OF REPORT UNCLASSIFIED	18. SECURITY CLASSIFICATION OF THIS PAGE UNCLASSIFIED	19. SECURITY CLASSIFICATION OF ABSTRACT	20. LIMITATION OF ABSTRACT	

7. (Concluded).

USAEWES, Information Technology Laboratory
3909 Halls Ferry Road
Vicksburg, MS 39180-6199;

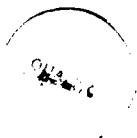
Department of Welding Engineering
Ohio State University
190 W. 19th Ave.
Columbus, OH 43210-1366

14. (Concluded).

Highly constrained welded connections
Residual stress
Thermal mechanical modeling
Thermal strain

Toughness
Weld access holes
Welded joint design
Welding

Accession For	
NTIS GRA&I	<input checked="checked" type="checkbox"/>
DTIC TAB	<input type="checkbox"/>
Unannounced	<input type="checkbox"/>
Justification	
By	
Distribution/	
Availability Codes	
Dist	Avail and/or Special
A-1	




PREFACE

The research described in this report was conducted by the Scientific and Engineering Application Group of the Computer Aided Engineering Division (CAED), Information Technology Laboratory (ITL), US Army Engineer Waterways Experiment Station (WES), for the US Army Engineer District, Portland (NPP). Mr. John Jaeger, formerly with the CAED, was Project Manager under the general supervision Mr. H. Wayne Jones, Chief, Scientific and Engineering Applications Center, and Dr. Edward E. Middleton, former Chief, CAED, and Dr. N. Radhakrishnan, Director, ITL. Technical Monitor for NPP was Mr. Jeffery Sedey.

The investigation was performed at the Ohio State University, Department of Welding Engineering, Design Group, under the supervision of Dr. Chon L. Tsai. Principal Investigators were Zhili Feng, Dong S. Kim, Sung G. Lee, and Yong L. Shim. In addition, Dr. James C. Papritan, Ohio State University, Department of Agricultural Engineering, and Messrs. Omer W. Blodgett, Bud Fletcher, Thomas J. Black, Harold A. Sadler, Bob Bandy, and Larry Ash from the Lincoln Electric Company contributed to the experimental research performed in this report. All labor and equipment provided by the Lincoln Electric Company were donated to the research effort. Acknowledgment is made to Messrs. Jim Snyder, Bethlehem Steel Corporation, who provided the rolled shapes used in the experiments; Tom Campbell, J. T. Edwards Company, for cutting and delivering the material; Ken Runyon, John Bosworth, and Bruce Hornbourger, Beasley Company, for their support in preparing the FCAW joints; and Cort Reiser, Ohio State University, for welding the test coupons.

At the time of the publication of this report, Director of WES was Dr. Robert W. Whalin. Commander and Deputy Director was COL Leonard G. Hassell, EN.

92-15366


CONTENTS

	<u>Page</u>
PREFACE	1
LIST OF TABLES	3
LIST OF FIGURES	3
CONVERSION FACTORS, NON-SI TO SI (METRIC) UNITS	6
PART I: INTRODUCTION	7
Identification of Field Problem	7
Objectives	9
Summary of Activities	9
PART II: EXPERIMENTAL INVESTIGATION	12
Instrumentation for Welding Analysis	12
Welding, Data Acquisition, and Analysis	14
Fracture Toughness	29
PART III: PROBLEM DEFINITION FOR FINITE ELEMENT MODELING (FEM) ANALYSIS	32
Material Property	32
Joint Type and Preparation Proposed for FEM Analysis	33
Welding Process and Variable Proposed for FEM Analysis	34
Thermo-Mechanical Parameter	36
PART IV: FINITE ELEMENT ANALYSIS	40
Thermal Analysis	48
Stress Analysis	53
Comparison with Experimental Data	68
PART V: CONCLUSIONS AND RECOMMENDATIONS	89
Conclusions	89
Recommendations	90
PART VI: FUTURE WORK	92
Fracture Toughness of EGW Weldments	92
Technology Transfer	93
REFERENCES	94

LIST OF TABLES

<u>No.</u>		<u>Page</u>
1	Test Variables	16
2	Welding Parameters and Variables of Test 1	18
3	Welding Parameters and Variables of Test 2	19
4	Welding Parameters and Variables of Tests 3 and 4	20
5	Welding Parameters and Variables of Test 5	21
6	Residual Stress Measurement Results	28
7	Results of Charpy Impact Tests	30
8	Results of Transverse Microhardness	31
9	Ramp Heat Input	46
10	Comparison of CUP Time	78

LIST OF FIGURES

<u>No.</u>		<u>Page</u>
1	Navigation lock diaphragm wall	8
2	Experimental setup for strain gage and thermocouple measurements	13
3	Schematic diagram of basic system with VTR	15
4	Testing setup of infrared system	15
5	Specimen dimensions of W36x300 shape used in the experimental study	16
6	Details of joint and access hole geometry	17
7	Joint details and pass sequences of Test 1	18
8	Joint details and welding pass sequences of Test 2	19
9	Joint details and pass sequences of Tests 3 and 4	20
10	Joint details and pass sequences of Test 5	21
11	Thermal strain gage layout of Test 1 at Ohio State University	23
12	Strain gage and thermocouple layout of Test 2	24
13	Thermal strain gage and thermocouple layout of Test 3	24
14	Thermal strain gage and thermocouple layout of Test 4	25
15	Thermal strain gage and thermocouple layout of Test 5	25
16	Thermal strain variations during the first pass of Test 4	26
17	Thermal strain variations during the final pass of Test 1	26
18	Illustration of the positions of strain gages and coordinate system used in residual stress measurements (Tests 3 through 5)	27
19	Illustration of strain gage positions and coordinate system used in residual stress measurements (Test 2)	27
20	Strain relief versus hole depth in residual stress measurement (Test 2, Location E)	28
21	Temperature dependent material properties used in the FEM analysis	32
22	Specimen dimensions used in finite element analysis (W36x359)	33

<u>No.</u>		<u>Page</u>
23	Access hole details used in finite element analysis . . .	34
24	Weld edge preparation and fit up for FCAW used in finite element analysis	35
25	Weld edge preparation and fit up for SAW and EGW in finite element analysis	35
26	Weld passes for FCAW used in finite element analysis . . .	37
27	Weld passes for SAW process used in finite element analysis	38
28	Weld passes for EGW process used in finite element analysis	38
29	Finite element meshes	41
30	Lumped passes for flange weld in FCAW	42
31	Lumped passes for flange weld (FCAW: single V-groove) . .	43
32	Lumped passes for flange weld (FCAW: double V-groove) . .	44
33	Model of Case A in FCAW (W36x359)	47
34	Model of Case B in FCAW (W36x359)	47
35	Model of Case C in FCAW (W36x359)	49
36	Model of Case D in FCAW (W36x359)	49
37	Isotherm plots for Case A in FCAW process (1-1/8-in.- diam access hole)	50
38	Isotherm plots for Case B in FCAW process (1-1/8-in.- diam access hole)	53
39	Isotherm plots in SAW process (2-in.-diam access hole)	57
40	Isotherm plots in EGW process (2-in.-radius semicircle access hole)	59
41	Stress distribution for Case A with FCAW (1-1/8-in.- diam access hole)	61
42	Stress distribution for Case B with FCAW (1-1/8-in.- diam access hole)	63
43	Stress distribution for Case C with FCAW (1-1/8-in.- diam access hole)	64
44	Stress distribution after welding the outside half of the flange for Case D with FCAW (1-1/8-in.-diam access hole)	65
45	Stress distribution after welding the outside half of the flange and one side of the web for Case D with FCAW (1-1/8-in.-diam access hole)	66
46	Stress distribution after welding both sides of the flange and one side of the web for Case D with FCAW (1-1/8-in.-diam access hole)	67
47	Final residual stress distribution for Case D with FCAW (1-1/8-in.-diam access hole)	69
48	Stress distribution for Case A with FCAW (1-1/2-in.- diam access hole)	70
49	Stress distribution for Case B with FCAW (1-1/2-in.- diam access hole)	71
50	Final residual stress distribution for Case A with SAW (W36x359, elongated access hole)	72
51	Final residual stress distribution for Case B with SAW (W36x359, elongated access hole)	73
52	Final residual stress distribution for Case A with EGW (W36x359, semicircle access hole)	74

<u>No.</u>		<u>Page</u>
53	Final residual stress distribution for Case B with EGW (W36x359, semicircle access hole)	75
54	Final residual stress distribution for Case A with EGW (W36x359, elongated access hole)	76
55	Final residual stress distribution for Case B with EGW (W36x359, elongated access hole)	77
56	Thermal strains in the x-direction during the flange weld with EGW (Case A: web not welded yet, elongated access hole)	79
57	Thermal strains in the y-direction during the flange weld with EGW (Case A: web not welded yet, elongated access hole)	80
58	Thermal strains in the x-direction during the flange weld with EGW (Case B: web not welded yet, elongated access hole)	81
59	Thermal strains in the y-direction during the flange weld with EGW (Case B: web not welded yet, elongated access hole)	82
60	Comparison of final residual stress in the x-direction for Case A with EGW (elongated access hole)	83
61	Comparison of final residual stress in the y-direction for Case A with EGW (elongated access hole)	84
62	Comparison of final residual stress in the x-direction for Case B with EGW (elongated access hole)	85
63	Comparison of final residual stress in the y-direction for case B with EGW (elongated access hole)	86
64	Comparison of final residual stress in the x-direction for Case A with SAW (elongated access hole)	87
65	Comparison of final residual stress in the y-direction for Case A with SAW (elongated access hole)	88
66	Comparison of residual stress (ksi) in x-direction at weld access hole	89
67	Improvement through heat treatment of notch-toughness of electroslog-deposited metals	92

CONVERSION FACTORS, NON-SI (METRIC)
UNITS OF MEASUREMENT

Non-SI units of measurement used in this report can be converted to SI (metric) units as follows:

<u>Multiply</u>	<u>By</u>	<u>To Obtain</u>
degrees (angle)	0.01745239	radians
Fahrenheit degrees	5/9	Celsius degrees or Kelvins*
feet	0.3048	metres
foot-pounds (force)	1.355818	metre-newtons or joules
inches	2.54	centimetres
kips (force) per square inch	6.894757	megapascals
pounds (force) per square inch	6.894757	kilopascals

* To obtain Celsius (C) temperature readings from Fahrenheit (F) readings, use the following formula: $C = (5/9) (F - 32)$. To obtain Kelvin (K) readings, use: $K = (5/9) (F - 32) + 273.15$.

FINITE ELEMENT MODELING OF WELDED THICK PLATES
FOR BONNEVILLE NAVIGATION LOCK

PART I: INTRODUCTION

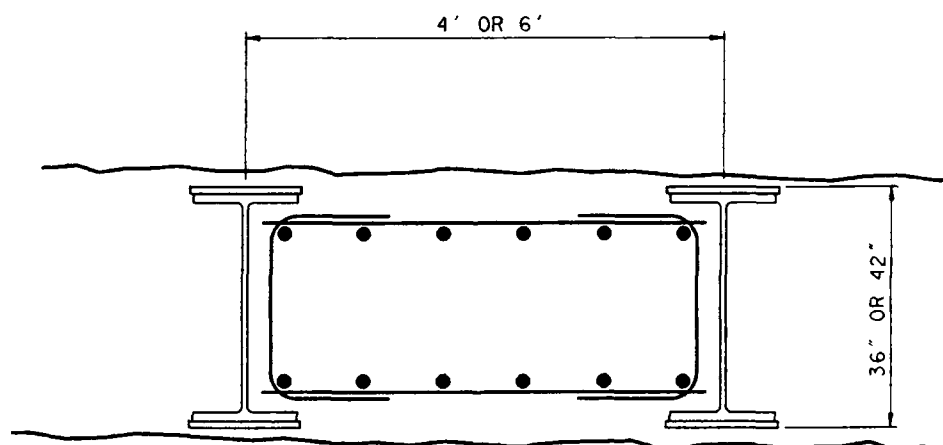
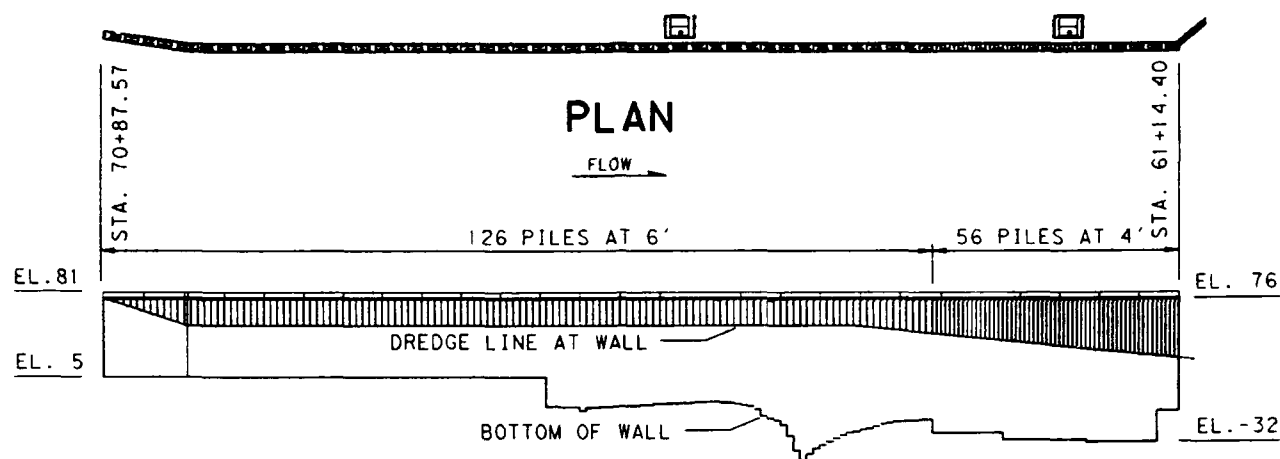
Identification of Field Problem

1. Cracking and fracture problems have recently been associated with groove weld splicing of thick plates and rolled shapes (American Institute of Steel Construction (AISC) 1989). Problems were reported in 1981 at the Orange County Convention Center in Orlando, FL (Fisher and Pense 1987), and more recently at the American Airlines hanger under construction at the Dallas/Fort Worth International Airport in 1988 (Engineering News Record 1988). Segregation and slow cooling at the midthickness region of the flange and web intersection cause a reduction in base metal toughness. In addition to reduced toughness, high residual stress from the nonlinear thermal cycles created by the welding process and geometric irregularities at the weld access holes increase the potential for cracking.

2. Field experience has shown that the welding sequence can have a controlling effect on cracking of heavy wide-flange butt joint connections. When the sequence is such that the flanges are welded prior to the web, cracks can initiate from the web access holes and propagate through the web material. If the weld sequence is such that the web is welded first followed by the flanges, again cracks initiate at the web access holes; however, the cracks then tend to propagate through the flange material.

3. An integral part of the structural design on the Bonneville Navigation Lock was the 1,088-ft*-long lock diaphragm wall or guide wall along the upstream approach to the lock (Figure 1). The guide wall structural system primarily consisted of a 42-in.-thick slurry trench wall, reinforced by large wide-flange steel beams placed vertically on 4- to 6-ft centers and joined by reinforcing cages and concrete. Since these thick members would be subjected to tensile loads, there was concern for cracking. The US Army Engineer District (USAED), Portland, requested that the Information Technology

* A table of factors for converting non-SI metric units of measurement to SI (metric) units is presented on page 6.



TYPICAL SECTION

(PILE WITH AND WITHOUT COVERPLATES)

Figure 1. Navigation lock diaphragm wall

Laboratory, US Army Engineer Waterways Experiment Station (WES), perform a thermal mechanical finite element analysis to calculate the influence of welding parameters and joint geometry on the magnitude and distribution of residual stress caused by welding.

4. Initially it was proposed to use ASTM A 572 Grade 50 "Fritenar steel" for the large wide-flange shapes. Since continuous lengths up to 133 ft are necessary for construction, complete penetration groove welded butt joints were required. Bolted connections were not selected because the bolt heads would interfere with the slurry wall construction techniques. Originally it was proposed to fabricate the large beams from W33x387, W36x393, W36x650, and W36x848 steel shapes manufactured by Trade Arbed. Flange thickness for these shapes ranges from 2.20 to 4.53 in. with web thicknesses varying from 1.22 to 2.52 in. thick. As the project progressed, purchase of foreign material was prevented, and the design was revised to use W36x300 and W36x359 members that would be built up with flange cover plates ranging in thickness from 3/8 to 3 in. thick.

Objectives

5. The primary objective of this study was to evaluate what influence welding parameters and joint geometry had on the magnitude and distribution of residual stress on thick section butt joints. This study also provides the USAED, Portland, with an initial finite element modeling technique that can be applied to future structural analysis and design of weldments.

Summary of Activities

6. This study was originally initiated by the USAED, Portland, to perform thermal mechanical finite element analysis on thick section butt joints. As the study developed, other nongovernmental organizations became interested in complementing the Portland-sponsored finite element analysis with experimental data and material testing at no additional cost to the District.

7. Bethlehem Steel Corporation donated W36x300 A572 Grade 50 rolled shape for instrumenting. Edge preparation was donated by John F. Beasley Construction Company and the Lincoln Electric Company. Welding was donated by the Lincoln Electric Company and the Ohio State University Welding Engineering

Department, with electrogas welding (EGW) equipment being provided by Oregon Iron Works.

8. The guide wall design is based on using W36x359 rolled shapes from A572 Grade 50 steel. The finite element analysis was conducted for this shape. However, the experimental and testing results were based on the W36x300 shapes that were donated. The structural dimensions of these two shapes are similar. The thermo-mechanical responses of these shapes to the welding heat source were also similar. No finite element analysis was conducted for W36x300 shapes because of the time restraint of this project.

9. This study investigated the effect of welding sequence on residual stress and the variance in the residual stress distribution between the root pass and the final weld pass. In addition, the effect that weld access hole diameter has on residual stress distribution was also investigated. The weld access hole diameter is an important parameter since it can act as a stress concentrator that promotes cracking.

10. Another parameter investigated was the effect that weld joint geometry has on residual stress. This study looked at the variance in magnitude and distribution of residual stress associated with joining the flanges with single-v-groove versus double-v-groove joint geometry.

11. The welding processes that were studied included flux cored arc welding (FCAW), submerged arc welding (SAW) and EGW. FCAW test coupons were welded in the Welding Engineering Laboratory at the Ohio State University. SAW and EGW test coupons were welded in the Research and Development Laboratory at the Lincoln Electric Company.

12. During welding, temperature at various locations in the weldment was measured using thermocouple and a noncontact infrared pyrometer. Transient welding stresses were measured by high temperature strain gages. After completion of welding, residual stresses in the weldment were determined by blind hole drilling technique. Fracture toughness of weld metal (WM), heat-affected zone (HAZ), and base metal (BM) was obtained from Charpy V-notch tests.

13. Since the actual weld joint geometry and welding procedures were not submitted to the USAED, Portland, by the contractor prior to initiation of this study, recommended guidance by Trade Arbed and AISC was used as a starting point to initialize the study. The finite element code ABAQUS was used to evaluate both joint and access hole geometries and welding procedures in this study. Experimental welding tests were conducted for comparison purposes with

the finite element model. These studies resulted in recommendations for improved design of thick-shape welded connections. Formal welding procedures submitted later by the contractor can be analyzed using this finite element model, which can be easily revised to reflect the actual welding conditions.

PART II: EXPERIMENTAL INVESTIGATION

14. The experimental investigation details were finalized after the finite element study was in progress. The actual testing used W36x300 shapes, whereas the finite element analysis used W36x359 shapes. The major difference is that larger W36x359 shapes needed more welding passes. Variations in the other factors, such as joint and access hole geometry and welding parameters, have been kept to a minimum. Therefore, the thermo-mechanical response of these shapes to the welding heat source will be similar.

Instrumentation for Welding Analysis

Data acquisition system

15. A specially designed data acquisition system was used to monitor the temperature and thermal strain changes at specific points during welding. This system was also used to measure the residual stresses in combination with the blind hole drilling method. The system configuration is shown in Figure 2. Thermocouples and electric strain gages were used to measure the temperature and strain changes during welding. Details about the system and the principles of strain gage and thermocouple measurements are described in WES report "Determination of Residual Stress and Effects in Thick Section Weldments for Hydraulic Structures" (Jaeger, in preparation).

Infrared pyrometer

16. The Inframetrics Model 525 system was used to measure and record on videotape the overall surface temperature field during and after welding. This system has -4° to $2,700^{\circ}$ F temperature measurement range and has four basic display functions:

- a. IMAGE. Normal picture with brightness indicating temperature difference and a calibrated gray scale.
- b. LINE SELECT. Normal picture is displayed with a brightened line indicating vertical position of the line scan that will be displayed in the line scan mode.
- c. LINE SCAN. Temperature versus horizontal position is displayed for a continuous horizontal scan fixed in the scene vertically by the line position potentiometer.
- d. ISOTHERM. Constant temperature contours are intensified over the normal image for selected temperature levels. A marker at the left of the display indicates the difference temperature as a fraction of the temperature for a given range set.

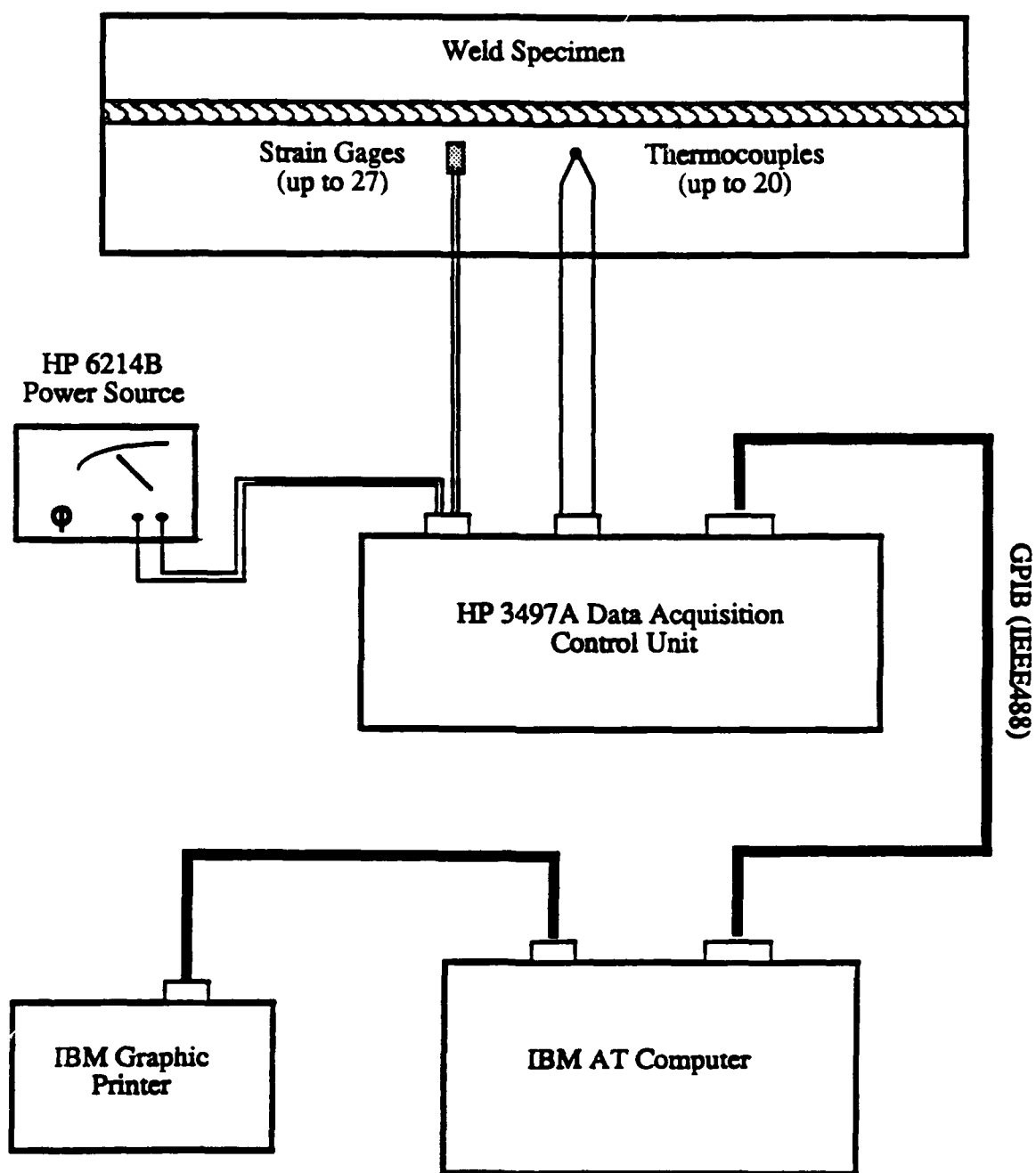


Figure 2. Experimental setup for strain gage and thermocouple measurements

17. As the surface of a specimen is scanned, the naturally emitted infrared radiation is converted by a liquid nitrogen cooled mercury, cadmium, telluride (HgCdTe) detector to an electrical signal that is processed through a monitor that displays the temperature contours on the screen.

18. A calibrated temperature scale is presented across the bottom of the screen in the normal imaging mode to gage the displayed image. In addition, there are two quantitative modes, Isotherm and Line Scan. There are seven different temperature ranges with full-scale settings 50, 68, 122, 212, 392, 932, 2700 °F. A 4:1 zoom feature is also provided on the scanner. Figure 3 illustrates the infrared system with a videotape recorder (VTR). The specimen is viewed through the scanner, and the infrared signal is converted to a temperature field by the control/electronic unit. The videotape recorder saves all the temperature readings from the monitor. A typical test set is shown in Figure 4.

Welding, Data Acquisition, and Analysis

19. The experiments were initiated in August and completed on 15 September 1989. The effects on the final residual stresses and thermal strain changes for different welding processes, welding sequences, and the geometry of the access hole were evaluated by using the blind hole drilling technique and high temperature strain gages. An infrared pyrometer was also used to monitor the temperature changes during welding. The strain gage locations were predetermined from the finite element analysis results where the stresses and strains were predicted to be high. These locations were close to the access hole. Since the temperature around the access hole during welding was relatively high (up to 300 °F), the effects of temperature change during welding on the strain gage readings had to be considered and compensated. Temperature effect on the final residual stresses measurements was ignored, since these measurements were obtained after the weldment returned to the ambient temperature.

20. A total of five welding specimens were tested on W36x300 A572 Grade 50 rolled shapes donated by Bethlehem Steel Corporation. One of them was conducted at the Department of Welding Engineering, Ohio State University (OSU). The other four tests were conducted at Lincoln Electric Co, Cleveland, OH. Table 1 lists the welding process, hole geometry, and welding sequence of each test.

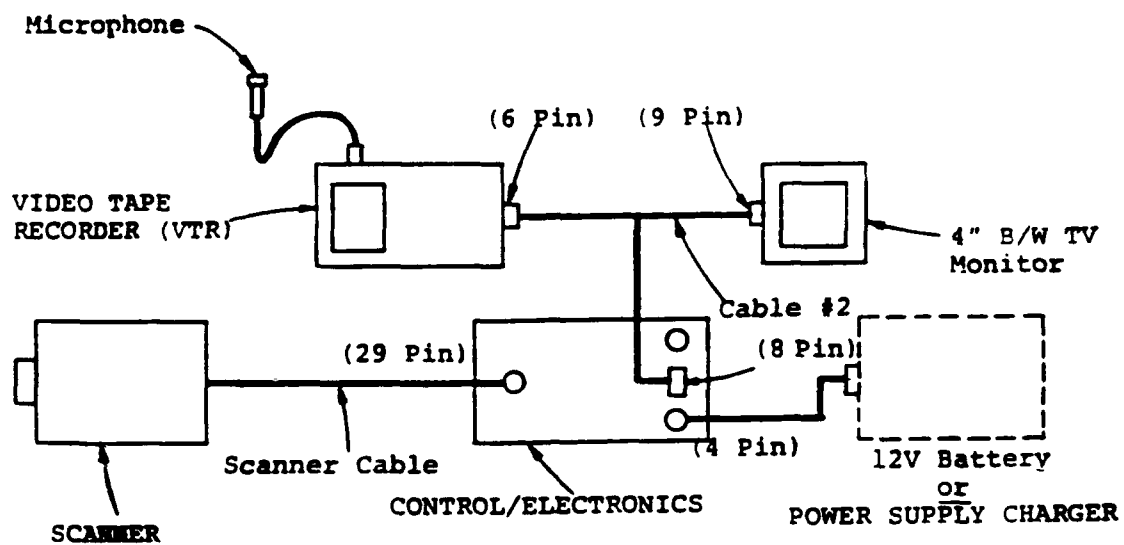


Figure 3. Schematic diagram of basic system with VTR

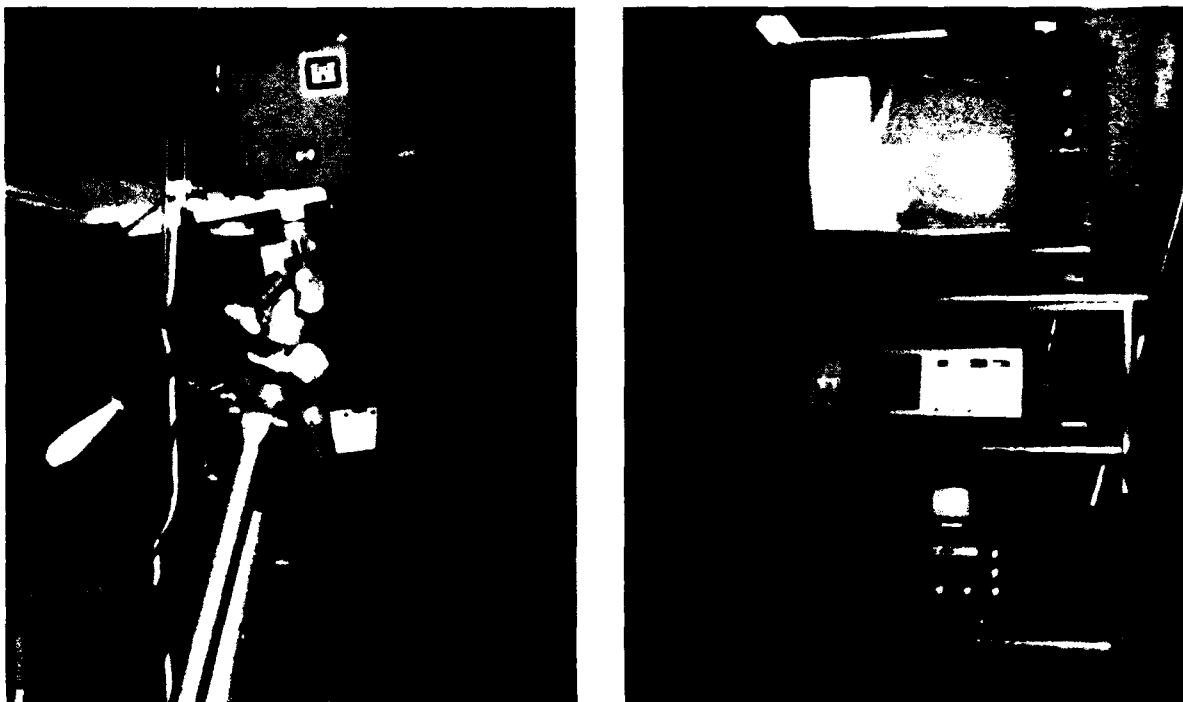


Figure 4. Testing setup of infrared system

Table 1
Test Variables

<u>Test No.</u>	<u>Welding Process</u>	<u>Access Hole Geometry</u>	<u>Welding Sequence</u>	<u>Location</u>
1	FCAW	Figure 7	Flanges first	OSU
2	EGW for flanges, SAW for web	Figure 8	Web first	Lincoln Electric Co.
3	EGW for flanges, SAW for web	Figure 9	Flanges first	Lincoln Electric Co.
4	EGW for flanges, SAW for web	Figure 9	Web first	Lincoln Electric Co.
5	SAW	Figure 10	Flanges first	Lincoln Electric Co.

21. Three welding processes, FCAW, EGW, and SAW, were investigated. The dimensions of specimen, joint, and access hole details are given in Figures 5 and 6. The associated variables including welding parameters,

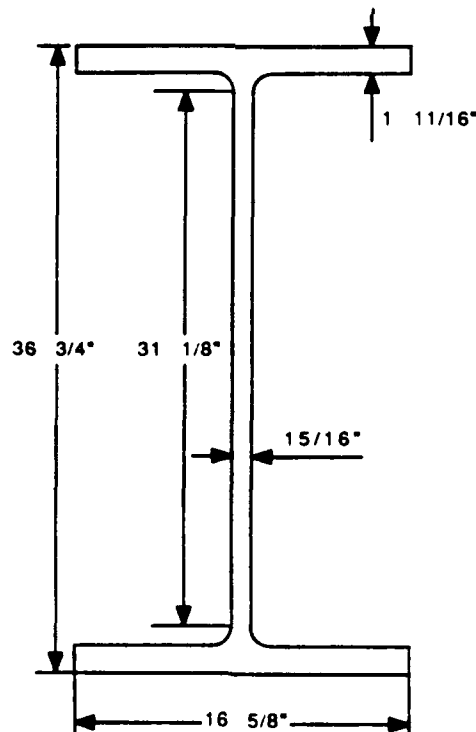


Figure 5. Specimen dimensions of W36x300 shape used in the experimental study

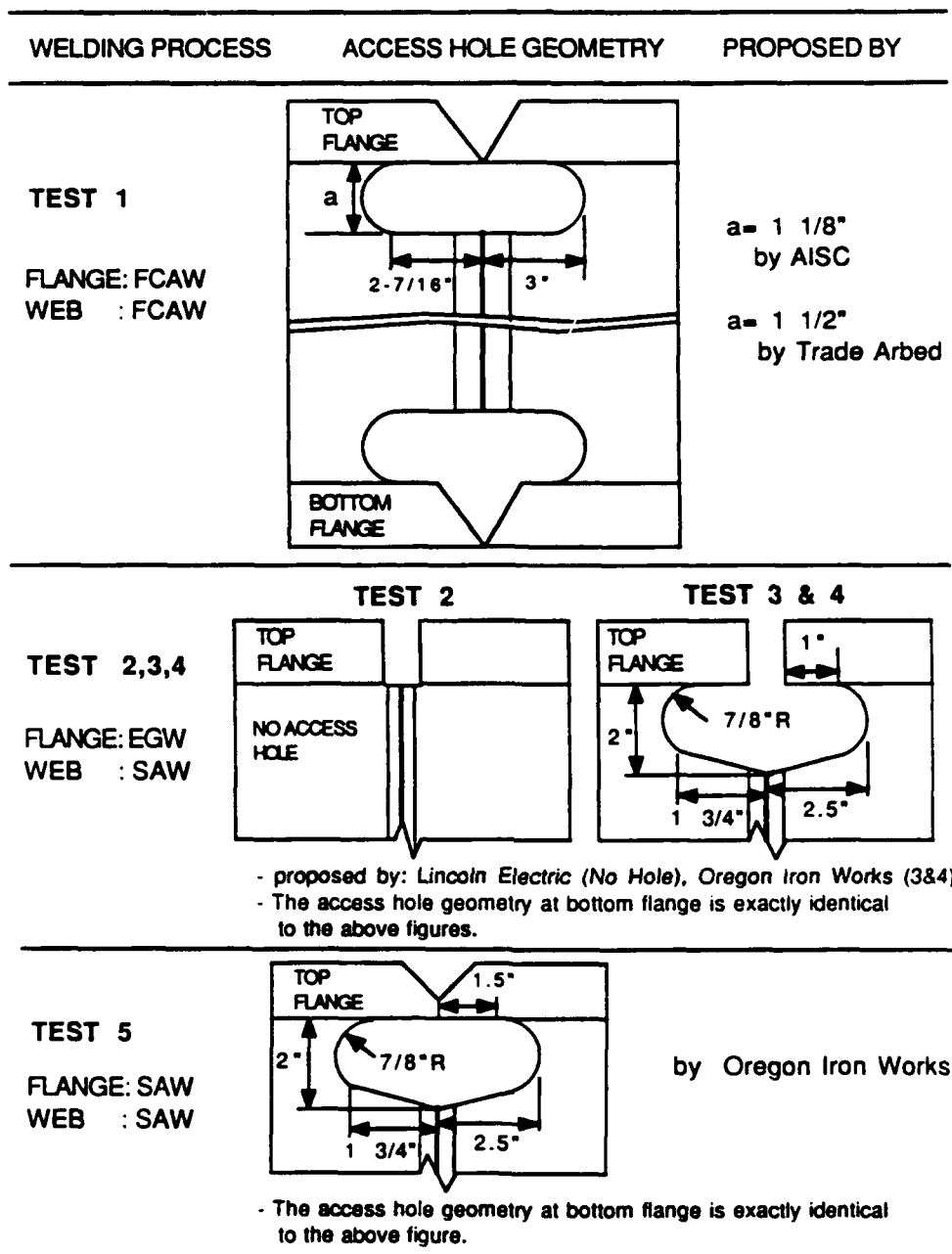


Figure 6. Details of joint and access hole geometry

sequence, number of passes, joint and access hole geometries, and materials are given in Tables 2 through 5 and in Figures 7 through 10 in detail. It should be pointed out that the welding variables used in the actual welding tests were similar but not exactly the same as those used in the finite element analysis. In addition, the actual welding passes were also different from those used in the finite element analysis. These differences would be understandable if one noticed that most of the finite element analysis had been finished before the actual tests were initiated and the dimensions of

Table 2
Welding Parameters and Variables of Test 1

<u>Joint</u>	<u>Thick in.</u>	<u>Groove</u>	<u>Amp.</u>	<u>Volt.</u>	<u>Speed(IPM)</u>	<u>Passes</u>	<u>Position</u>	<u>Remarks</u>
Top flange	1-11/16	V	190- 230	24-27	8-14	23	Flat	One side welding
Bottom	1-11/16	V	195- 220	24-27	8-14	28	Flat	One side welding
Web	15/16	X	155- 160	21-22	3-7	11	Vertical	No back gouge

Note: Specimen: ASTM A572 Gr. 50 (W-shapes 36x300)
 Process: FCAW
 Consumables: AWS E71T-1 (0.05"), 75Ar-25CO2 Gas
 Weld Sequence: Top Flange - Bottom Flange - Web

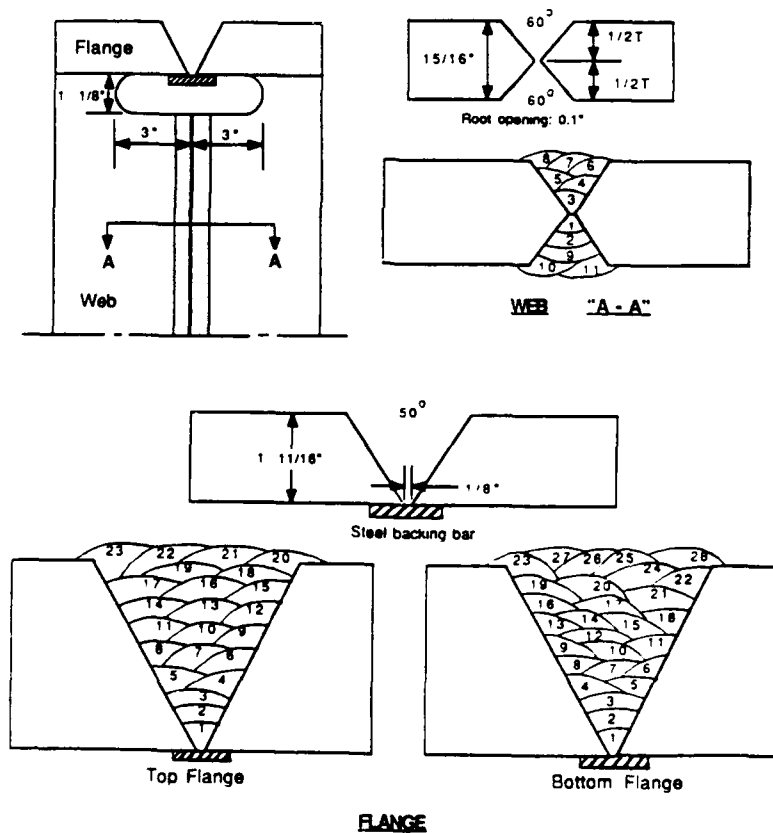


Figure 7. Joint details and pass sequences of
 Test 1

Table 3

Welding Parameters and Variables of Test 2

<u>Joint</u>	<u>Thick in.</u>	<u>Groove</u>	<u>Amp.</u>	<u>Volt.</u>	<u>Speed(IPM)</u>	<u>Passes</u>	<u>Position</u>	<u>Remarks</u>
Top flange	1-11/16	Square	540* 640**	37 37	1.6 1.6	1	Vertical	2 Poles *SP, † **RP
Bottom flange	1-11/16	Square	540* 640**	37 37	1.6 1.6	1	Vertical	
Web	15/16	V	330- 340	31	7.0- 15.0	10	Flat	Back gouge (2nd side)

Note: Specimen: ASTM A572 Gr. 50 (W-shapes 36x300)

Process: EGW for Flange Weld

SAW for Web Weld

Consumables: Lincoln EGW-NR431(0.12"), SAW-L61(5/64")&Flux 980

Weld Sequence: Web - Top Flange - Bottom Flange

No Access Hole: (suggested by Lincoln Electric Co.)

† SP = straight polarity; RP = reversed polarity

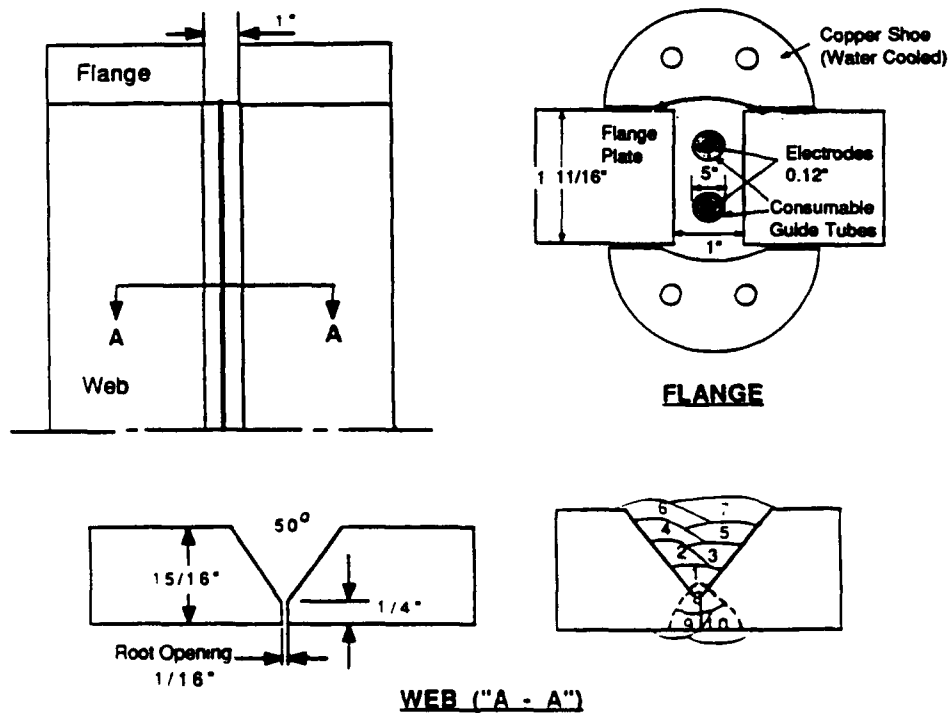


Figure 8. Joint details and welding pass sequences of Test 2

Table 4
Welding Parameters and Variables of Tests 3 and 4

<u>Joint</u>	<u>Thick in.</u>	<u>Groove</u>	<u>Amp.</u>	<u>Volt.</u>	<u>Speed(IPM)</u>	<u>Passes</u>	<u>Position</u>	<u>Remarks</u>
Top flange	1-11/16	Square	900	42	1.2	1	Vertical	1 Pole (oscil- lation)
Bottom flange	1-11/16	Square	900	41.5	1.2	1	Vertical	
Web	15/16	V	330- 340	31	7.0- 12.2	8	Flat	Gouging (2nd side)

Note: Specimen: ASTM A572 Gr. 50 (W-shapes 36x300)
 Process: EGW for Flange Weld
SAW for Web Weld
 Consumables: Lincoln EGW-NR431(0.12"), SAW-L61(5/64")&Flux 980
 Weld Sequence: TEST 3: Top Flange - Bottom Flange - Web
TEST 4: Web - Top Flange - Bottom Flange

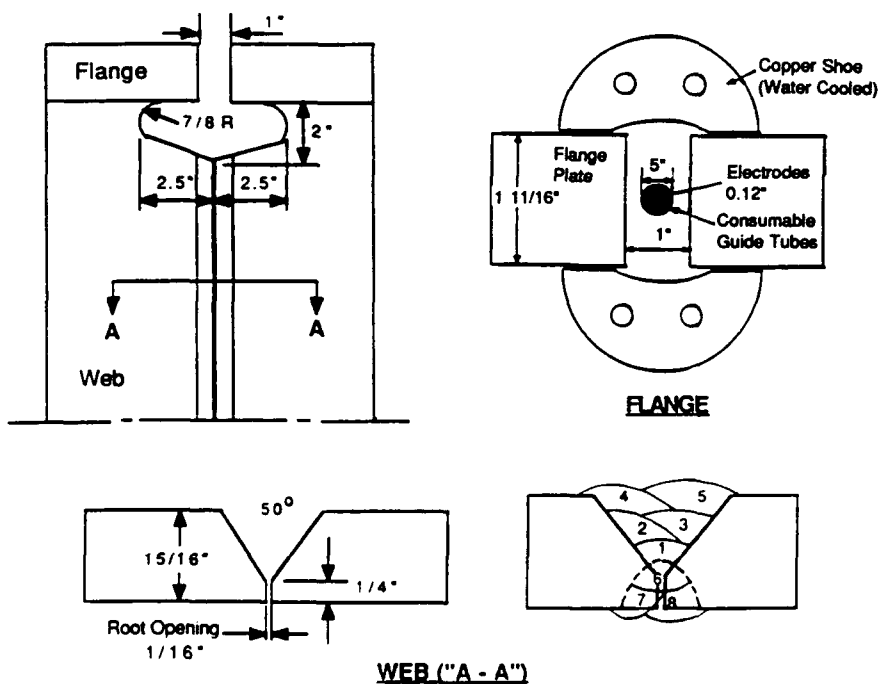


Figure 9. Joint details and pass sequences of
 Tests 3 and 4

Table 5

Welding Parameters and Variables of Test 5

<u>Joint</u>	<u>Thick in.</u>	<u>Groove</u>	<u>Amp.</u>	<u>Volt.</u>	<u>Speed(IPM)</u>	<u>Passes</u>	<u>Position</u>	<u>Remarks</u>
Top flange	1-11/16	V	350- 370	31	10.1-13.3	22	Flat	Gouge (2nd side)
Bottom flange	1-11/16	V	350- 370	31	10-13	22	Flat	Gouge (2nd side)
Web	15/16	V	330- 360	31	7.0-12.2	12	Flat	Gouge (2nd side)

Note: Specimen: ASTM A572 Gr. 50 (W-shapes 36x300)
 Process: SAW for Flange Weld
SAW for Web Weld
 Consumables: Lincoln L61(5/64")&Flux 980
 Weld Sequence: Top Flange - Bottom Flange - Web

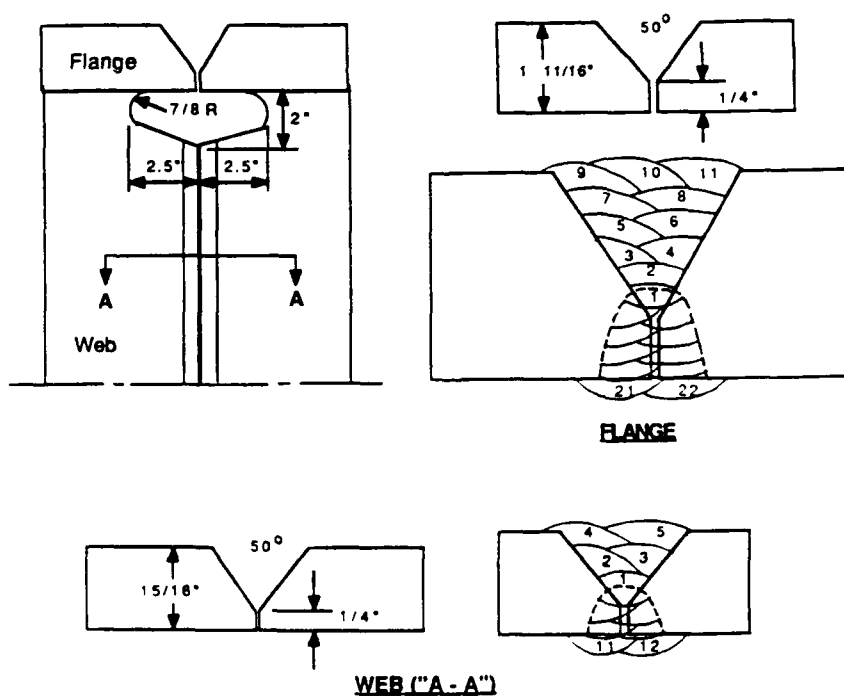


Figure 10. Joint details and pass sequences of Test 5

W36x300 shapes used in the actual testing were different from those of W36x359 used in the finite element analysis.

22. The temperature and strain measurements were obtained via a data acquisition system developed at the Department of Welding Engineering, Ohio State University. All testing data files were collected and stored on the hard disk of an IBM AT. The files were then transferred to floppy diskettes after testing.

Thermal strain results

23. Usually welding one test was too long for the data collection of the whole welding process to be finished without interruptions. As an example, the strain gages had to be disconnected with the data acquisition system for gouging, and power line surge interrupted the data acquisition a few times. Thus, a test was divided into some "small" experiments due to these considerations. An experiment is referred to as a data collection period from the time the data acquisition system begins to collect data until the system is turned off or interrupted. This is how the actual thermal strain measurements were arranged and how the thermal strain testing data were stored in the diskettes.

24. The location of the thermal strain gages and thermocouples near the access hole are depicted in Figures 11 through 15. All strain gages were 3/8 in. from the edges of the access holes. The thermal strain variation for the first pass of Test 4 and final pass of Test 1 are plotted in Figures 16 and 17 as examples of the experimental results. More testing results are presented when comparing with the finite element analysis results (see Part IV).

Residual stress results

25. After the weldments returned to the ambient temperature, residual stress measurements were made. The blind hole drilling technique was used to measure residual stress near the access holes. A 1/16-in.-diam high-speed drill bit was used to drill the hole. The residual stresses were calculated following the American Society for Testing and Materials (ASTM) Standard E837-85 "Determining Residual Stresses by the Hole-Drilling Strain Gage Method." Two locations were selected on each specimen. All strain gages were 3/8 in. from the edges of the access holes for Tests 3 through 5, as shown in Figure 18. For Test 2, the strain gages were at a distance of 3/8 in. from the fusion line of the web weld. One gage was 1-7/8 in. from the inside face of the flange, and the other gage was 3 in. from the flange, inside face, as

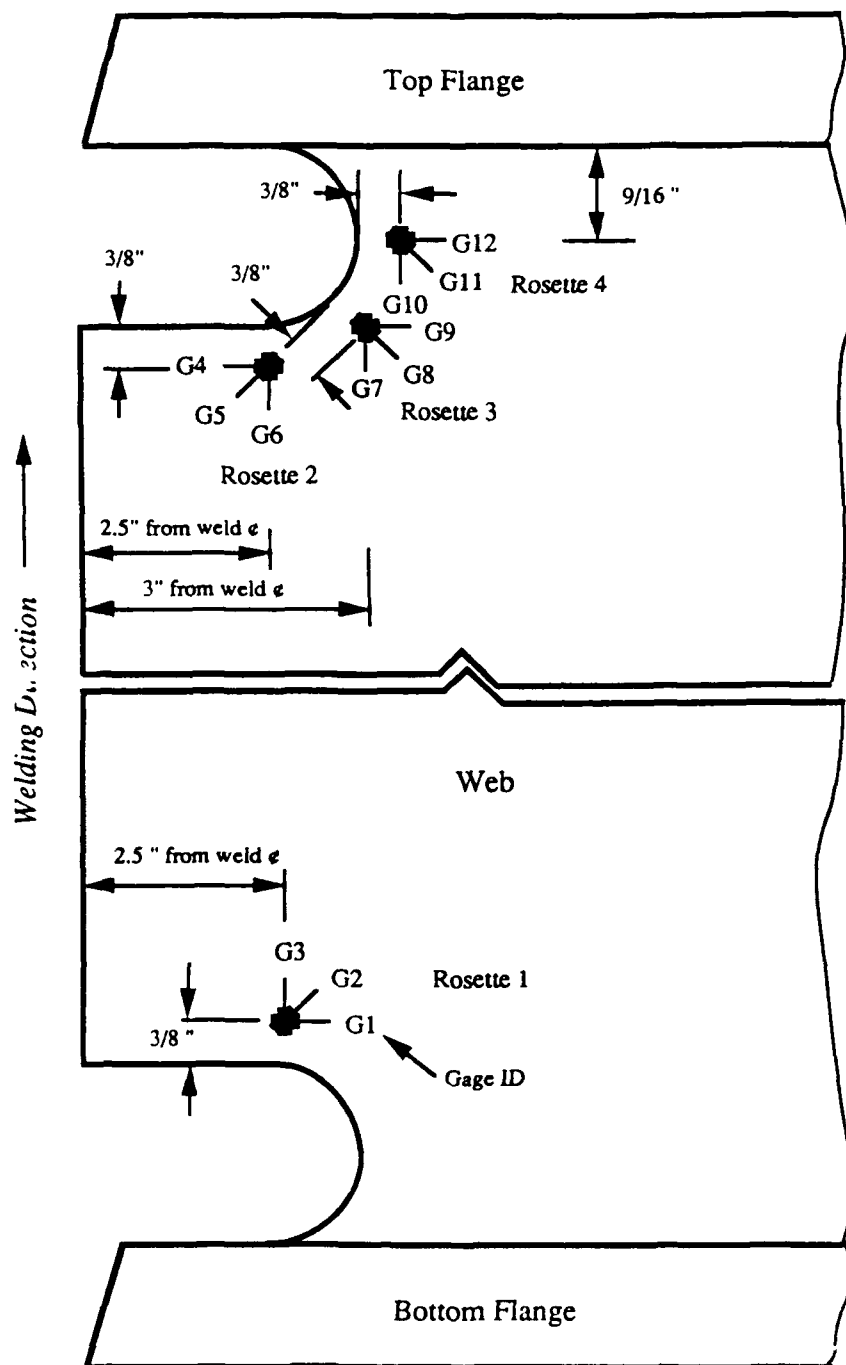


Figure 11. Thermal strain gage layout of Test 1 at Ohio State University

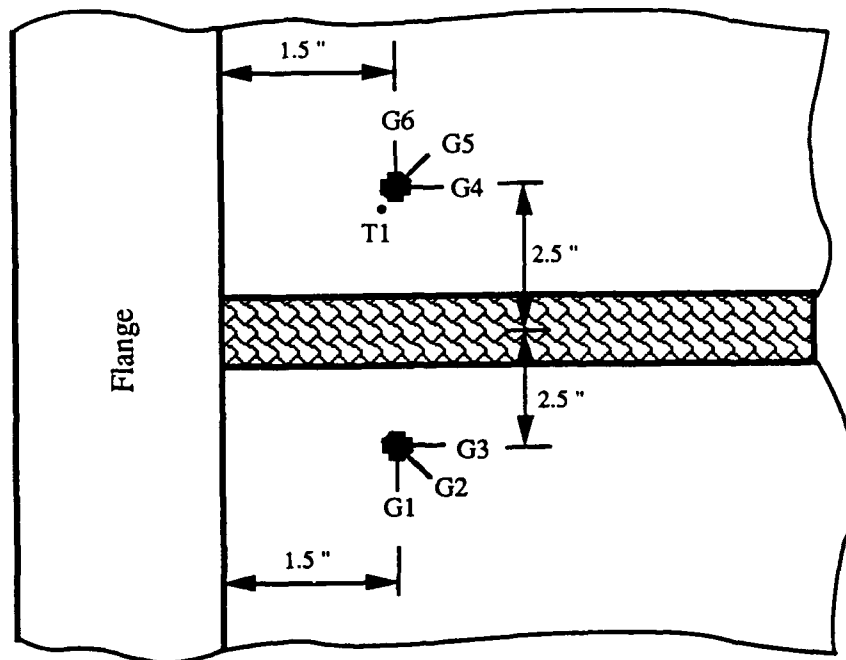


Figure 12. Strain gage and thermocouple layout of Test 2

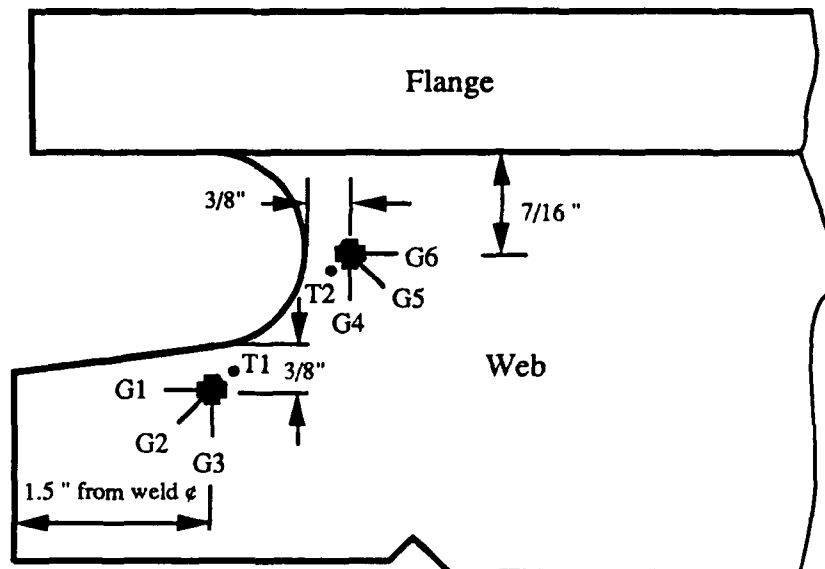


Figure 13. Thermal strain gage and thermocouple layout of Test 3

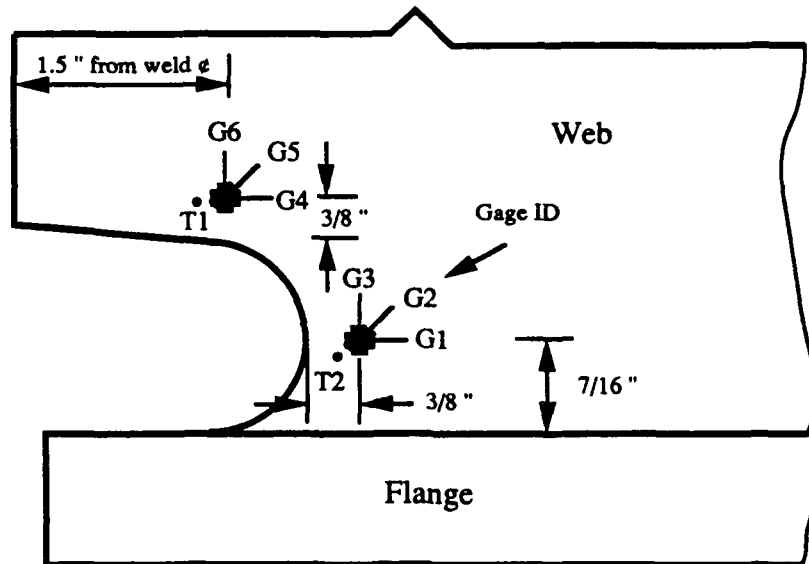


Figure 14. Thermal strain gage and thermocouple layout of Test 4

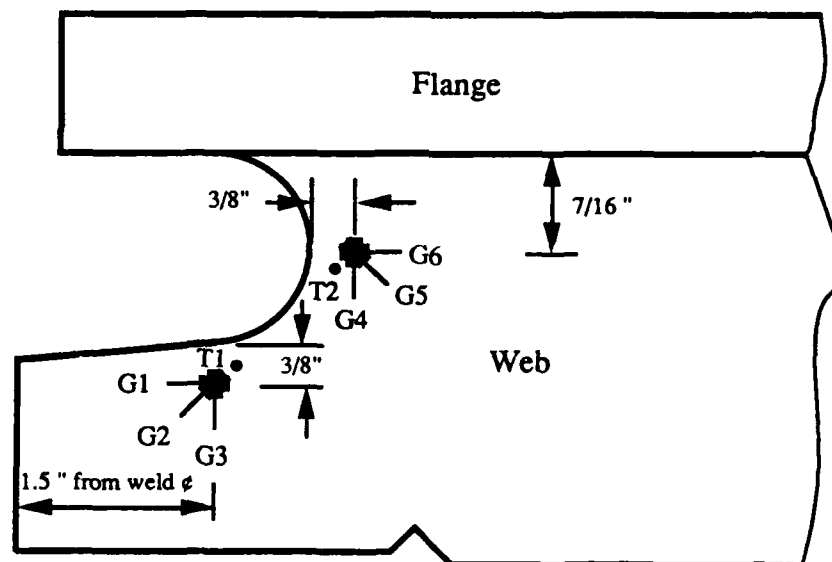


Figure 15. Thermal strain gage and thermocouple layout of Test 5

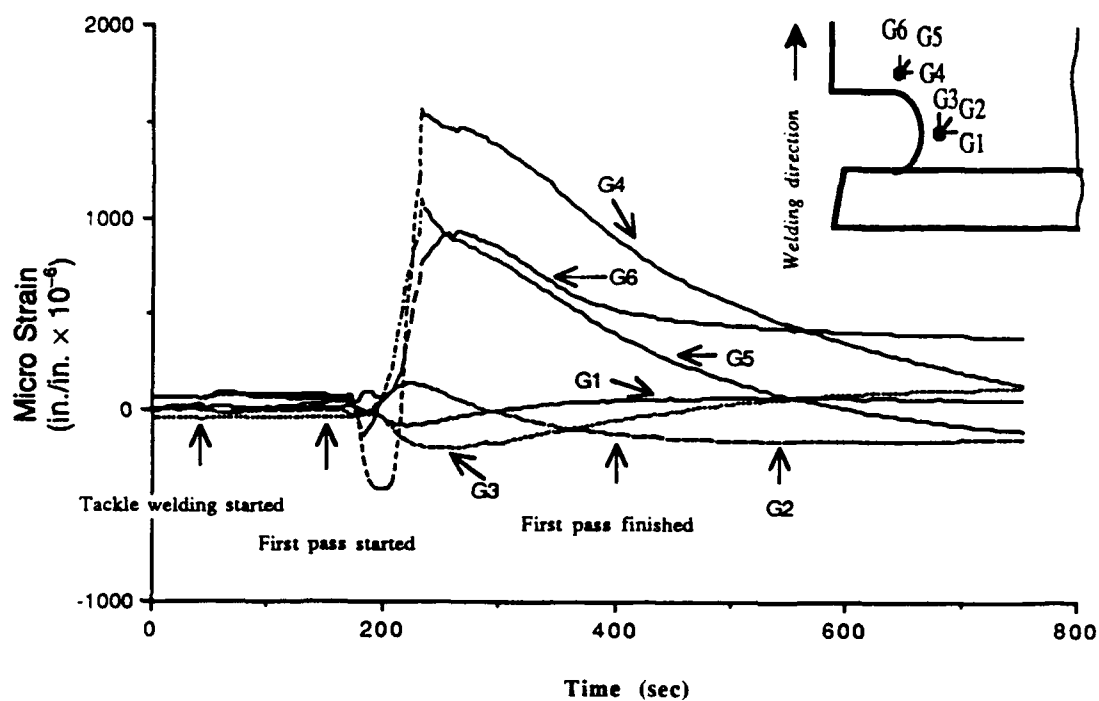


Figure 16. Thermal strain variations during the first pass of Test 4

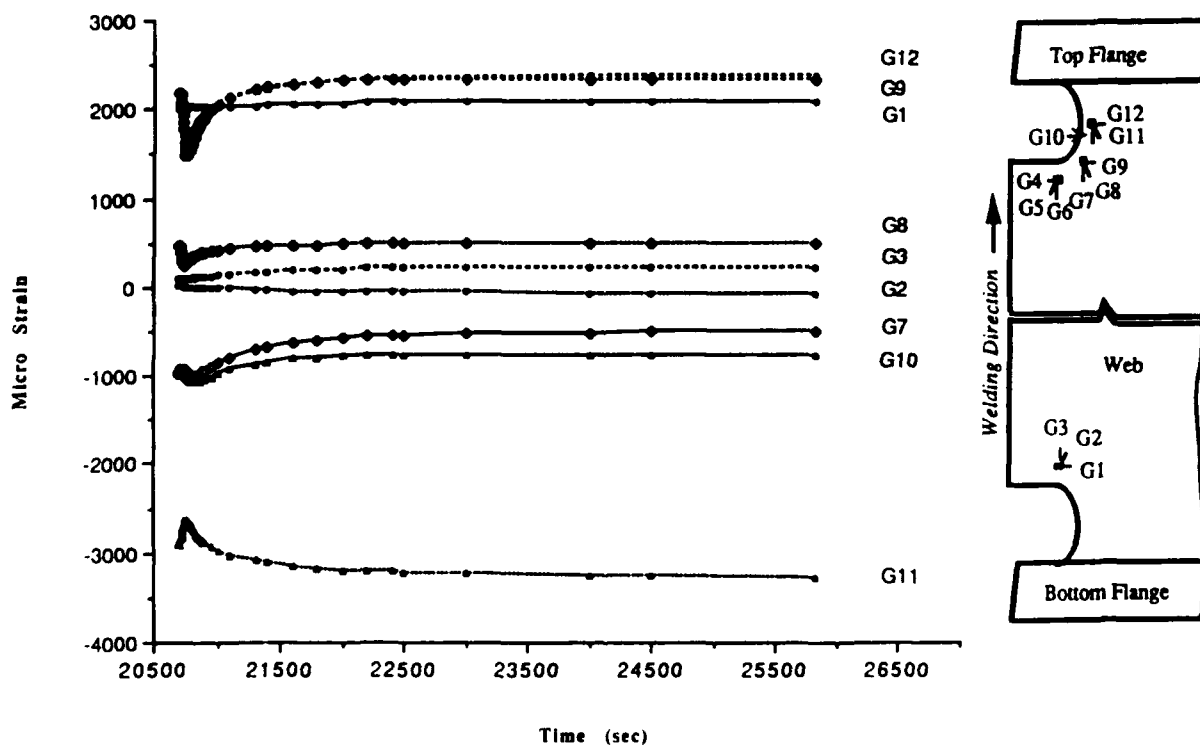


Figure 17. Thermal strain variations during the final pass of Test 1

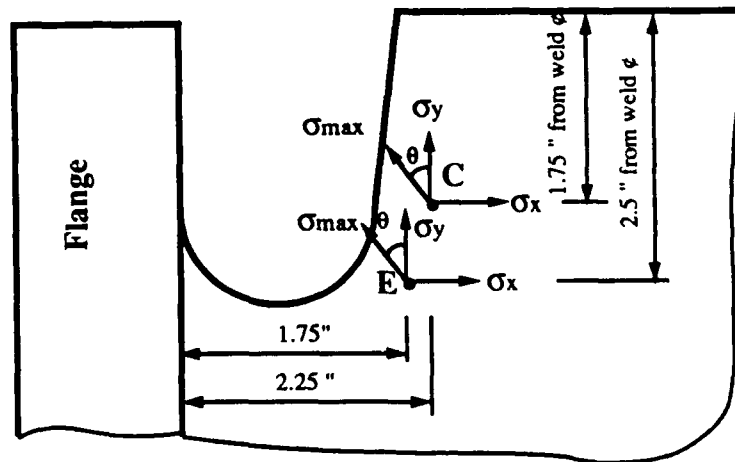


Figure 18. Illustration of the positions of strain gages and coordinate system used in residual stress measurements (Tests 3 through 5)

shown in Figure 19. No residual stress measurements were obtained from Test 1. These strain gage locations were suggested by the finite element analysis, in order to compare with the finite element analysis results. The notations C and E were the same as used in the finite element analysis.

26. By using the developed data acquisition system, strain relaxation during the hole drilling could be recorded. Figure 20 shows the relieved strain as a function of the hole depth for Test 2 at location E (Figure 19). The plot indicated that at approximately 3/32-in. depth, the surface residual

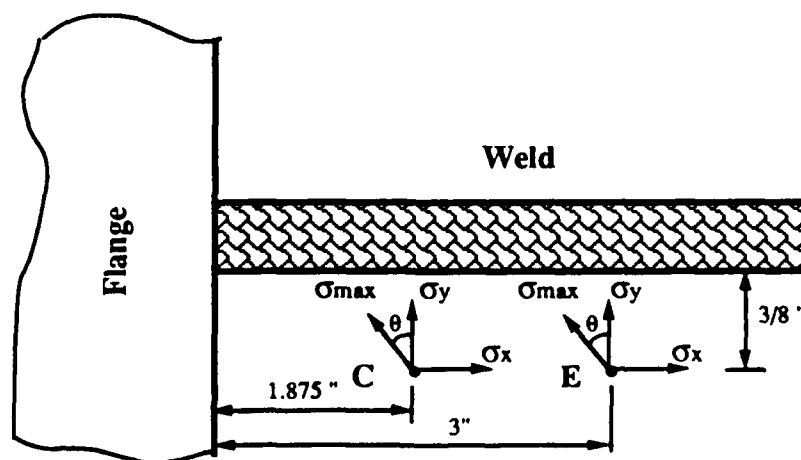


Figure 19. Illustration of strain gage positions and coordinate system used in residual stress measurements (Test 2)

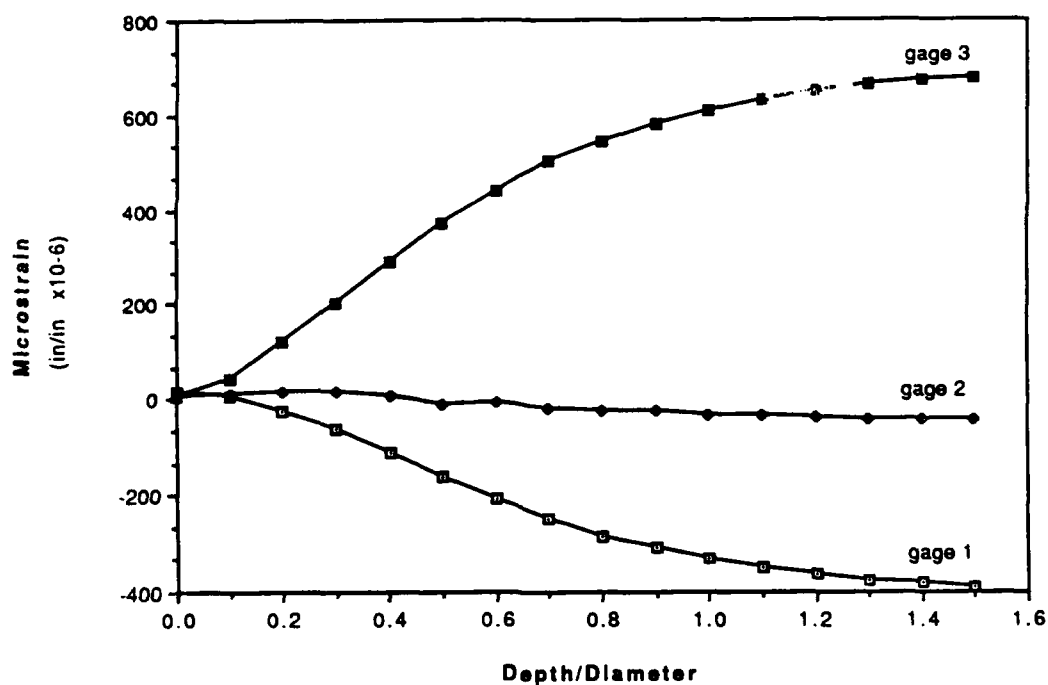


Figure 20. Strain relief versus hole depth in residual stress measurement (Test 2, Location E)

stress near the point of drilling was relieved. The surface residual stress values are tabulated in Table 6.

Table 6
Residual Stress Measurement Results

Test No. Coupon	Test 2 A	Test 3 B	Test 4 C	Test 5 D
<u>Location C</u>				
σ_{\max} (ksi)	21.5	67.0	-17.3	74.4
σ_{\min} (ksi)	-64.0	8.7	-92.2	10.4
θ (deg)	80	-38	63	-31.0
σ_x (ksi)	18.9	30.8	-33.5	27.4
σ_y (ksi)	-61.4	44.9	-76	57.4
<u>Location E</u>				
σ_{\max} (ksi)	5.4	58.7	-2.1	90.1
σ_{\min} (ksi)	-65.0	20.0	-65.9	18.7
θ (deg)	87	55	57	-30
σ_x (ksi)	5.18	46.0	-20.3	36.6
σ_y (ksi)	-64.8	32.7	-47.7	72.3

Note: Locations C and E are shown in Figures 18 and 19. θ is the angle from the σ_y direction to the maximum principal stress direction.

Fracture Toughness

27. Coupons from the FCAW test (Test 1) were mechanically tested by the Welding Consultants, Inc., in Columbus, OH. Prior to removal of mechanical test specimens, the welds were ultrasonically tested in accordance with American Welding Society (AWS) D1.1. The web was satisfactory. However, there were some sidewall slag inclusions and incomplete fusion in the flange welds. All test samples were taken from sound weld areas.

28. Oxyacetylene cutting was used to remove rough sections from both the web and one of the flanges. Individual specimens were then carefully machined to eliminate any possible thermal effects of the flame cutting operation. The following samples were removed from both the web and flange:

- a. One-microhardness macrosection.
- b. Five-base metal charpys.
- c. Five-weld metal charpys.
- d. Five-heat-affected zone charpys.

29. The charpy specimens were prepared and tested in accordance with ASTM E23. The test temperature was 40 °F. The results of these mechanical tests appear in Tables 7 and 8.

30. The microhardness data show a slight increase in hardness for the HAZs of both flange (20 to 27 Rockwell hardness C-scale (RC)) and web joints (24 to 31 RC). The higher hardness in the web welds than the flange welds is due to the smaller welding heat input required for the thinner web joint.

31. The charpy data show inconclusive results that indicate higher toughness in the flange-HAZ and web-HAZ than their respective base metal. Also, the flange toughness is much higher than the web toughness in all three zones.

32. Charpy tests were also conducted on SAW and EGW welded samples by the Lincoln Electric Company. However, test results were not yet made available as of the time when this report was written.

Table 7
Results of Charpy Impact Test

<u>Location</u>	<u>Specimen Number</u>	<u>Test Temperature °F</u>	<u>Breaking Energy, ft-lb</u>
Web-weld	1	40	61.0
	2	40	68.0
	3	40	66.5
	4	40	62.0
	5	40	31.0*
Web-HAZ	1	40	31.0
	2	40	55.0
	3	40	69.0
	4	40	85.0
	5	40	48.0
Web-base metal	1	40	22.0
	2	40	28.0
	3	40	24.0
	4	40	22.5
	5	40	31.5
Flange-weld	1	40	112.0
	2	40	103.0
	3	40	86.5
	4	40	98.0
	5	40	97.0
Flange-HAZ	1	40	109.0
	2	40	122.0
	3	40	104.5
	4	40	105.0
	5	40	121.5
Flange-base metal	1	40	88.0
	2	40	61.0
	3	40	60.0
	4	40	29.0
	5	40	13.5

* Slag present in sample.

Table 8
Results of Transverse Microhardness

<u>Location</u>	<u>Distance, in.</u>	<u>Knoop Hardness Number</u>	<u>Equivalent HRB/HRC*</u>
Web-weld	0	239	98 (B)
	0.02	246	99 (B)
	0.04	258	22 (C)
	0.06	265	23 (C)
	0.08	273	24 (C)
Web-HAZ	0.1	270	24 (C)
	0.12	318	31 (C)
Web-base metal	0.14	213	92 (B)
	0.16	184	86 (B)
	0.18	145	73 (B)
	0.2	132	67 (B)
	0.22	113	56 (B)
	0.24	117	58 (B)
Flange-weld	0	125	63 (B)
	0.02	132	66.5 (B)
	0.04	177	84 (B)
	0.06	191	88 (B)
	0.08	221	94 (B)
Flange-HAZ	0.1	289	27 (C)
	0.12	220	94 (B)
	0.14	249	20 (C)
Flange-base metal	0.16	224	95 (B)
	0.18	230	96 (B)
	0.2	180	85 (B)
	0.22	238	98 (B)
	0.24	194	89 (B)
	0.26	186	87 (B)
	0.28	258	22 (C)

Note: Distance was measured from the weld center line.

* HRB = hardness Rockwell B-scale; HRC = hardness Rockwell C-scale.

PART III: PROBLEM DEFINITION FOR FINITE ELEMENT MODELING (FEM) ANALYSIS

Material Property

33. Material properties of A572 Grade 50 steel are summarized in Figure 21. These properties, which are temperature dependent, include thermal conductivity, specific heat, thermal expansion coefficient, Young's modulus, yield stress, and strain hardening exponent. Their values were used in the finite element analysis.

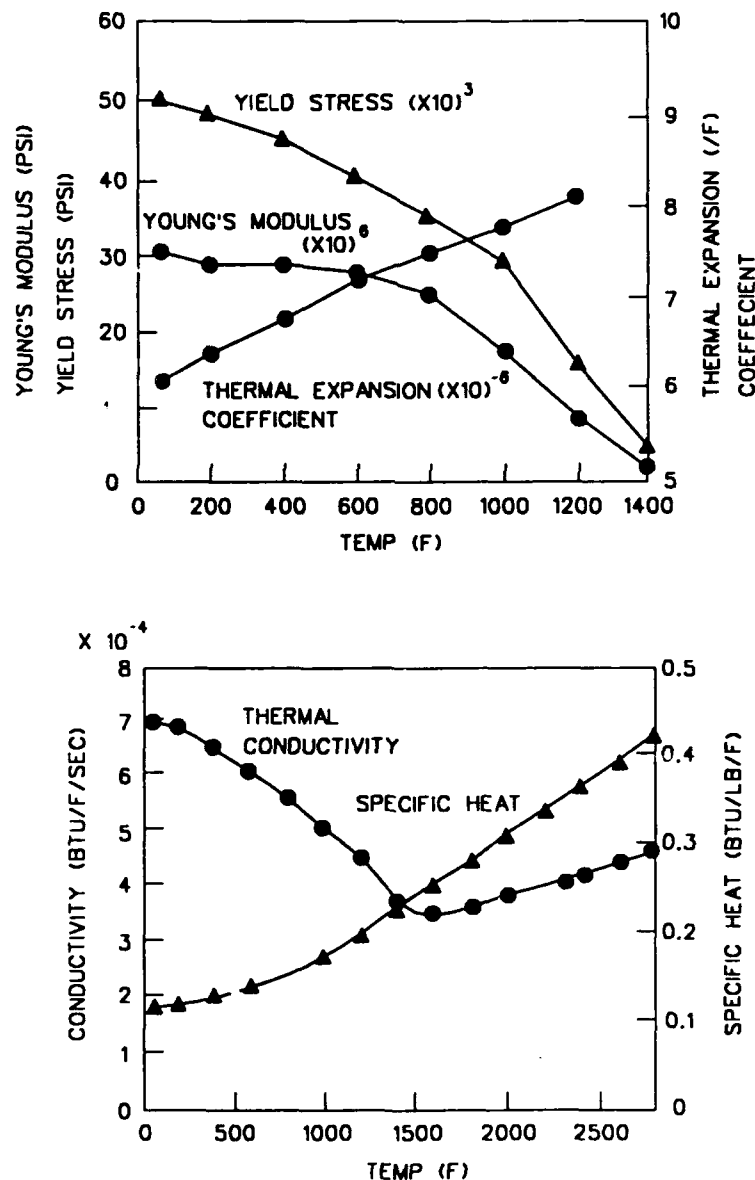


Figure 21. Temperature dependent material properties used in the FEM analysis

Joint Type and Preparation Proposed for FEM Analysis

34. In this study, the wide-flange shapes were joined by a complete penetration groove weld butt joint. Trade Arbed, AISC, and Oregon Iron Works (OIW) recommend using single-V-groove welds to join the flanges with a double-V-groove weld for the web. The finite element studies used W36X359 shapes, whose dimensions are shown in Figure 22. The geometry for the web access holes shown in Figure 23 as recommended by Trade Arbed, AISC, and OIW was investigated using the respective proposed welding processes. Trade Arbed recommends the largest hole diameter.

35. The weld joint edge preparation and fit up for the FCAW is presented in Figure 24. Figure 24a shows the geometry for the single-V-groove weld for the flanges with the double-V-groove geometry for the web

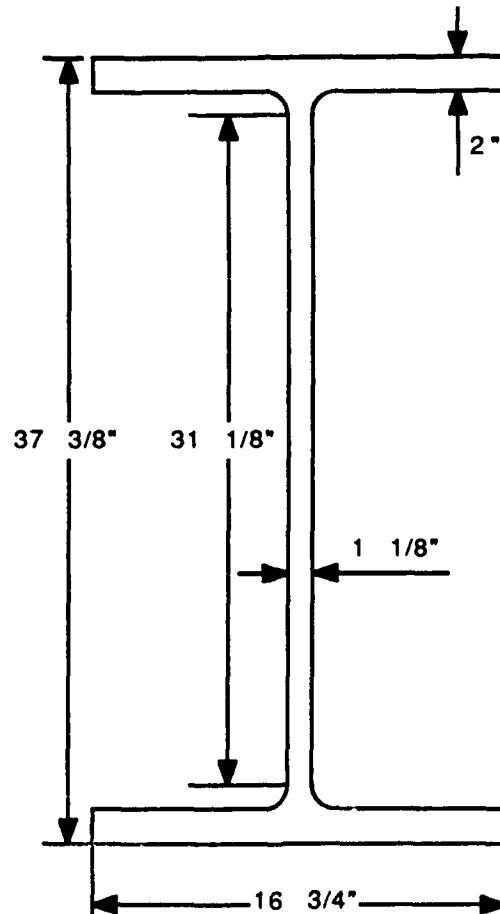


Figure 22. Specimen dimensions used in finite element analysis (W36x359)

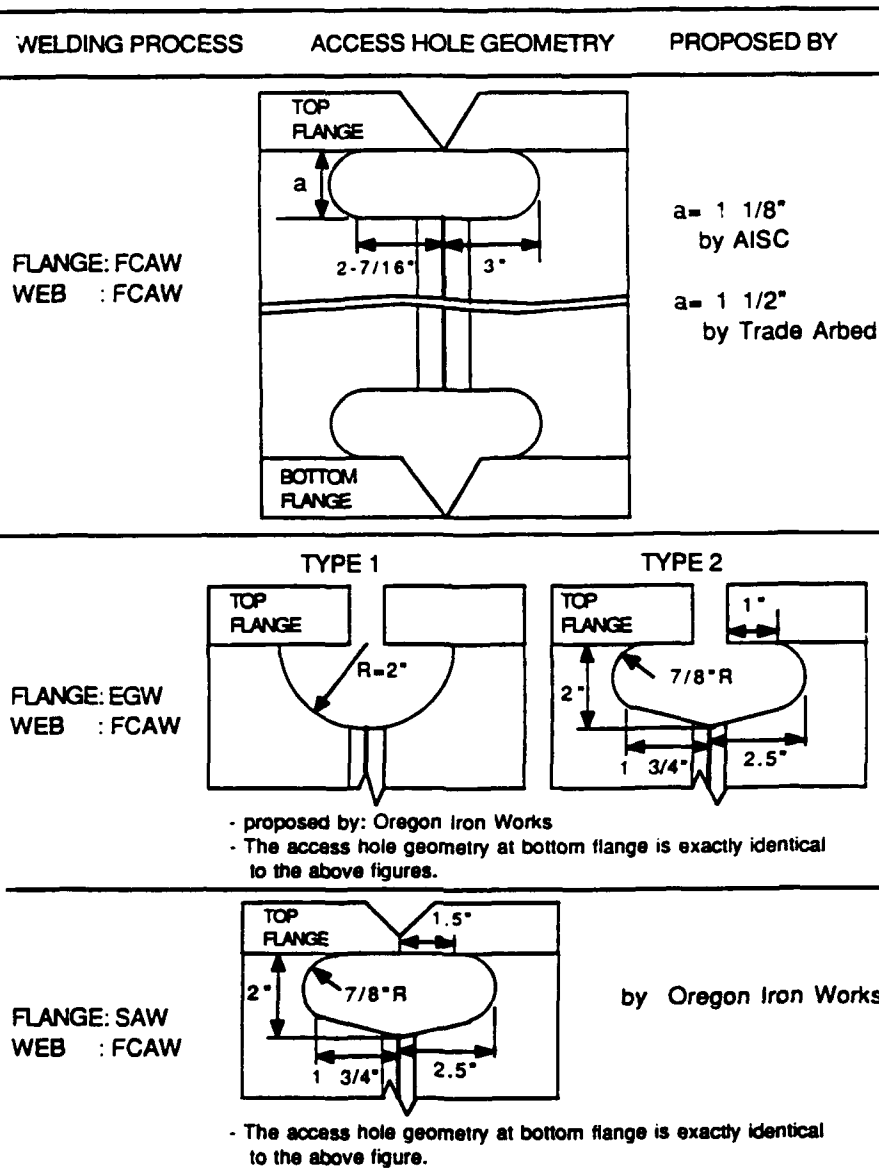


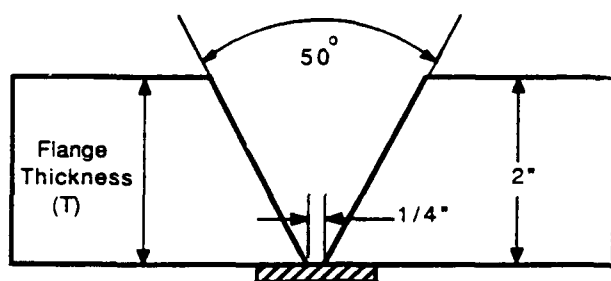
Figure 23. Access hole details used in finite element analysis

shown in Figure 24b. Figure 24c illustrates an alternate double-V-groove weld that will also be investigated for possible use in welding the flanges.

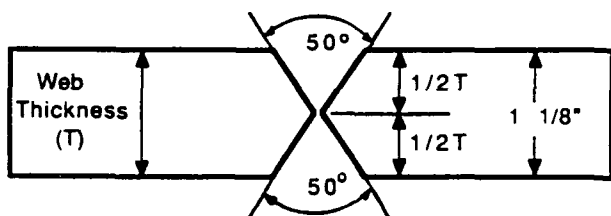
36. The weld joint edge preparation and fit up for the SAW and EGW processes are shown in Figure 25.

Welding Process and Variable Proposed for FEM Analysis

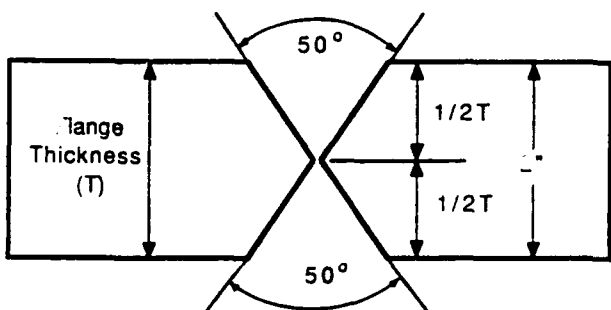
37. Three welding processes, FCAW, SAW, and EGW, were investigated in



(a) Proposed Flange Edge Preparation (Single-V)

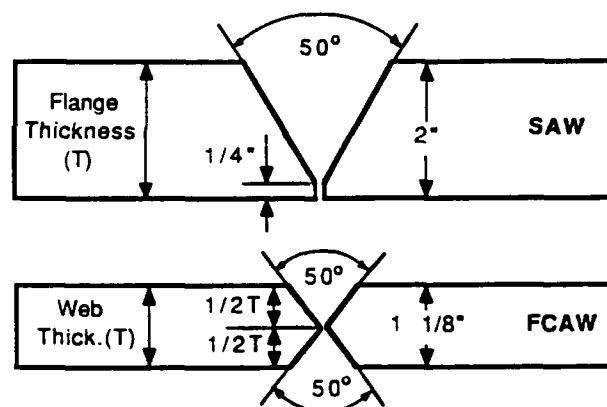


(b) Proposed Web Edge Preparation (Double-V)

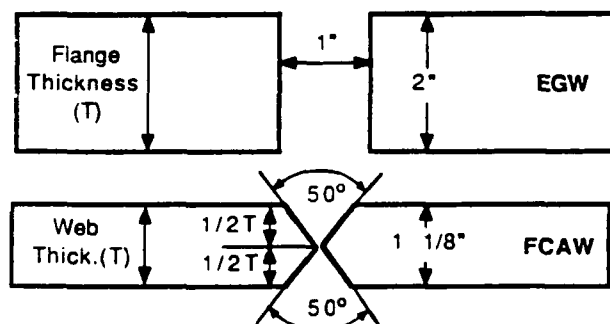


(c) Alternate Flange Edge Preparation (Double-V)

Figure 24. Weld edge preparation and fit up for FCAW used in finite element analysis



(a) Proposed Edge Preparations; SAW at Flange. FCAW at Web



(b) Proposed Edge Preparations; EGW at Flange. FCAW at Web

Figure 25. Weld edge preparation and fit up for SAW and EWG in finite element analysis

this study. The associated variables included welding current, voltage, travel speed, and sequence and number of weld pass.

Flux cored arc welding

38. The FCAW was used with E71T-1 (0.05 in.) electrode and a dual shield of CO₂ gas. The current, voltage, and travel speed for the root pass and second pass were in the range of 170 to 200 amp, 24 to 27 v with a travel speed of 5.9 to 7.5 in. per min (ipm). The remaining passes were deposited with welding parameters of 210 to 250 amp, 25 to 30 v and 10.6 to 15.7 ipm.

39. The double-V-groove flange weld required 26 passes, as shown in Figure 26-a while the single-V-groove required 37 passes, as shown in Figure 26-b. The double-V-groove web weld required 8 passes, as shown in Figure 26-c.

Submerged arc welding

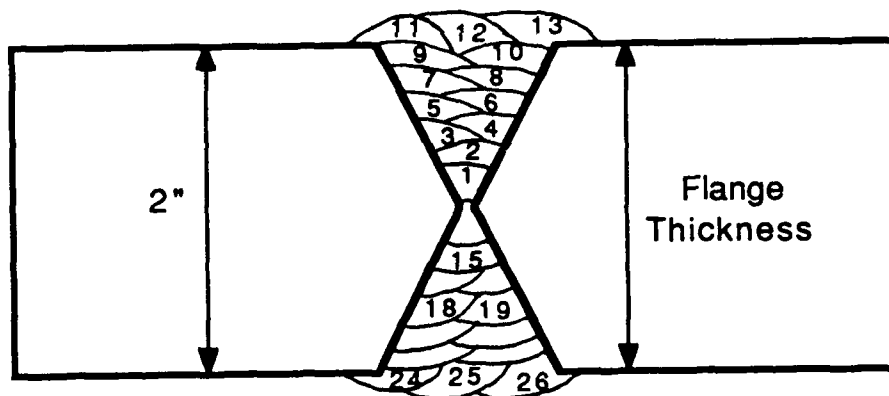
40. The SAW was used with a 6/64-in.-diam electrode. The current, voltage, and travel speed were in the range of 330 to 370 amp, 30 to 32 v, and 7.9 to 13.8 ipm. A total of 23 passes were used for the flange groove. The other side of the joint was back gouged and rewelded by 6 passes. The double-V-groove web weld required 8 passes, as shown in Figure 27.

Electrogas welding

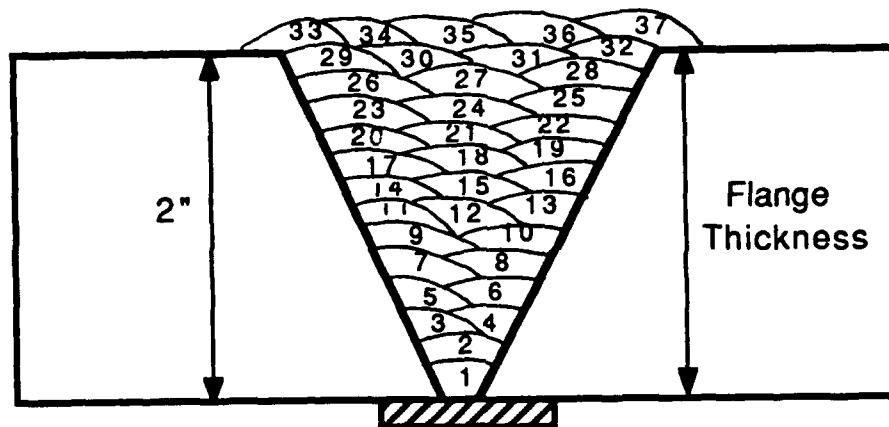
41. The ECW process was used as one method for flange welding. For the ECW process, 0.12-in. flux-cored wire was used with CO₂ shielding. The ECW process used square butt joint without any joint preparation (Figure 28). The flange was welded vertically up by a single pass with welding parameters in the range of 900 amp, 41 to 42 v, and 1.2 to 1.6 ipm. Copper cooling shoes were used to keep the molten metal in the groove during welding. The web was welded by the FCAW process in eight passes with welding parameters in the range of 170 to 230 amp, 24 to 30 v, and 7.9 to 11.8 ipm. Its joint geometry was the same as that shown in Figure 27.

Thermo-Mechanical Parameter

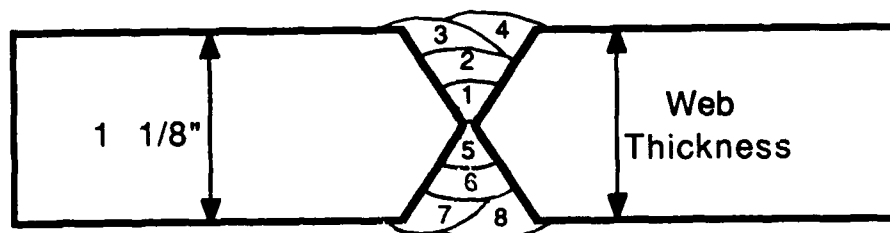
42. In this study, the thermo-mechanical responses of the weldment to the various welding processes and procedures were either calculated by the finite element analysis or measured experimentally during welding. These thermo-mechanical parameters included transient temperature and strain (or stress) variations of the weldment during heating and cooling periods and



(a) Alternate FCAW Double-V-Groove Flange Weld



(b) Proposed FCAW Single-V-Groove Flange Weld



(c) Proposed FCAW Double-V-Groove Web Weld

Figure 26. Weld passes for FCAW used in finite element analysis

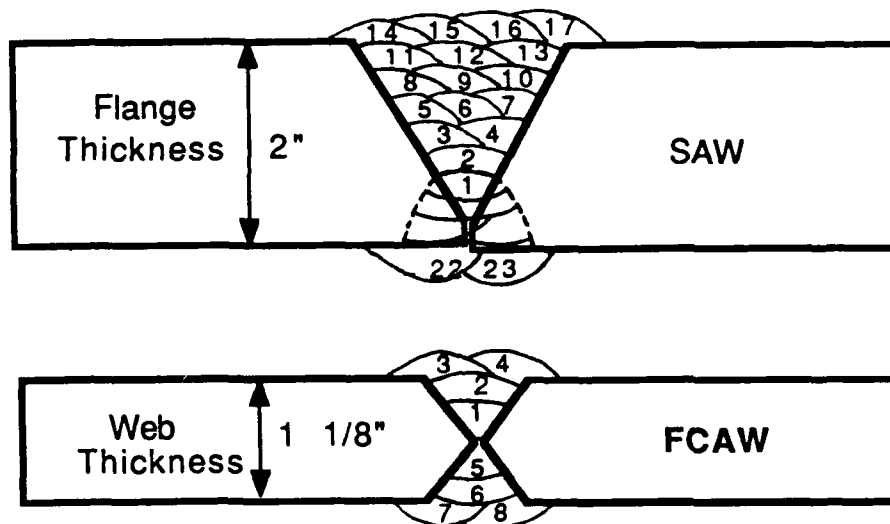


Figure 27. Weld passes for SAW process used in finite element analysis

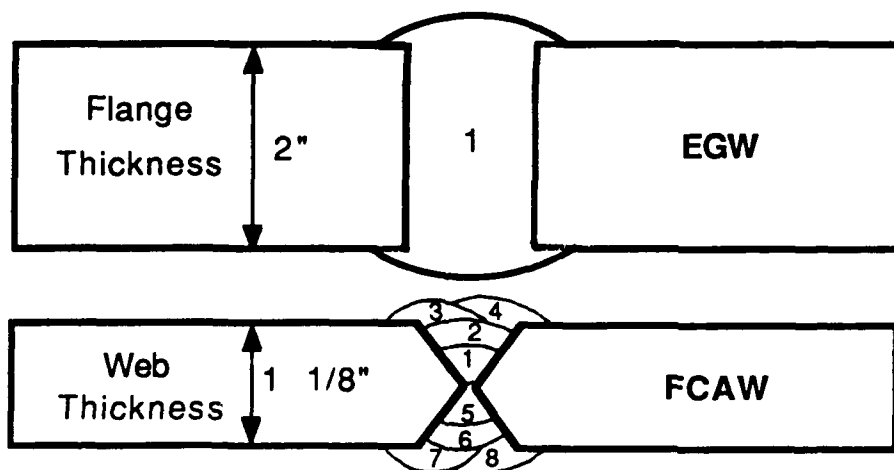


Figure 28. Weld passes for EGW process used in finite element analysis

residual stress distribution in the weldment after the weldment cooled down to room temperature.

PART IV: FINITE ELEMENT ANALYSIS

43. The thermal-mechanical analysis was performed using the ABAQUS finite element code. Since one of the parameters of interest pertained to effects from varying the diameter of the weld access hole, two finite element models for each welding process were required.

44. Assuming a condition of symmetry, a quarter of the joint was modeled (Figure 29). The finite element mesh for the 1-1/2-in.-diam weld access hole contained 374 elements while the 1-1/8-in.-diam weld access hole contained 368 elements for FCAW. Only the elongated weld access hole, which contained 234 elements, was modeled for SAW. Two models, semi-circle and elongated hole, were considered for EGW. They contained 207 and 234 elements, respectively. The thermal and stress analyses were both modeled as a two-dimensional problem in the plane of the web.

45. For the planar heat transfer analysis ABAQUS 8 node, quadratic interpolation element DC2D8 was used. The flange elements were given a thickness of 16.75 in. with 1.125 in. being used for the thickness of the web elements.

46. The heat input from the welding passes were lumped to make efficient use of the model. The 37 passes required to complete the full penetration single-V-groove flange weld using FCAW were lumped into 8 passes. The root and first pass were lumped into a single heat input. This heat input was then followed sequentially by lumping the passes, as shown in Figure 30.

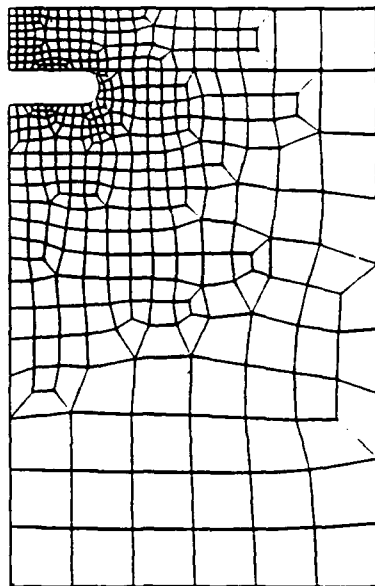
47. The heat input from the 26 passes required to complete the alternate double-V-groove flange weld using FCAW were lumped into 8 passes, as shown in Figure 30. The actual stair-step modeling of these lumped passes in the finite element analysis is shown in Figures 31 and 32.

48. For the SAW process, 23 flange weld passes were lumped into 10 heat input passes. The outer groove weld passes were lumped into 6 passes. Back gouging was considered as 1 lumped heat pass, but the root pass on the other side of the joint was removed from the model to simulate the gouging condition. The gouged groove at the inner surface was lumped into 3 passes.

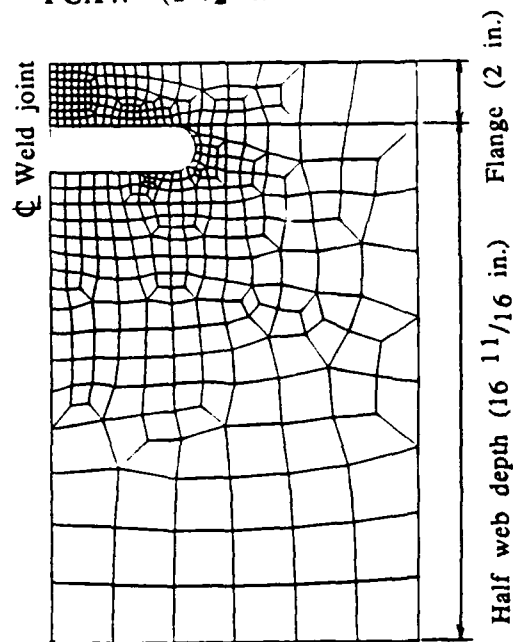
49. The EGW process makes a single, vertical up weld pass. Lumping the welding heat input is not needed for the finite element model for EGW.

50. The background for lumped heat input theory is discussed in detail in "Determination of Residual Stress and Effects in Thick Section Weldments

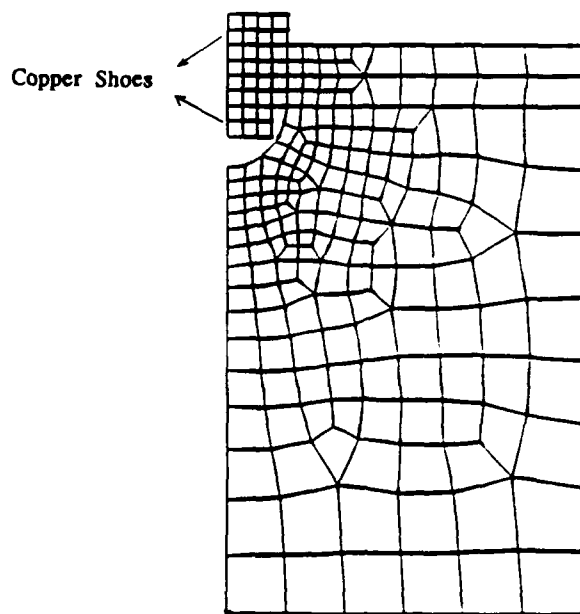
FCAW ($1\frac{1}{8}$ in. Diameter)



FCAW ($1\frac{1}{2}$ in. Diameter)



EGW (Semi-circle 2 in. Radius)



EGW & SAW (2 in. Diameter)

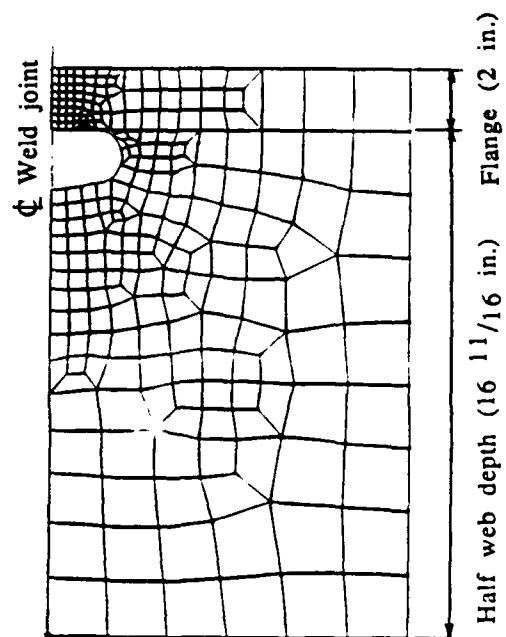


Figure 29. Finite element meshes

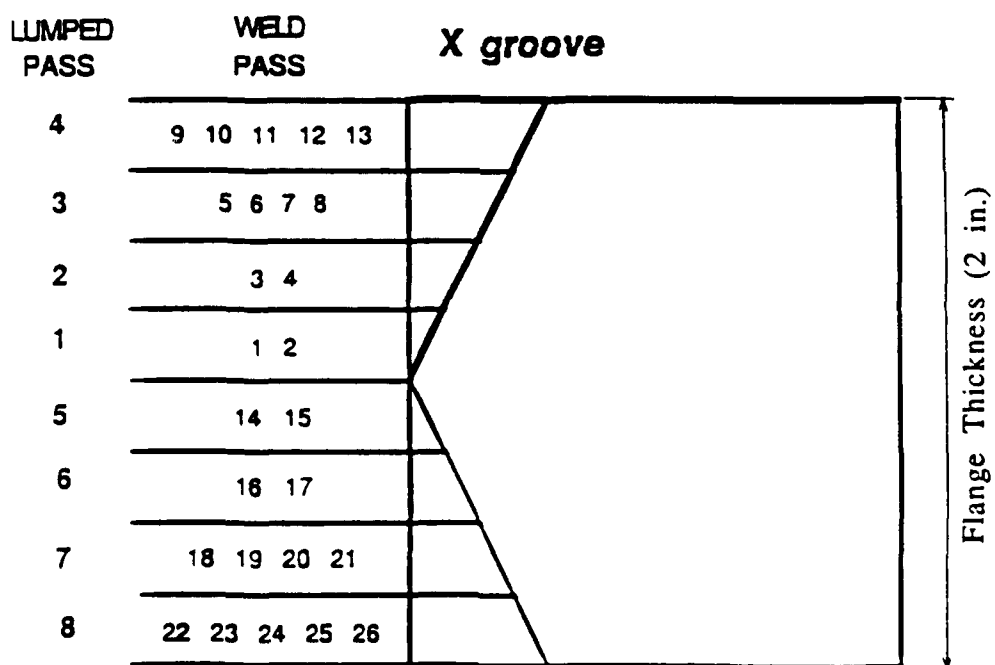
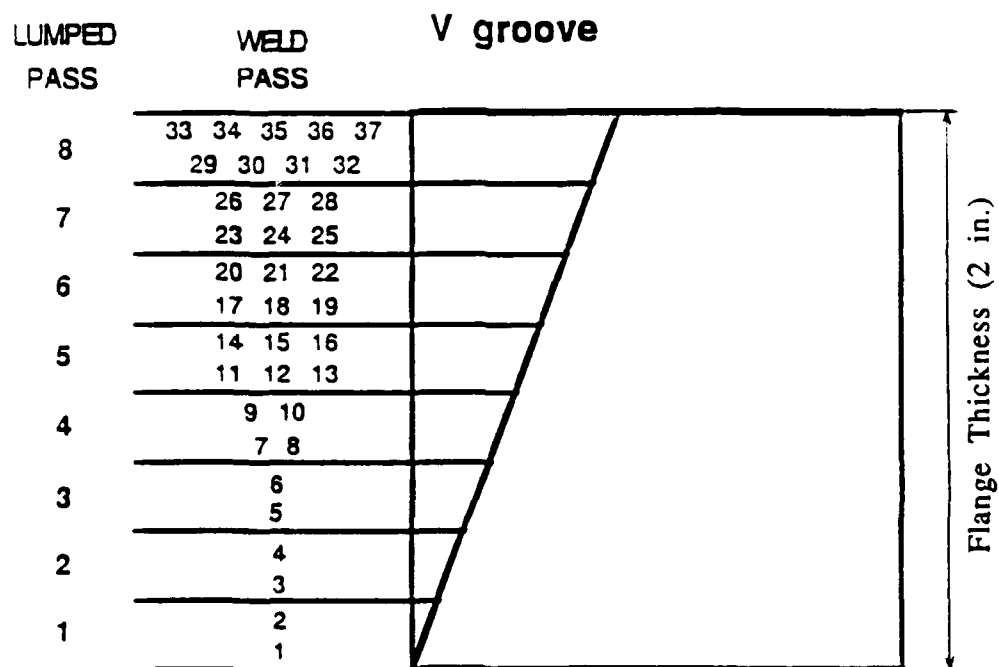


Figure 30. Lumped passes for flange weld in FCAW

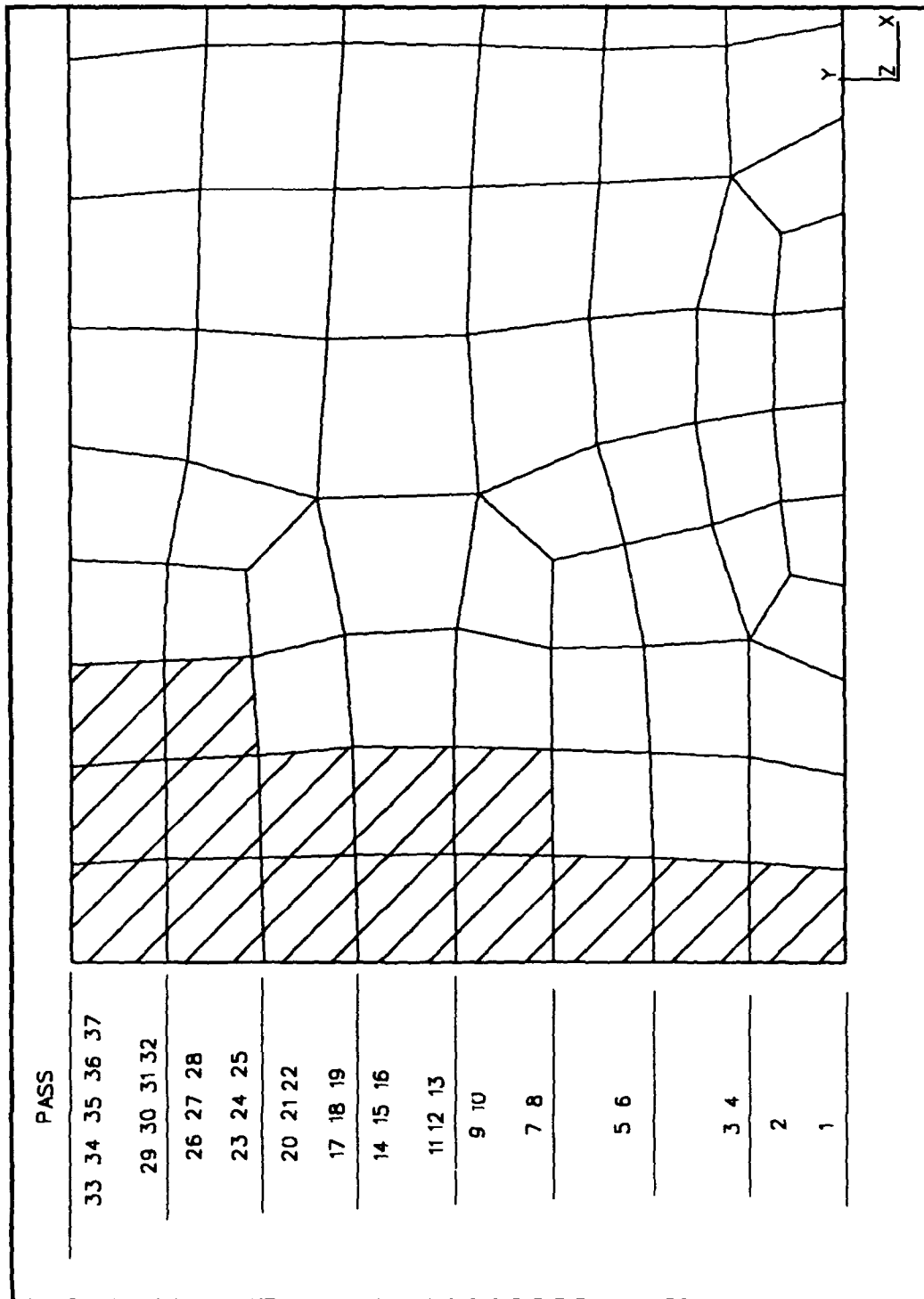


Figure 31. Lumped passes for flange weld (FACW: single-V-groove)

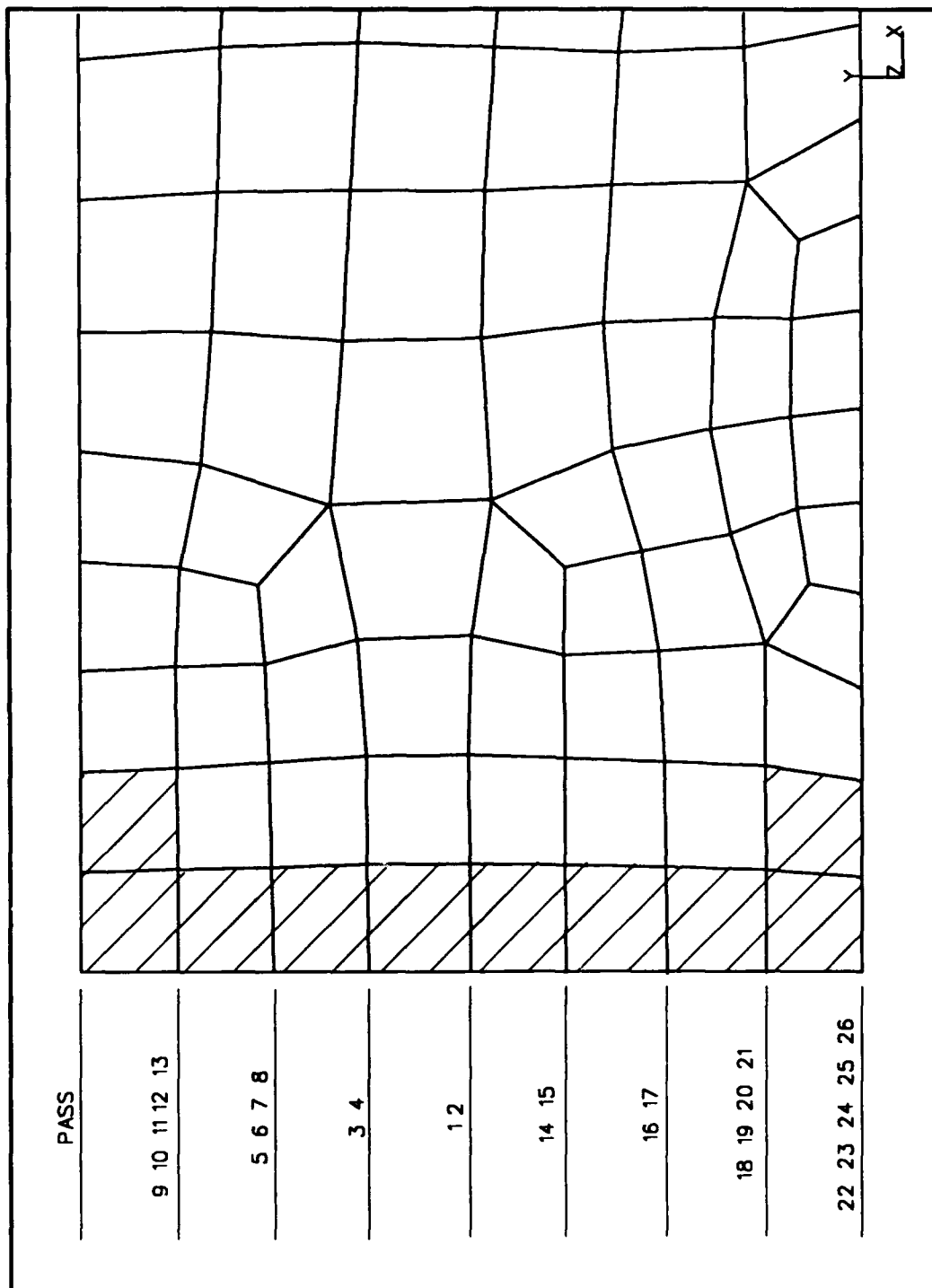


Figure 32. Lumped passes for flange weld (FACW: double-V-groove)

for Hydraulic Structures" (Jaeger, in preparation). For a brief summary, the FCAW lumped model is discussed here.

51. The single-V-groove flange weld geometry was modeled as a series of stair stepped elements as shown shaded in Figure 31. The eight lumped groups of weld passes were sequentially time-stepped through the thermal analysis from the root pass (passes 1 and 2) to the final cap passes (passes 29 through 37). Similarly the double-V-groove flange weld geometry was modeled as 8 lumped passes being deposited as shown in Figure 32. As the time-stepping was being performed, only those elements associated with the passes currently being deposited or those which had been previously deposited were considered active at the weld joint. Each pass of the web weld was modeled as a line heat source. A total of 8 passes were modeled in the thermal analysis. Ten minutes were allowed between each pass.

52. To represent the transient condition of the welding process, the thermal energy was input as a trapezoidal ramp function for each lumped pass. Ramp heat input time for each process is given in Table 9. Details of the ramp heat input are discussed in Jaeger (in preparation). An arc efficiency of 0.85 was assumed for the FCAW process, with 0.95 for the SAW and EGW processes. Preheat and interpass temperatures were modeled at 300 °F for both FCAW and EGW processes, and the ambient temperature was modeled at 70 °F. No preheating was modeled for SAW process.

53. Since welding sequence can have a significant effect on distortion and shrinkage, three different welding sequences were modeled. The first sequence assumed the flanges completely welded prior to welding the web. Since the flanges are welded first in this sequence, an edge constraint is developed at the flanges which restricts shrinkage of the subsequent web weld. Consequently, for this welding sequence, denoted as Case A, the web weld was modeled with boundary conditions fixing the translation of the edges of the flange along its thickness in the global X direction, as shown in Figure 33.

54. The second fabrication sequence modeled applies to a condition where the web is completely welded first followed by flange welding. This assembly sequence develops a translational constraint in the global X-direction along the spliced edge of the web during the final flange welding. This second welding sequence is referred to as Case B in this report and is shown in Figure 34.

55. The third procedure modeled is a staggered flange and web welding sequence. In this model, one face of one flange is welded, followed by

Table 9
Ramp Heat Input

<u>Pass</u>	<u>t1</u>	<u>t2</u>	<u>t3</u>	<u>Max.</u>	<u>Heat Input</u>
<u>(A) FCAW</u>					
Flange					
1	2.0	7.0	2.0	2.1	Btu/in./sec
2-8	1.0	4.1	1.0	3.0	
Web					
1	3.0	12.2	3.0	1.4	Btu/in./sec
2-4	2.0	7.0	2.0	1.9	
5	2.0	9.7	2.0	1.7	
6-8	2.0	7.0	2.0	1.9	
<u>(B) SAW</u>					
Flange					
1-2	0.8	3.2	0.8	4.0	Btu/in./sec
3-7	0.6	2.4	0.6	4.7	
8	0.8	3.2	0.8	4.0	
9-10	0.6	2.4	0.6	4.7	
Web					
1	0.6	2.5	0.6	3.1	Btu/in./sec
2-4	0.7	2.8	0.7	3.5	
5	0.6	2.5	0.6	3.1	
6-8	0.7	2.8	0.7	3.5	
<u>(C) EWG</u>					
Flange					
1	5.0	55.0	5.0	8.2	Btu/in./sec
Web					
1-8	1.0	4.6	1.0	3.3	Btu/in./sec

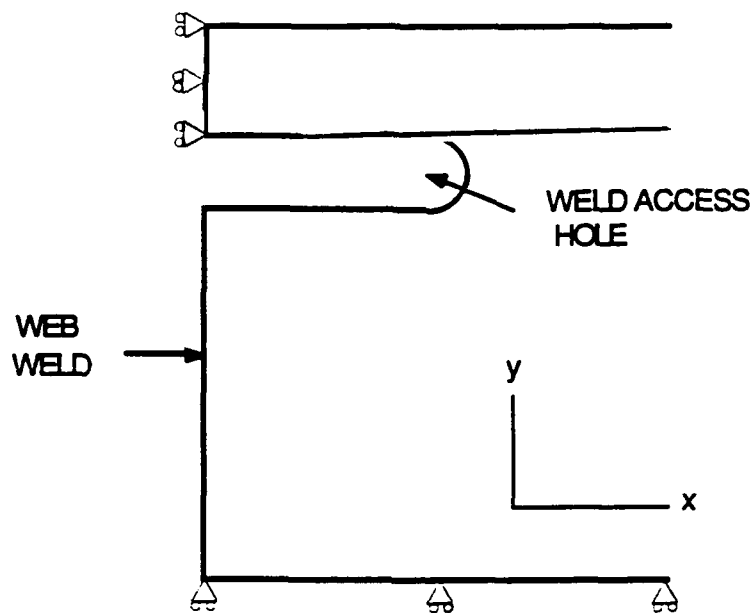


Figure 33. Model of Case A in FCAW (W36x359)

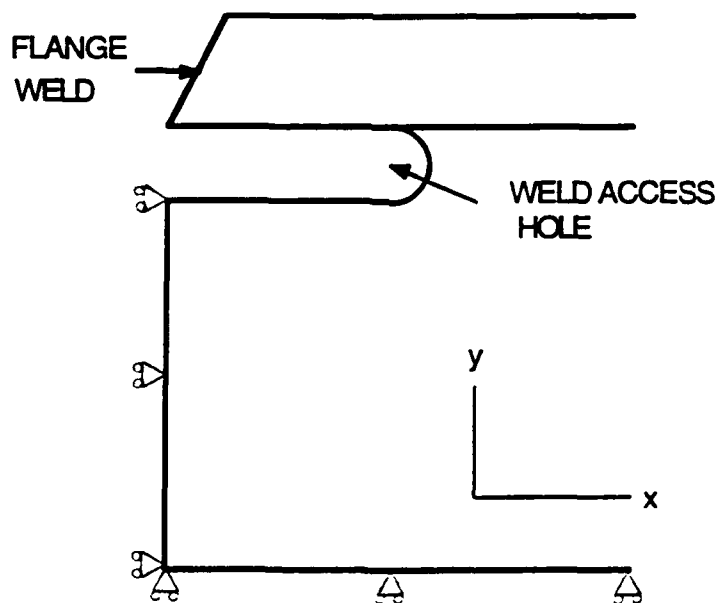


Figure 34. Model of Case B in FCAW (W36x359)

welding one side of the web and then one face of the other flange. This sequence is then repeated to complete the full penetration butt joint. This sequence is referred to as Case D and is shown in Figure 35.

56. In addition to the welding sequence selected, weld joint geometry may also have an effect on the final state of residual stress in the welded connection. For this reason, the effects of edge bevel and access hole diameter were also investigated.

57. Case B models a single-V-groove full-penetration flange weld with the root opening located at the inside face of the flange, as shown in Figure 34. Case C is the same single-V-groove weld; however, the root opening is located at the outside face of the flange, as shown in Figure 36.

58. Finally, to investigate what effect access hole diameter has on the magnitude and distribution of residual stress, Cases A through D were analyzed for both a 1-1/8-in.-diam and a 1-1/2-in.-diam access hole geometry for FCAW. Weld sequences of Cases A and B were analyzed for EGW and SAW.

Thermal Analysis

FCAW

59. Case A weld sequence models the constraint that the flange has on web weld shrinkage. The web weld was modeled as a line heat source in the thermal analysis. Instead of using a moving heat source to simulate the moving electrode, the line source assumed that the heat input from the electrode was distributed along the edge of the web (the whole weld bead) uniformly and simultaneously. But the heat input rate changed with time according to the specified ramp heat input function. Thus, the heat input from the electrode is simplified to reduce the finite element analysis time.

60. Isotherm plots from the thermal analysis for Case A with 1-1/8-in.-diam weld access hole are shown in Figure 37. The time elapse after welding for Figure 37 is 45, 187, 337, and 487 sec, respectively. The steep thermal gradient generated locally around the weld access hole can be seen in these plots.

61. The sequence modeled in Case B represents the conditions where the web is welded first, thus constraining flange weld shrinkage. Representative plots of the flange isotherms from this sequence are shown in Figure 38. The temperature profile for the final lumped pass (actual passes 29 through 37) is plotted in Figure 38. The passed times after welding for Figure 38 are 10,

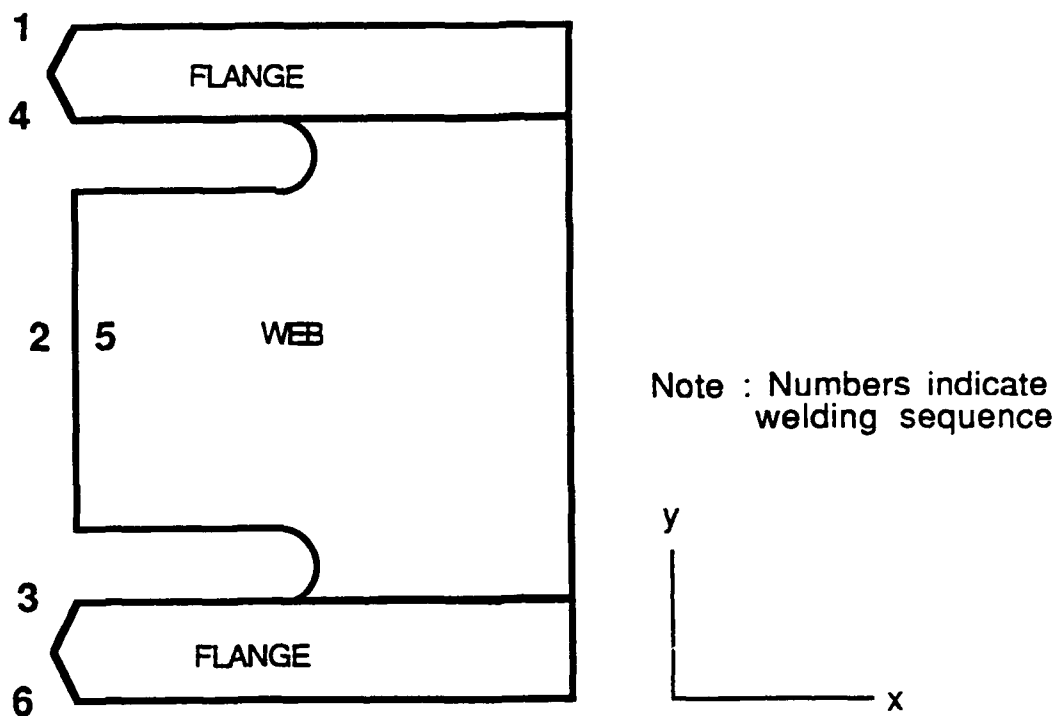


Figure 35. Model of Case D in FCAW (W36x359)

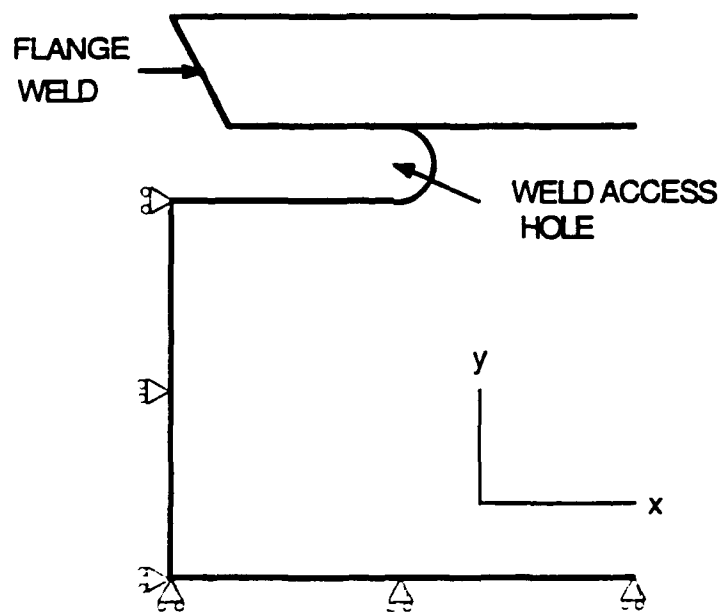


Figure 36. Model of Case C in FCAW (W36x359)

FCAW

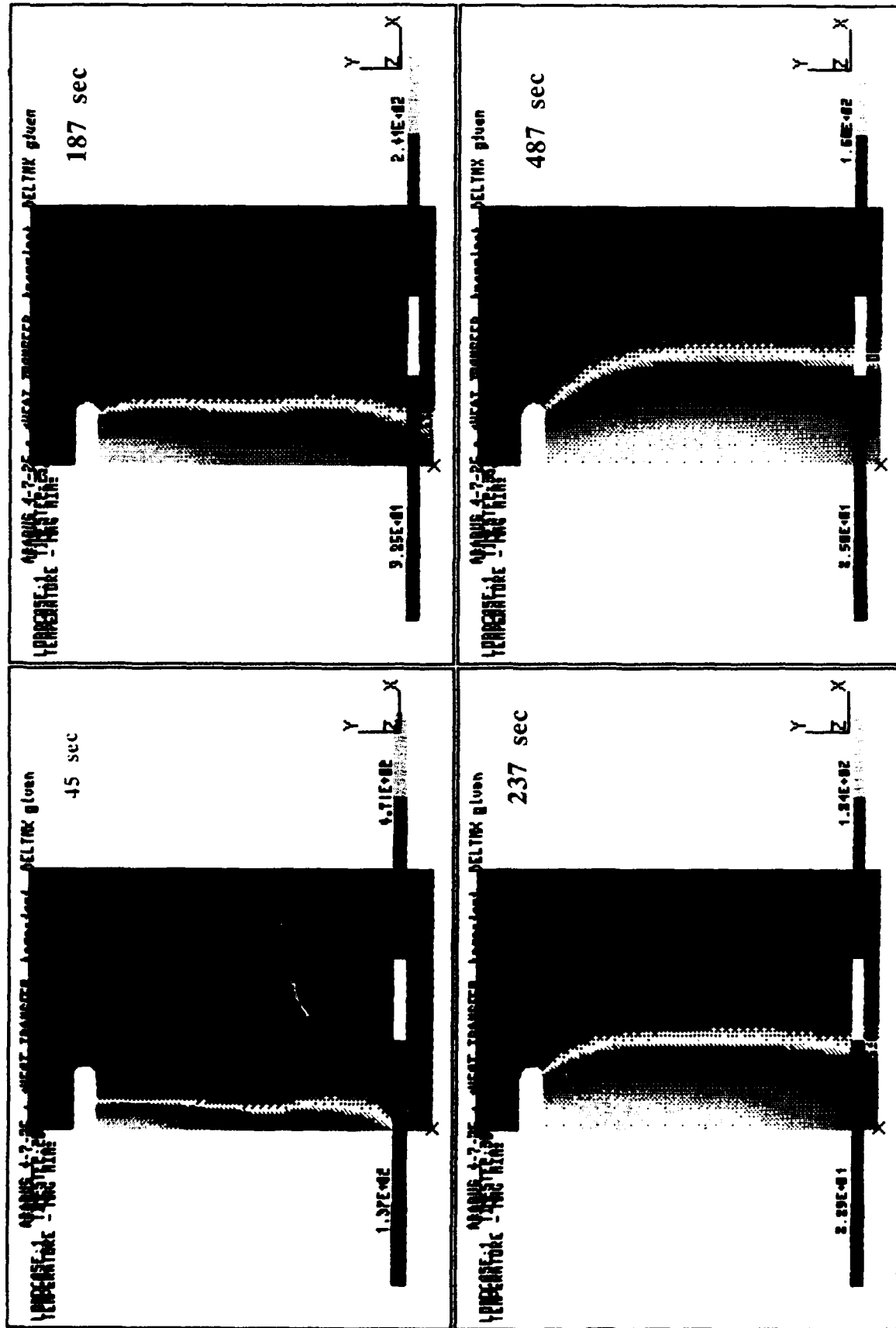


Figure 37. Isotherm plots for Case A in FCAW process (1-1/8-in.-diam access hole)

FCAW

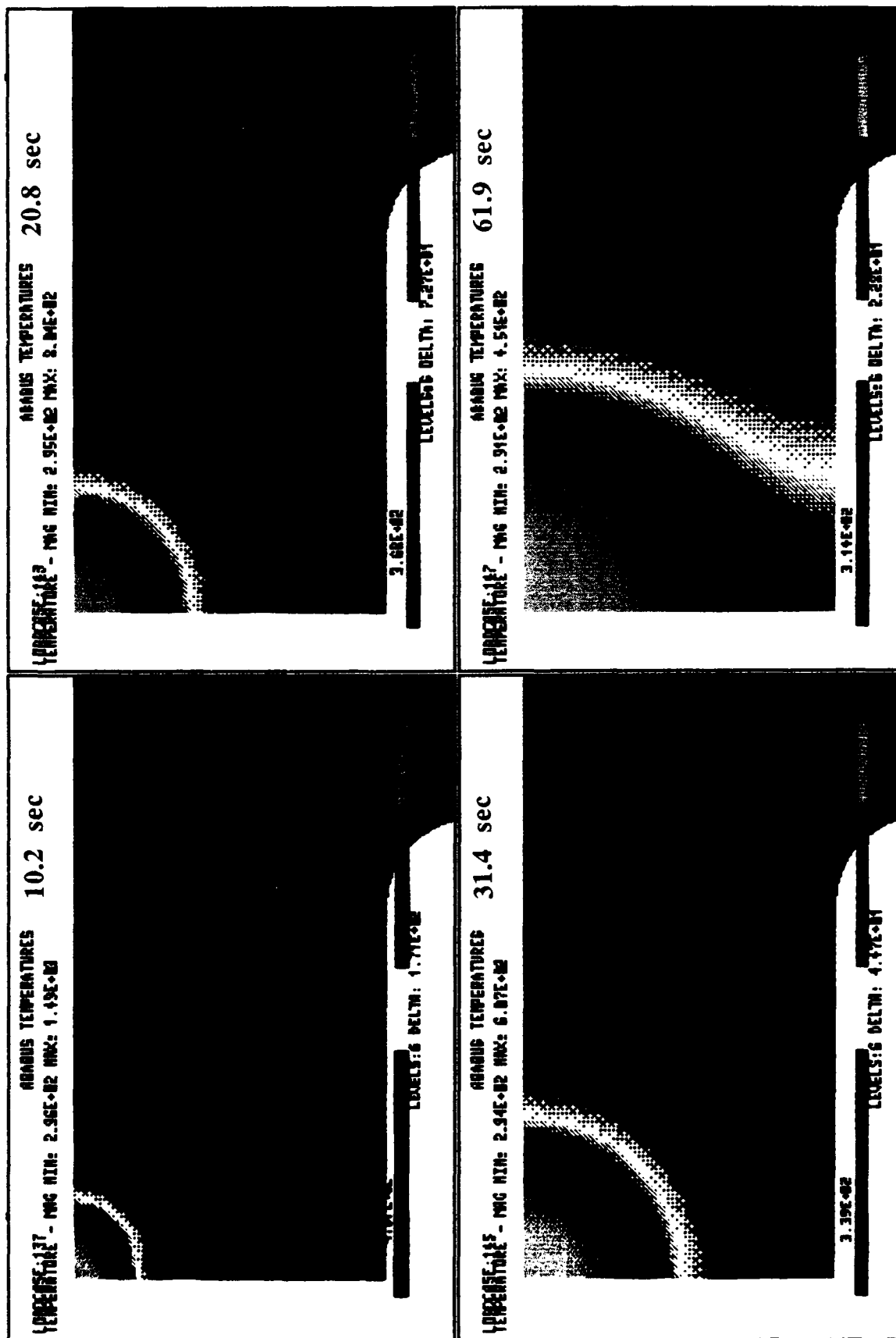


Figure 38. Isotherm plots for Case B in FCAW process (1-1/8-in.-diam access hole)

21, 31, and 62 sec. Similar plots were obtained for Cases C and D and provide information about width of heat-affected zone or cooling rate.

SAW

62. The weld sequence modeled in Case A is as follows: the flange is welded first and then, the web. The web is welded first in Case B. Isotherm plots for a flange with 2-in.-diam elongated weld access hole from the thermal analysis of final lumped pass for SAW process are shown in Figure 39. The elapsed times after welding are 36, 123, 213, and 300 sec.

EGW

63. Weld sequences for Cases A and B are the same as SAW. Isotherm plots for a flange with 2-in.-radius weld access hole from the thermal analysis for EGW process are shown in Figure 40. Copper shoes were modeled on both sides of the flange as shown in the figure. The elapsed times after welding are 67, 86, 120, and 193 sec.

Stress Analysis

FCAW

64. The temperature history obtained from the thermal analysis for the various weld sequences and joint geometries was used as thermal loading input in the stress analysis. Stress plots along the weld access hole are presented for the first lumped weld pass and the final lumped cap passes. Plots are provided for both the 1-1/8-in. and 1-1/2-in.-diam weld access holes. Tensile stress is plotted as a positive stress value.

65. The thermal stress plot (S_x) for Case A around the weld access hole for the initial web root pass with a 1-1/8-in. weld access hole diameter is shown in Figure 41 as a dashed curve. The maximum tensile stress approaches yield (50 ksi) near the lower tangent point of the access hole (point C). The final residual stress plot for Case A after the eighth web weld pass is shown in Figure 41 as a solid curve. The stress magnitude and distribution after the initial pass and final pass remain virtually unchanged around the weld access hole, suggesting future modeling may require consideration only for the first lumped pass for this case.

66. The model results agree well with cracking problems experienced in the field during construction. The tendency in the field for this welding sequence has been for cracks to initiate from the weld access hole and propagate through the web base metal material.

SAW

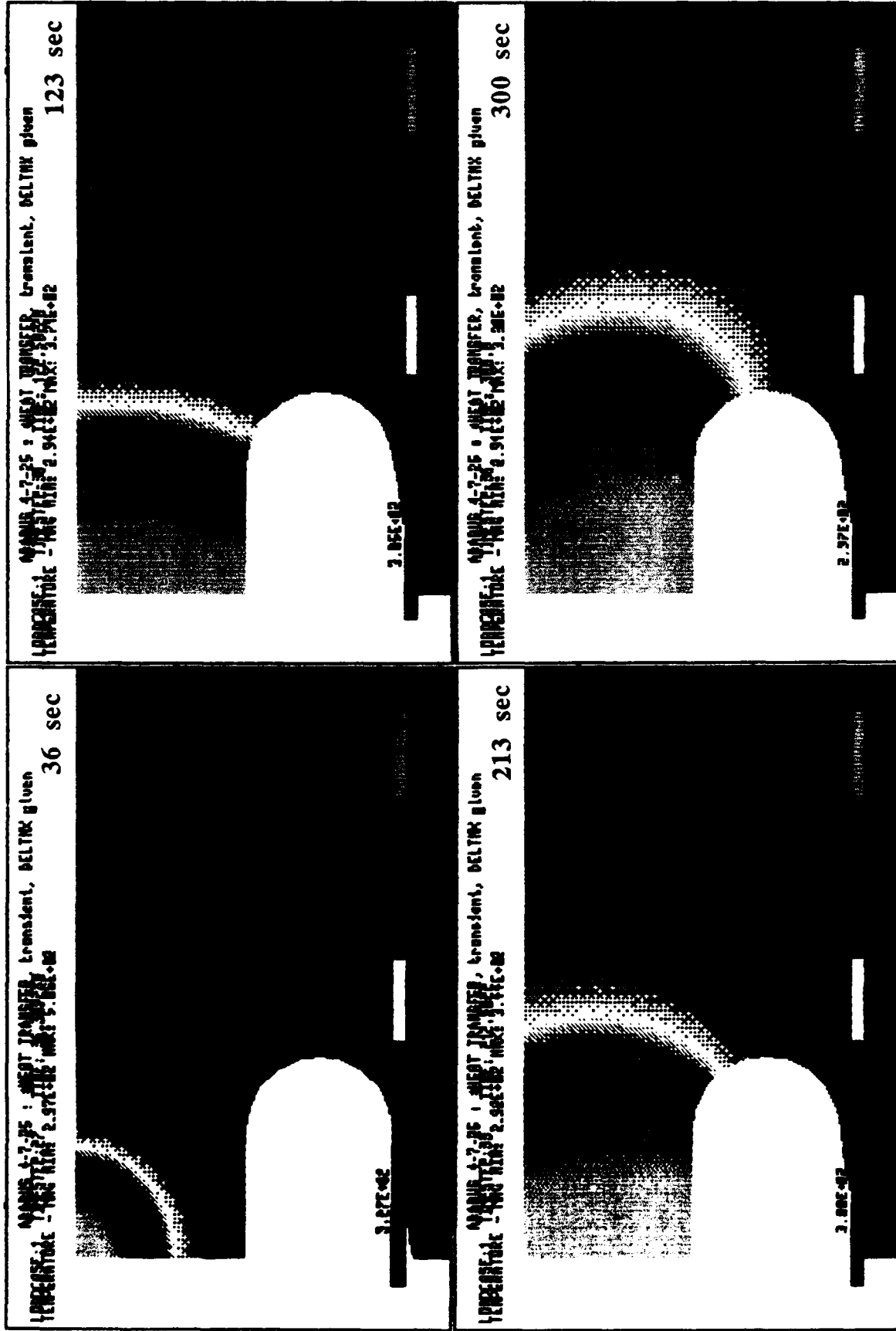
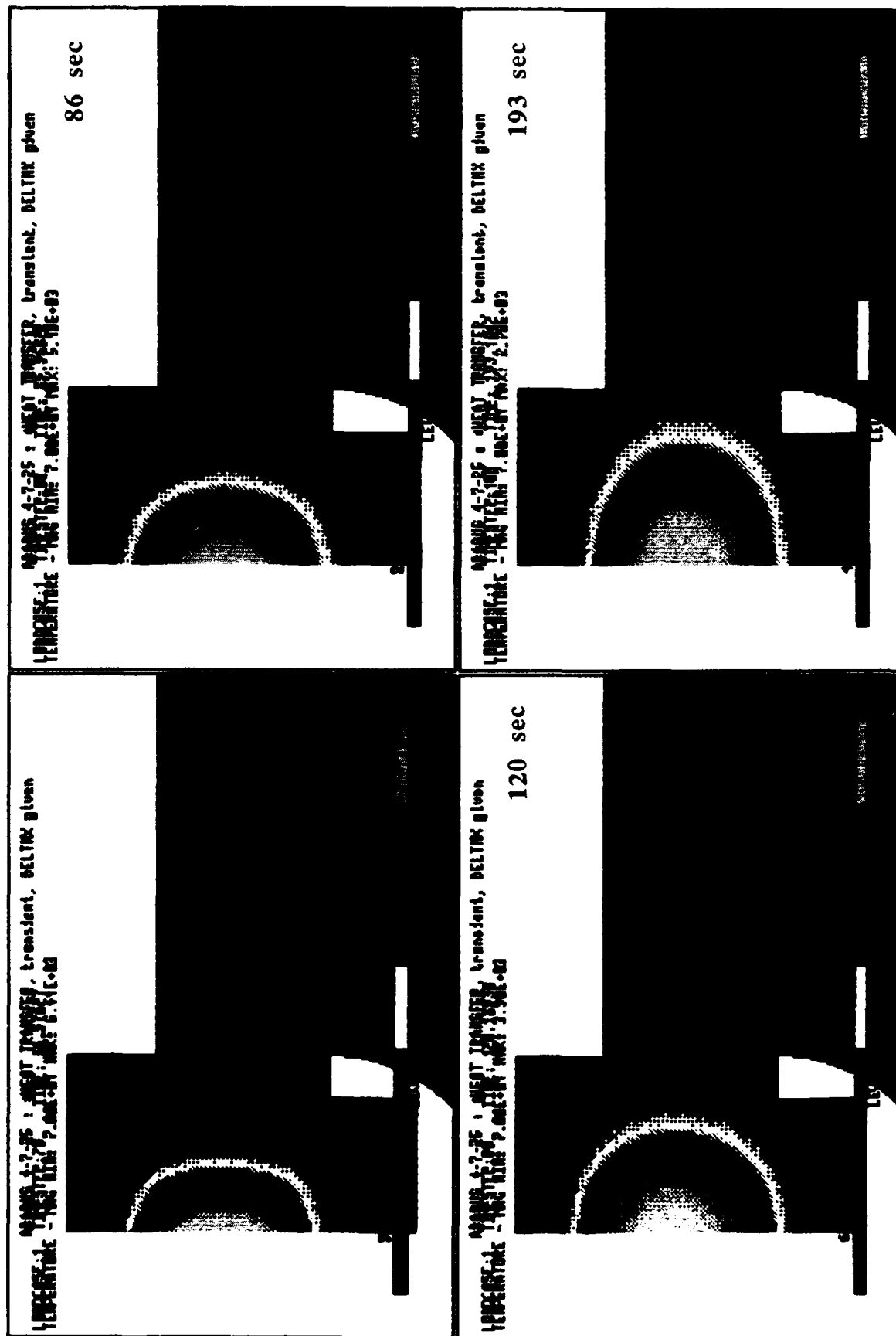


Figure 39. Isotherm plots in SAW process (2-in.-diam access hole)

EGW



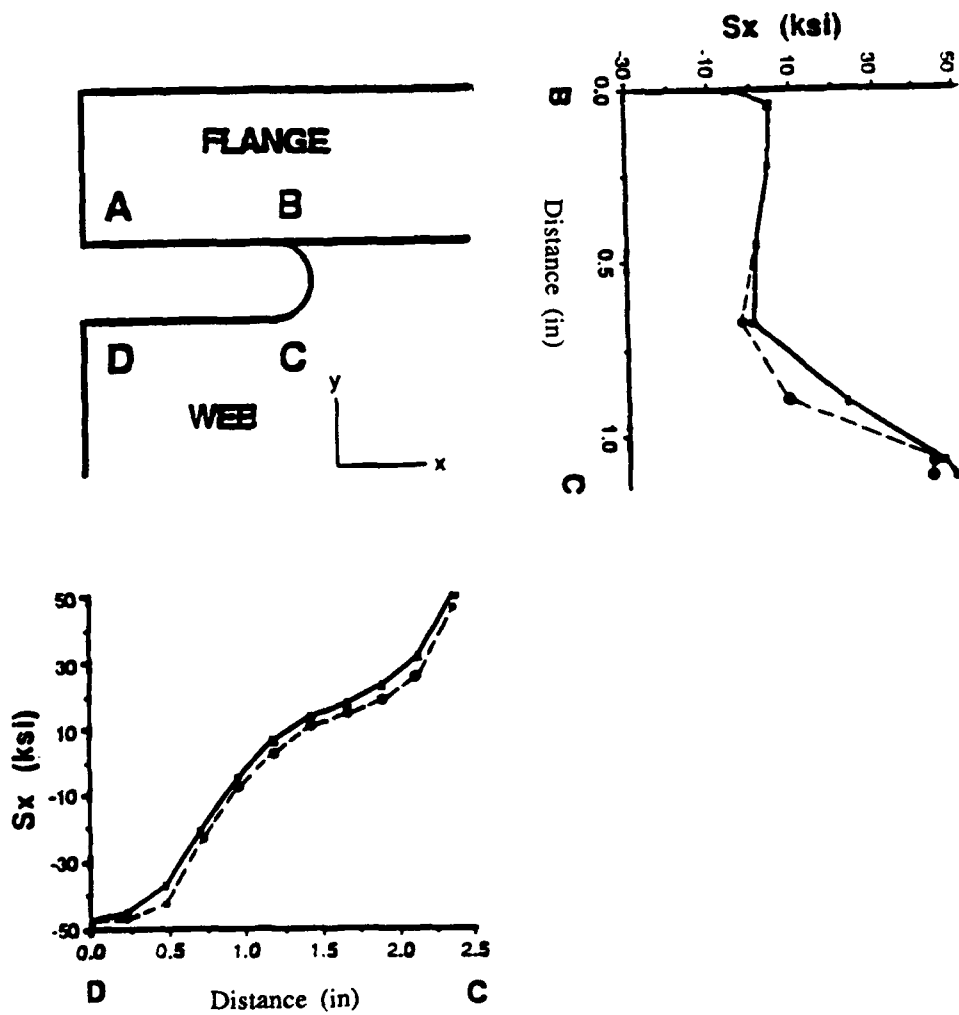


Figure 41. Stress distribution for Case A with FCAW (1-1/8-in.-diam access hole). Dashed line: after first pass; solid line: final residual stress

67. Thermal stress plots (S_x) after the initial lumped weld pass (actual weld passes 1 and 2) for Case B around the weld access hole are plotted as a dashed curve in Figure 42. Maximum tensile stress (50 ksi) occurs at the top of the weld access hole near the weld joint (point A) and at the upper tangent point of the 1-1/8-in.-diam hole (point B).

68. The final residual stress distribution (S_x) is plotted as a solid curve in Figure 42. The high tensile stress near the weld joint (point A) has been reduced approximately 75 percent from its initial value to 13 ksi. The final maximum residual tensile stress for this weld sequence and joint geometry is 33 ksi, located at the upper transition tangent of the weld access hole (point B), as shown in Figure 42. This is the area where cracking has been prone to occur in the field. For this welding sequence, field experience has shown that cracking tends to initiate near point B and propagate through the flange base material. The additional passes deposited to complete the joint tend to produce a more uniform temperature distribution with time near point A and consequently lower the final residual stress.

69. The initial pass thermal stress analysis results for Case C are plotted as a dashed line in Figure 43. The maximum tensile thermal stress for the first lumped pass is approximately 18 ksi near point B. The final residual stress distribution is plotted as a solid line in Figure 43. The maximum tensile residual stress of 50 ksi also occurs near point B.

70. The thermal stress distributions for Case D, alternating flange and web welding sequence, are shown plotted in Figures 44 through 46. Figure 44 shows the thermal stress distribution along the weld access hole after the outer half of the flange double-V-groove has been welded. The maximum tensile thermal stress of 26 ksi occurs at point B.

71. The thermal stress distribution developed after welding the outside half of the double-V-groove flange weld and one side of the double-V-groove web weld is plotted in Figure 45. There was no significant change in the magnitude or location of maximum tensile residual stress; however, there was a general increase in tensile stress (S_x) along the inside edge of the weld access hole.

72. Figure 46 contains a stress plot along the weld access hole after the welding of both sides of flange double-V-groove along with one half of the web double-V-groove. The maximum tensile thermal stress has doubled to approximately 50 ksi at point B.

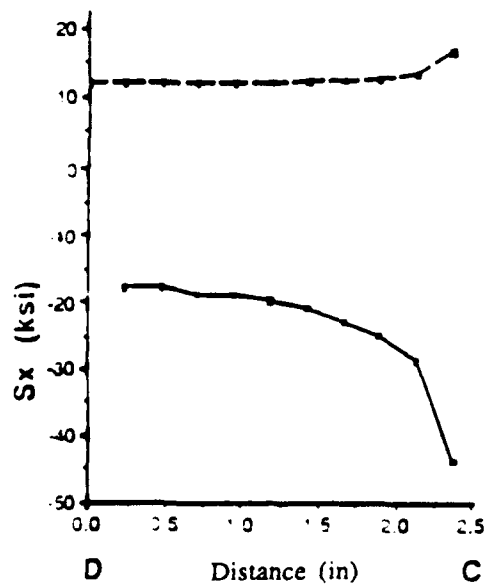
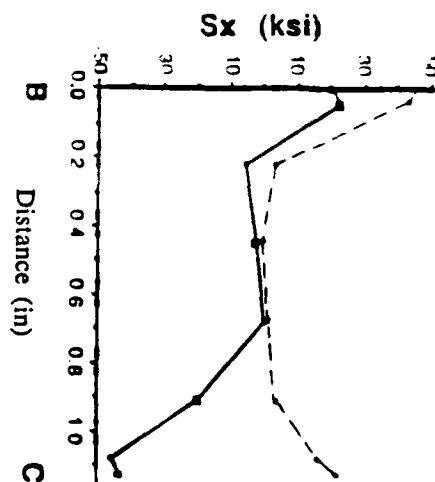
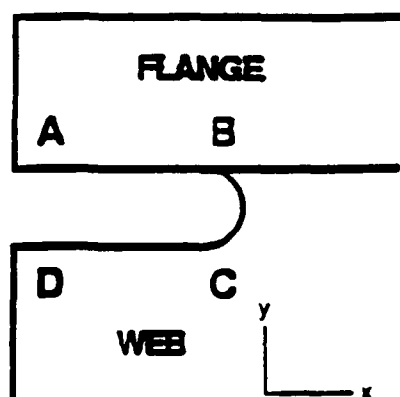
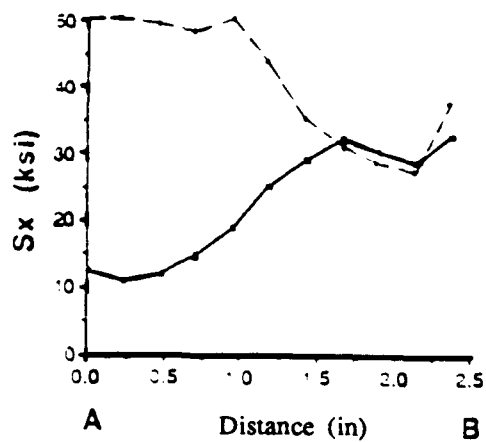


Figure 42. Stress distribution for Case B with FCAW (1-1/8-in.-diam access hole). Dashed line: after first pass; solid line: final residual stress

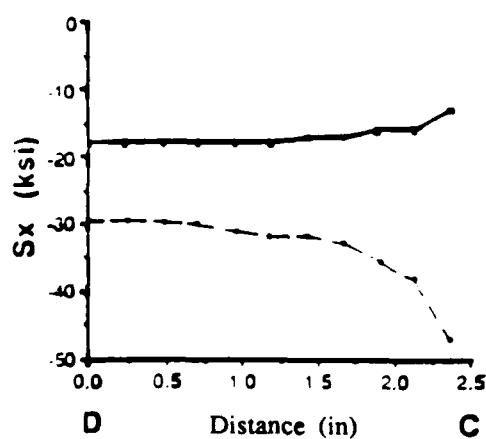
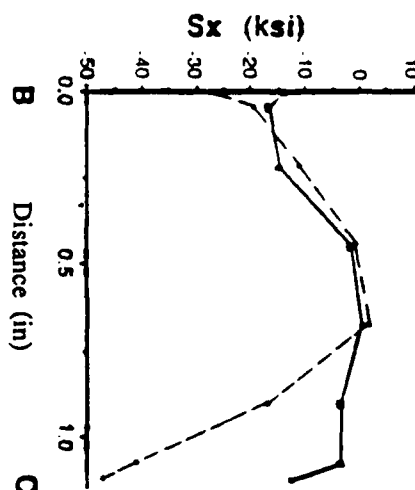
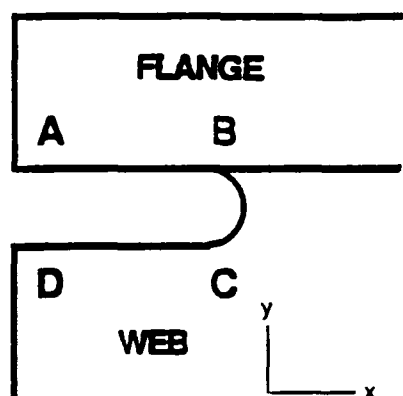
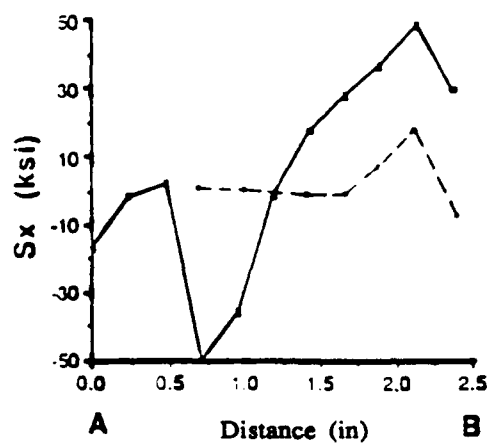


Figure 43. Stress distribution for Case C with FCAW (1-1/8-in.-diam access hole). Dashed line: after first pass; solid line: final residual stress

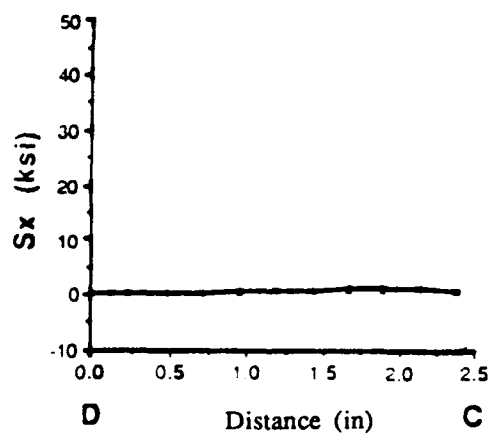
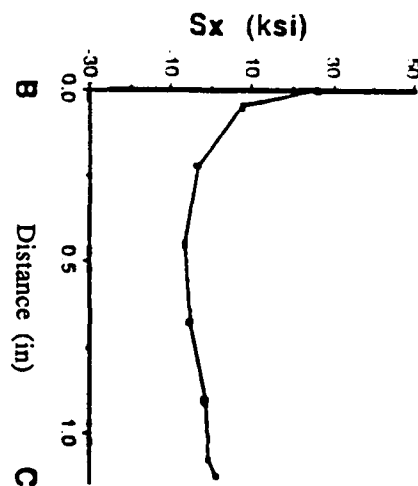
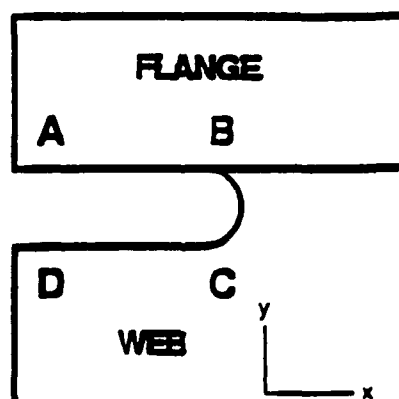
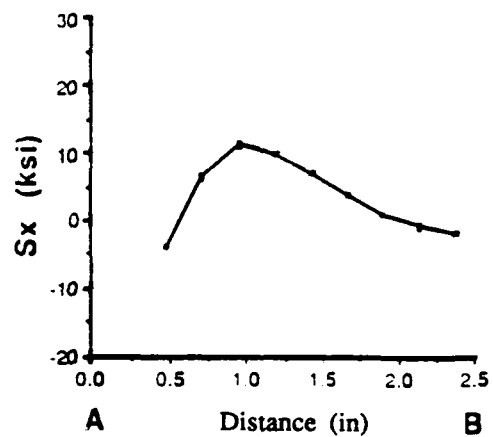


Figure 44. Stress distribution after welding the outside half of the flange for Case D with FCAW (1-1/8-in.-diam access hole)

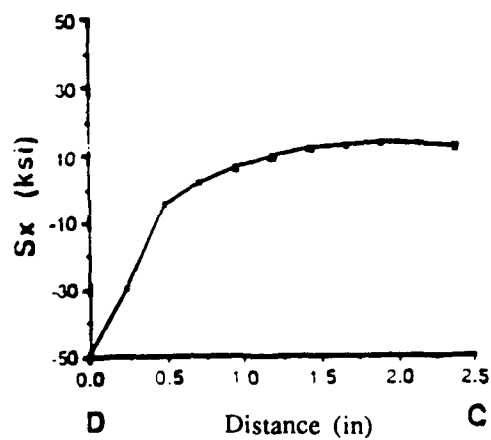
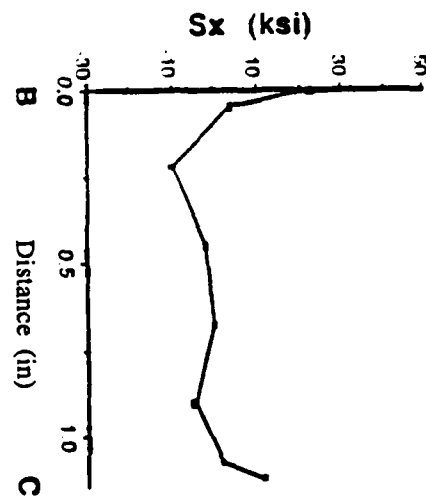
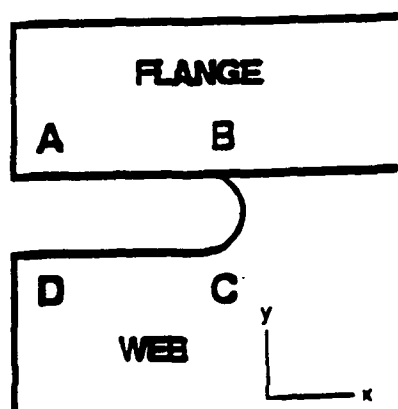
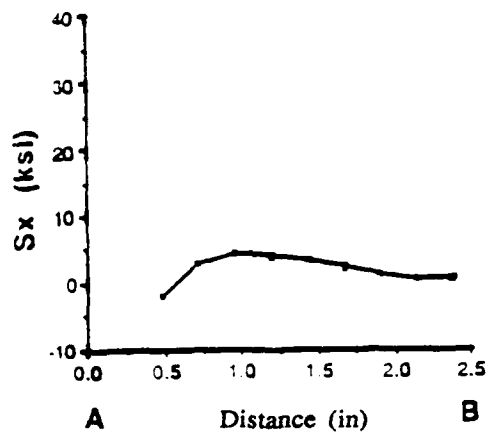


Figure 45. Stress distribution after welding the outside half of the flange and one side of the web for Case D with FCAW (1-1/8-in.-diam access hole)

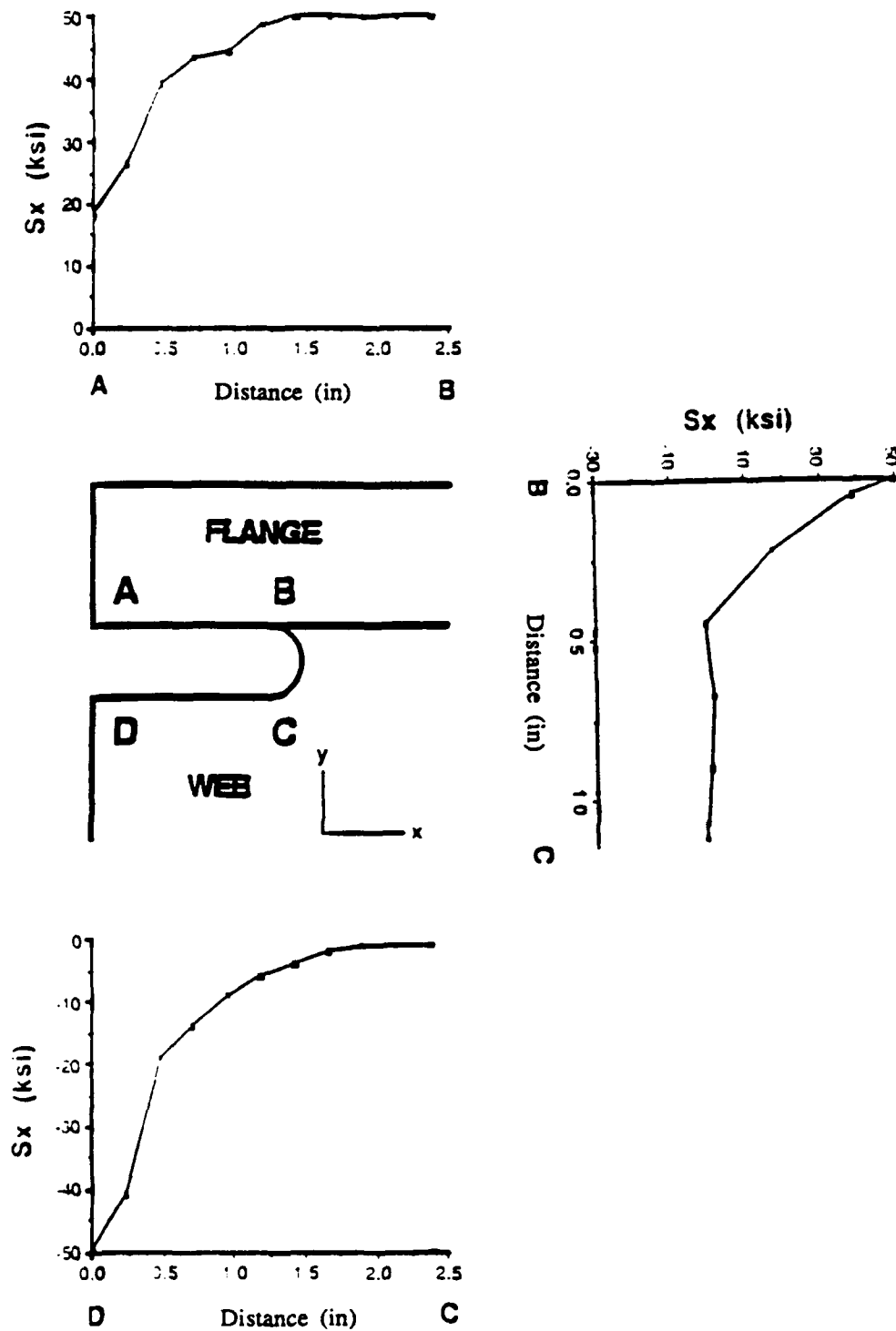


Figure 46. Stress distribution after welding both sides of the flange and one side of the web for Case D with FCAW (1-1/8-in.-diam access hole)

73. The final residual stress distribution along the weld access hole is plotted in Figure 47. The maximum tensile stress (40 ksi) occurs along the outer edge of the weld access hole along edges A to B.

74. To investigate the effect of weld access hole diameter on residual stress, the finite element model was revised from a 1-1/8- to 1-1/2-in.-diam hole. No other modifications were made to the thermal or stress analysis. Thermal and residual stress plots were developed along the 1-1/2-in.-diam weld access hole similar to the 1-1/8-in.-diam model. The thermal and residual stress plots for the 1-1/2-in.-diam weld access holes for Cases A and B are shown on Figures 48 and 49. The resulting thermal stress plots after the first lumped pass are shown as a dotted lines, and the final residual stress plots are shown as solid lines.

SAW and EGW

75. The SAW and EGW processes were simulated for Cases A and B. Figures 50 through 55 show the residual stress distributions along the access hole periphery of each simulated joint. Thermal stress distributions were not plotted for these two welding processes and, therefore, are not shown here.

76. Two types of access hole geometry were simulated for the EGW process, as shown in Figure 23. This was to study the effect of interface angle between the flange and web plates. The elongated hole geometry with a tangent interface resulted in lower residual stress than the normal interface access holes in both Cases A and B. Comparison of Central Processing Unit (CPU) times for the three processes studied are shown in Table 10.

Comparison with Experimental Data

77. The thermal strains in x-direction (E_x) calculated by a finite element analysis for the flange welding with EGW prior to web welding are shown in Figure 56. Experimental results for the same location using high temperature strain gage are also plotted for comparison. The thermal strains in the y-direction (E_y) for the same position are shown in Figure 57. The web is not welded in Figures 56 and 57. Figures 58 and 59 show thermal strains in the X and Y directions for the same process, but with web welded with SAW before the flange.

78. The initial correlation between FEM and experimental thermal strain data ($t < 350$ sec) shows a tendency for the FEM results to overpredict the experimental data. This may result from the two-dimensional modeling of the

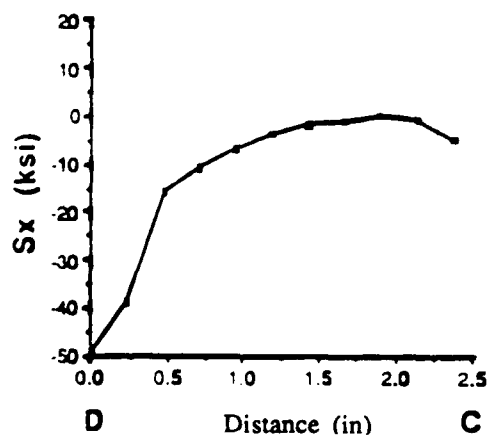
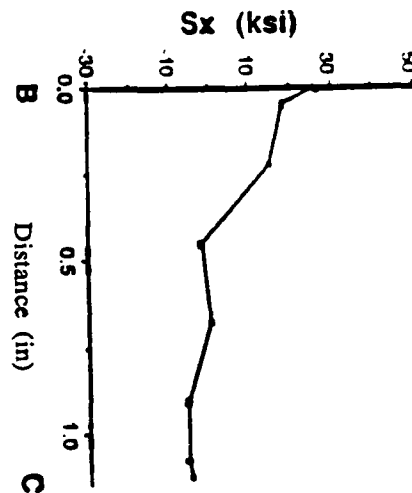
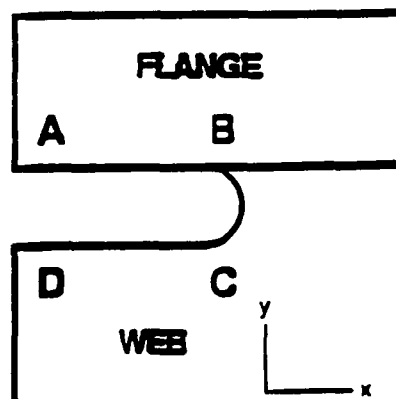
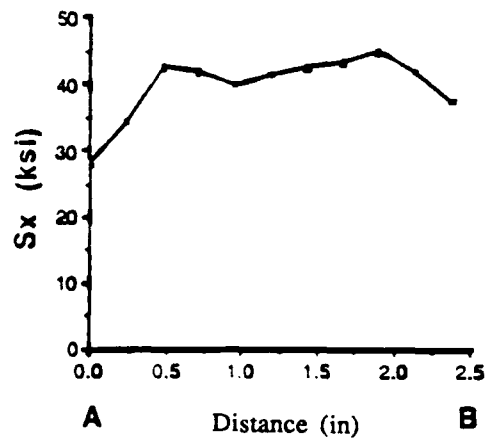


Figure 47. Final residual stress distribution for Case D with FCAW (1-1/8-in.-diam access hole)

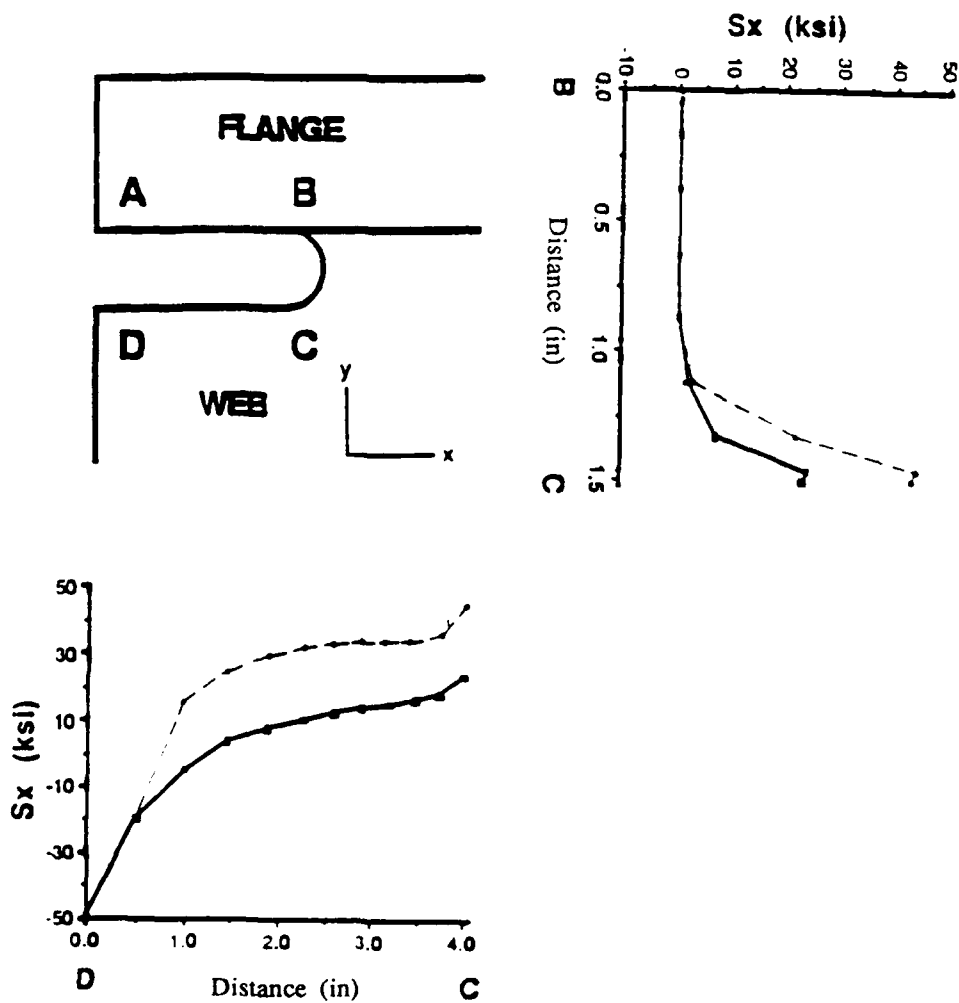


Figure 48. Stress distribution for Case A with FCAW (1-1/2-in.-diam access hole). Dashed line: after first pass; solid line: final residual stress

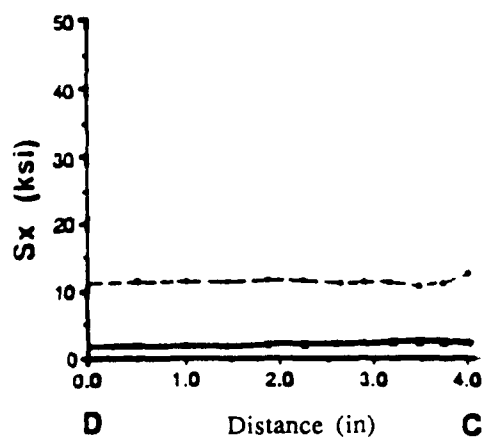
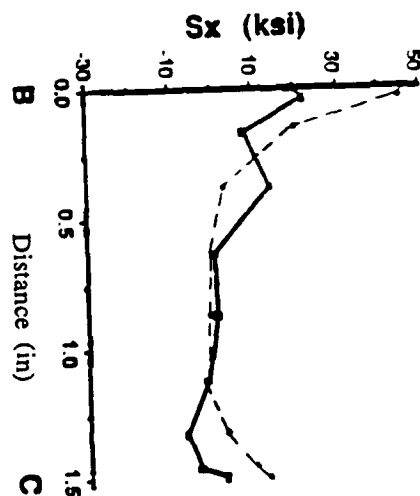
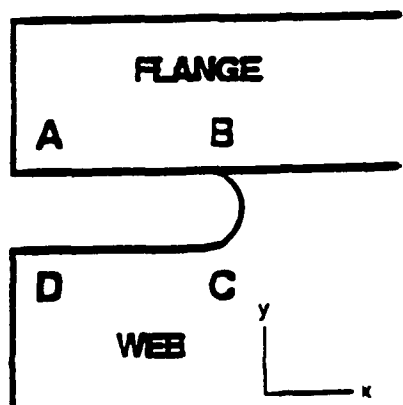
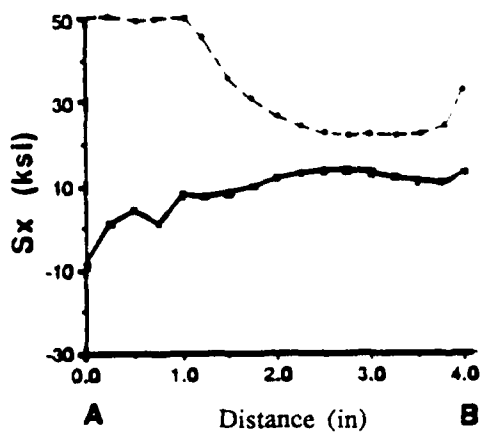


Figure 49. Stress distribution for Case B with FCAW (1-1/2-in.-diam access hole). Dashed line: after first pass; solid line: final residual stress

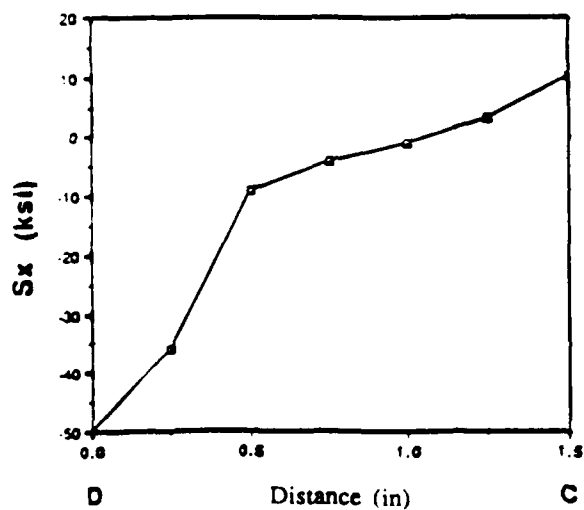
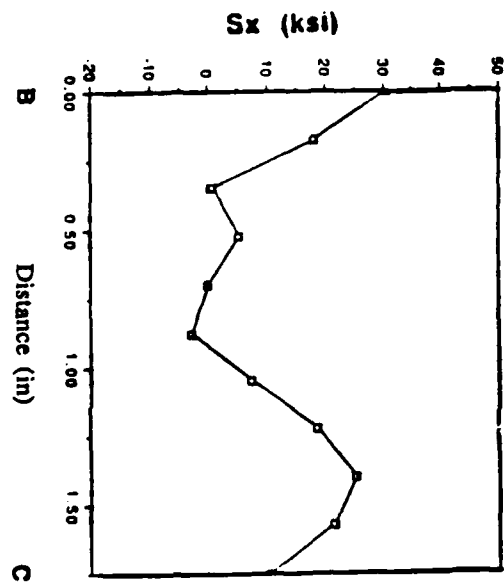
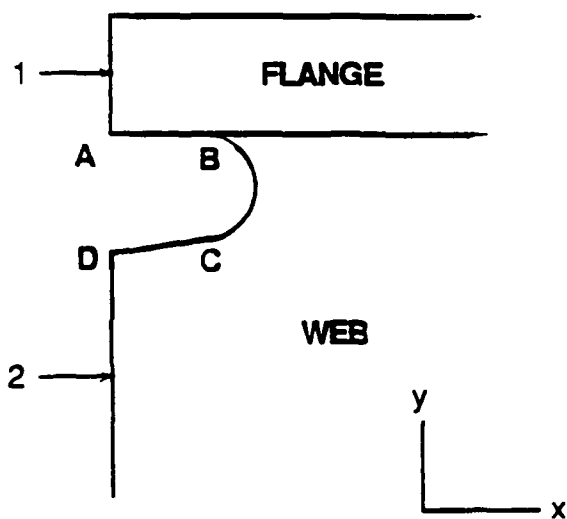
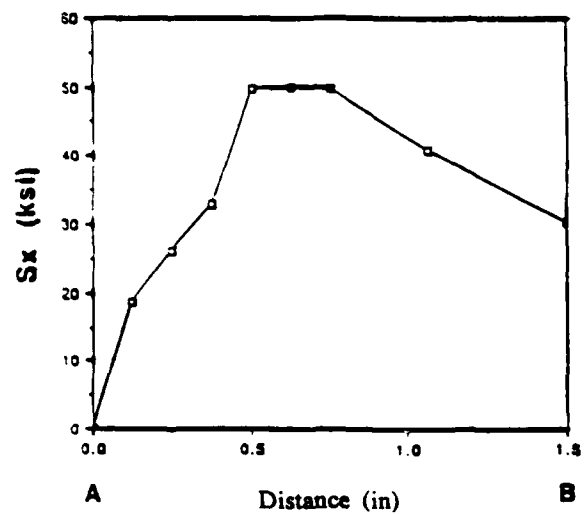


Figure 50. Final residual stress distribution for Case A with SAW (W36x359, elongated access hole)

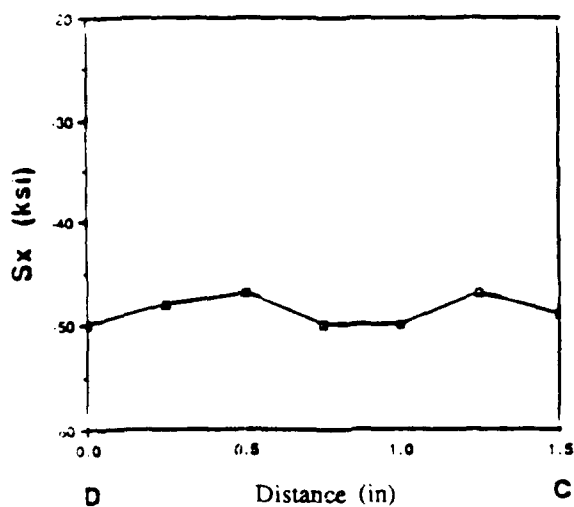
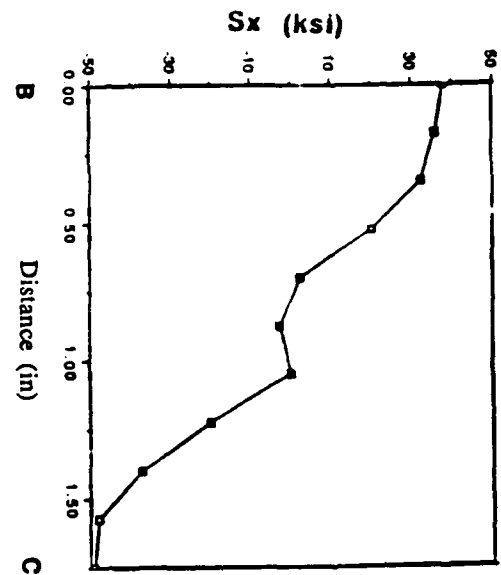
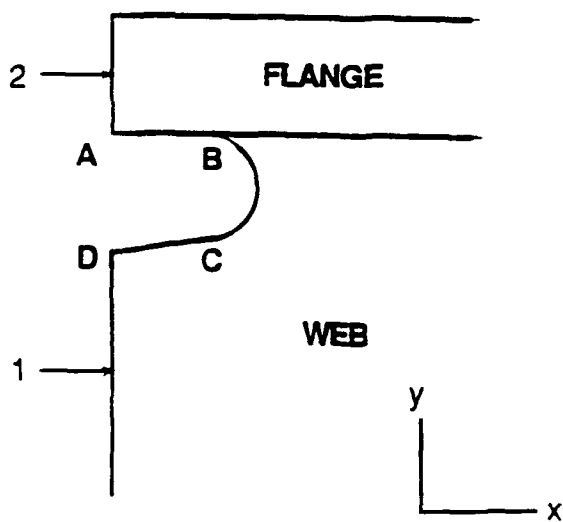
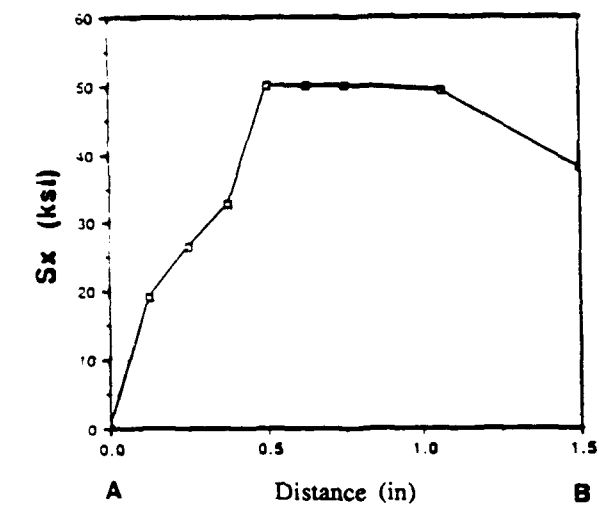


Figure 51. Final residual stress distribution for Case B with SAW (W36x359, elongated access hole)

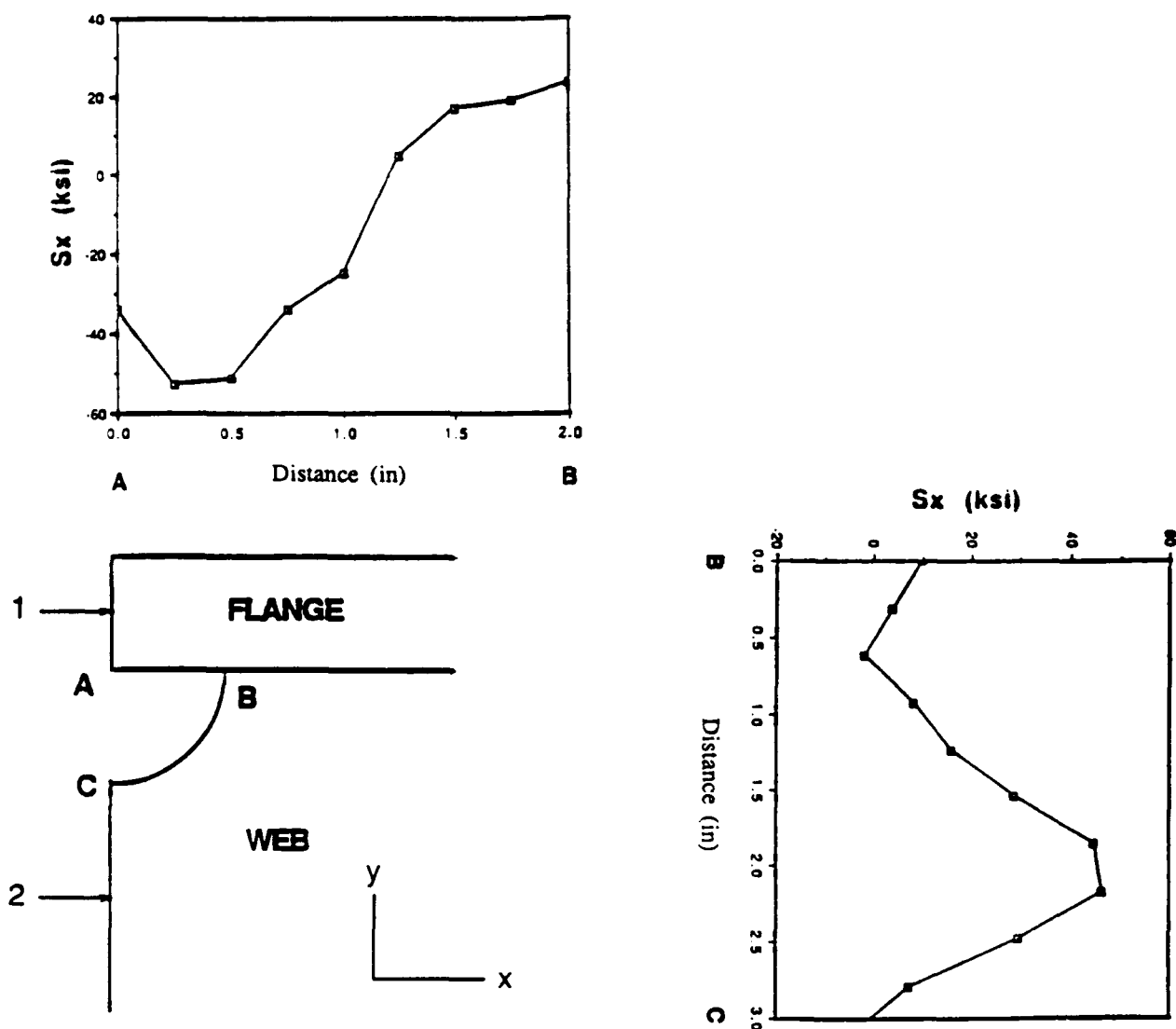


Figure 52. Final residual stress distribution for Case A with EGW (W36x359, semicircle access hole)

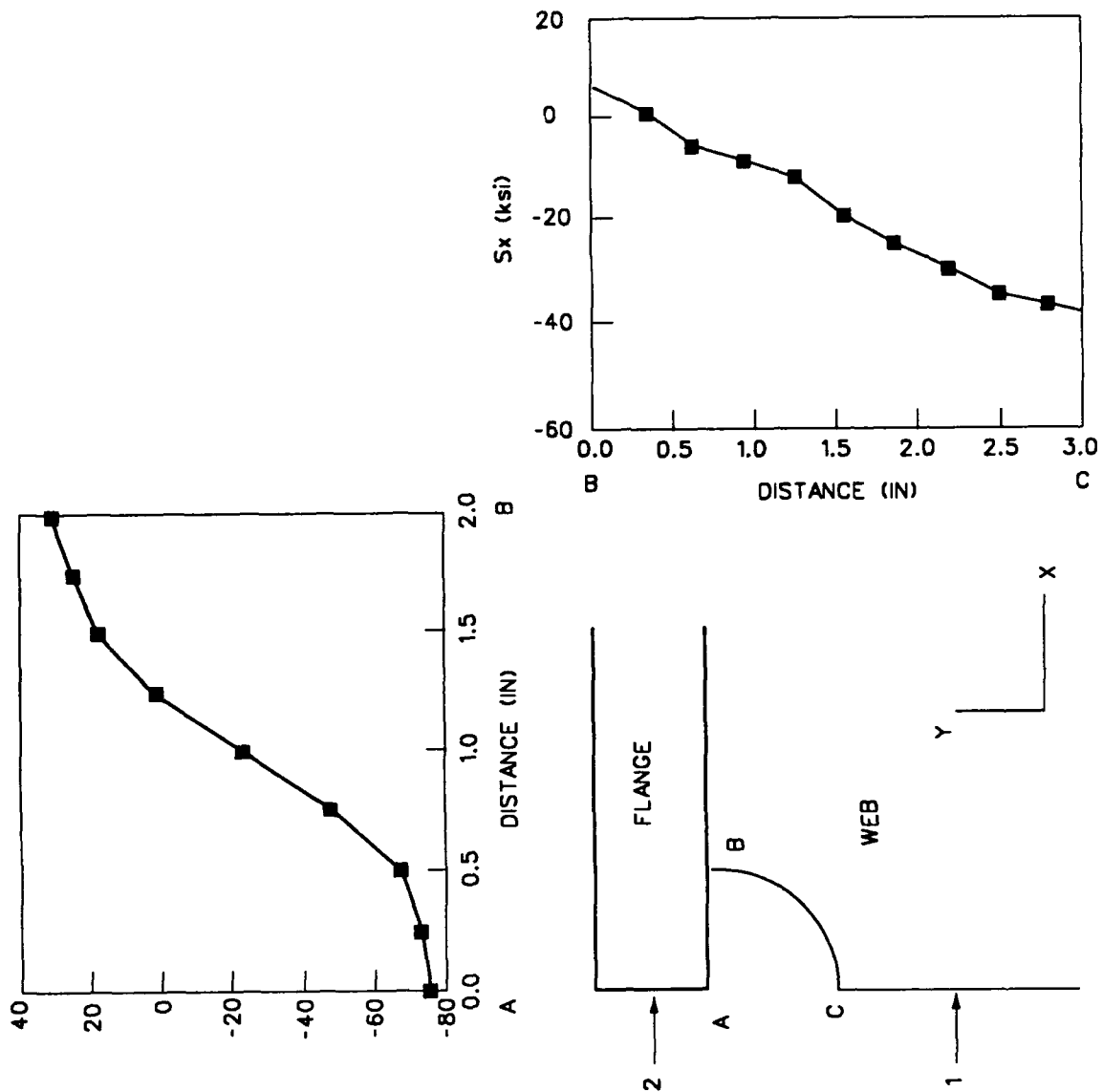


Figure 53. Final residual stress distribution for Case B with EGW (W36x359, semicircle access hole)

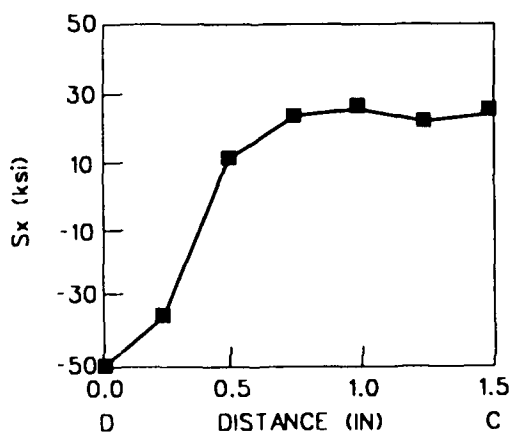
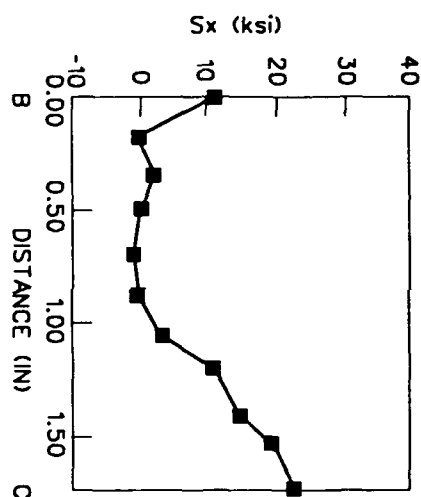
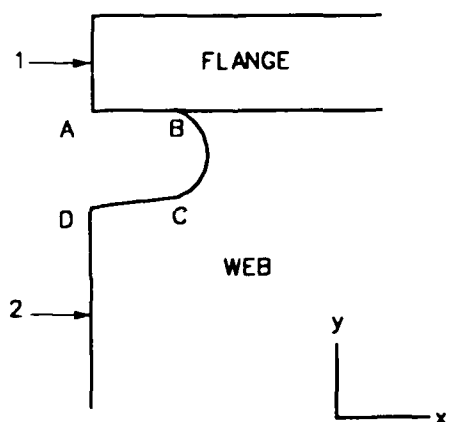
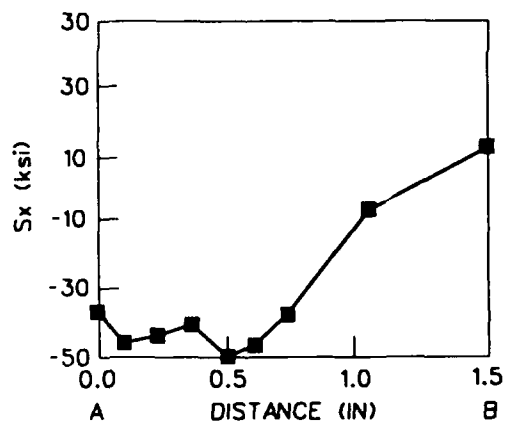


Figure 54. Final residual stress distribution for Case A with EGW (W36x359, elongated access hole)

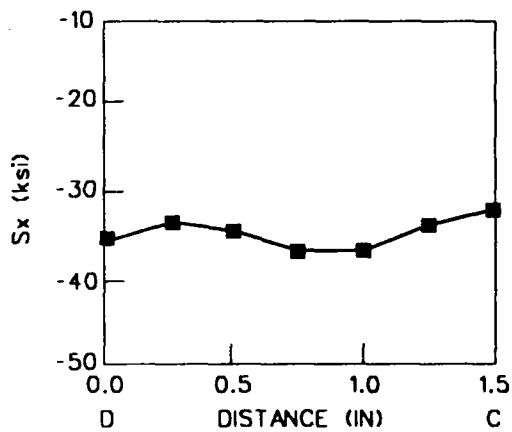
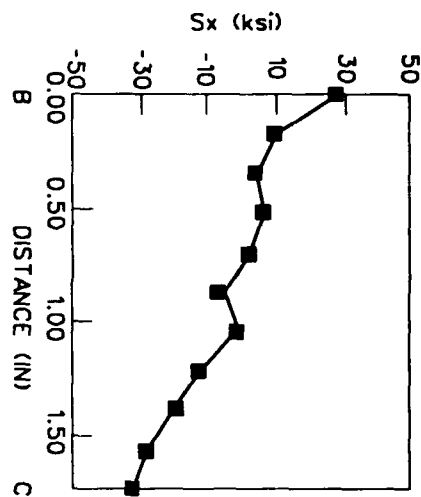
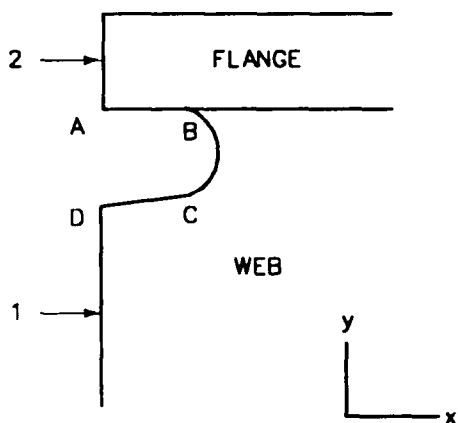
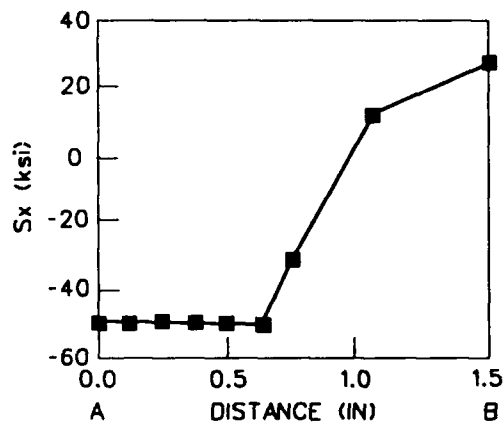


Figure 55. Final residual stress distribution for Case B with EGW (W36x359, elongated access hole)

Table 10
Comparison of CPU Time*

<u>Thermal Analysis, sec</u>	<u>Stress Analysis, sec</u>
EGW 450	400
SAW 1,350	1,550
FCAW 900 (lumped)	1,000 (lumped)
FCAW 2,000 (not lumped)	2,500 (not lumped)

* CPU Time: Super Computer (Cray).

moving electrode. The ramp heat input may not be sufficient for modeling of EGW. The FEM and experimental thermal strains tend to converge with time ($t > 350$ sec). The thermal strains in the y-direction (E_y) converged sooner than in the x-direction (E_x). In the actual welding, the welded part of the flange before the electrode reaches at the web location restricts the tensile thermal strains in the x-direction (E_x). This restriction in the x-direction may result in the longer required time for the thermal strains in the x-direction to converge.

79. Comparison of calculated final residual stresses with experimental data for EGW and SAW is shown in Figures 60 through 65. Surface residual stresses were experimentally measured by the blind hole drilling method at the web near the weld access hole.

80. The general trend is for the experimental residual stress values to exceed the calculated values by FEM. The graphs in the figures showing the results of the analysis are the values along the weld access hole, where the stress normal to the surface is zero. But stresses are measured at the locations about 3/8-in. from the weld access hole in experiment. This may cause the larger values of experimental data. The initial stress in the base metal is not relieved before welding and may be another source of deviation between calculated values and experimental data.

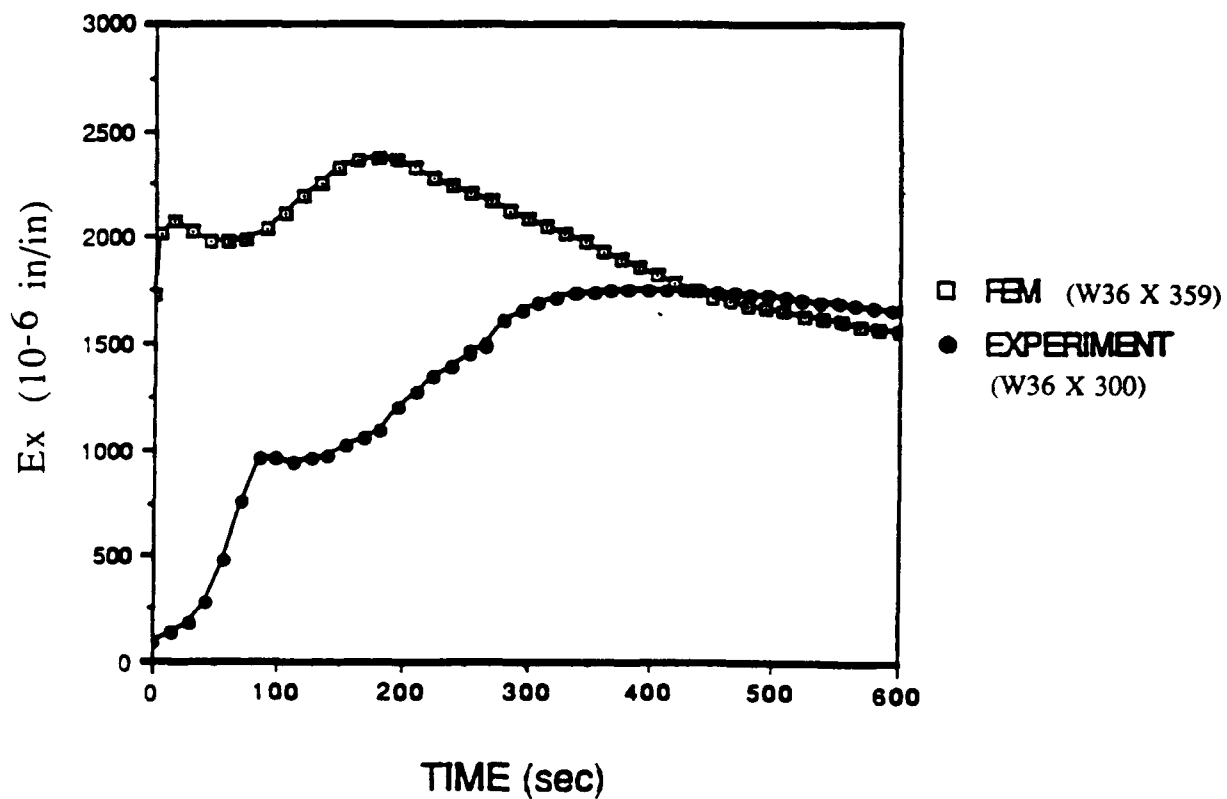
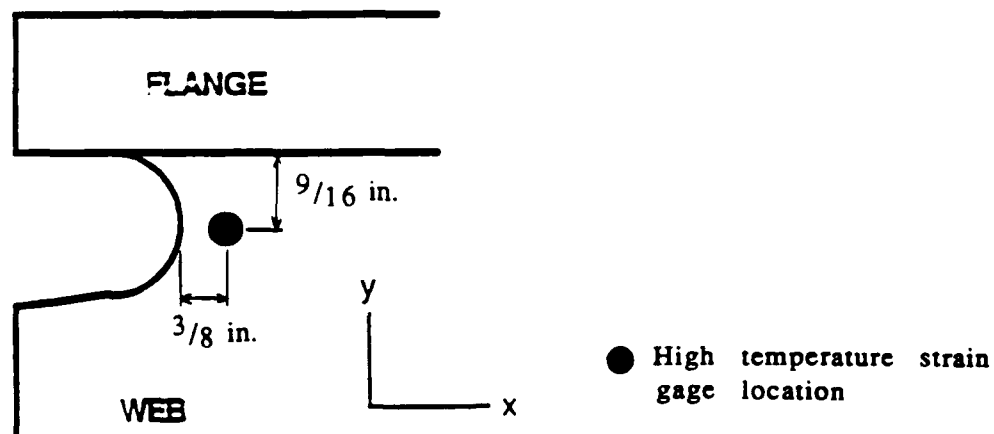


Figure 56. Thermal strains in x-direction during the flange weld with EGW
(Case A: web not welded yet, elongated access hole)

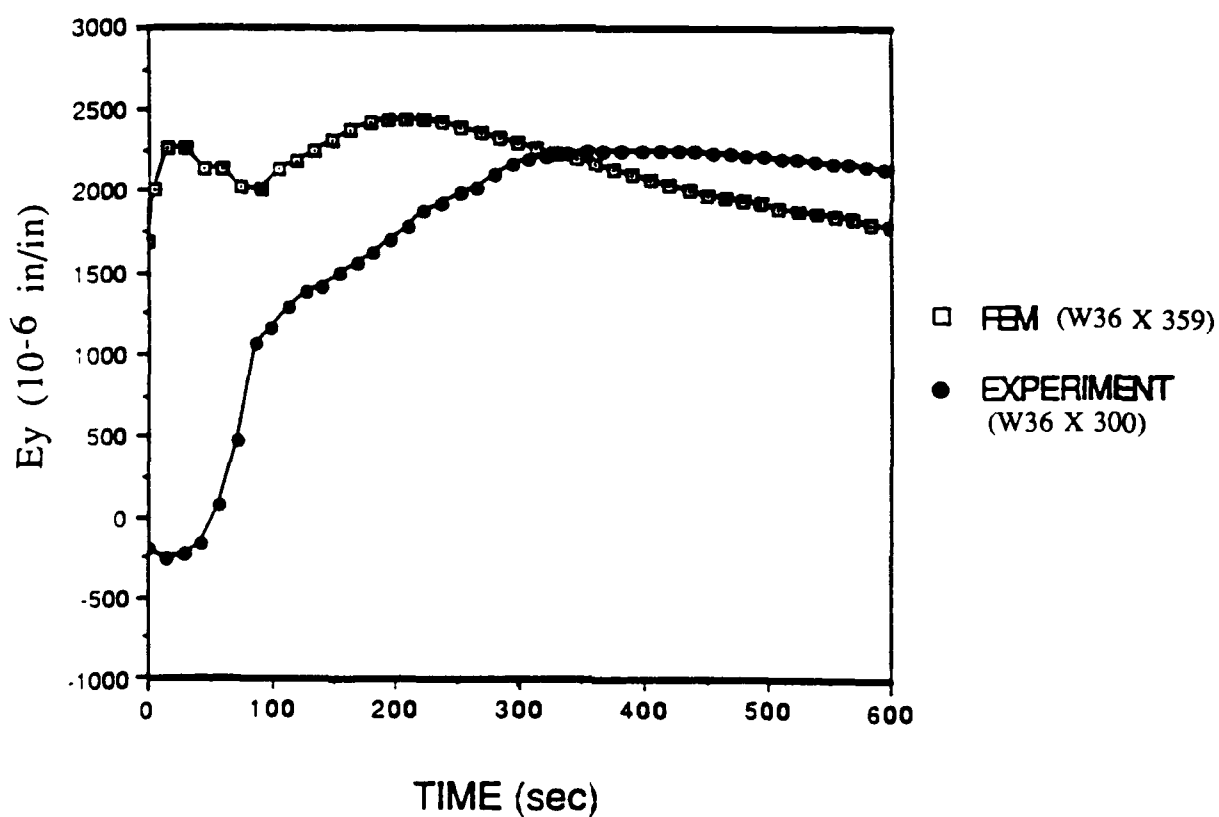
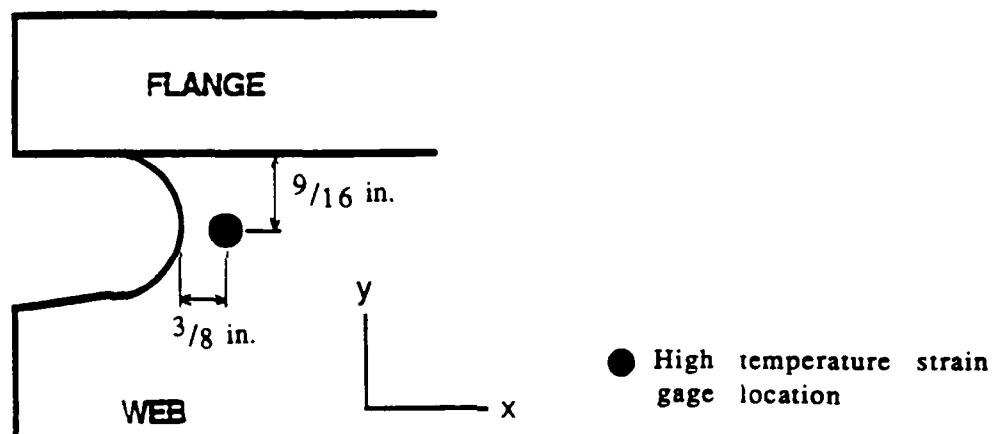


Figure 57. Thermal strains in y-direction during the flange weld with EGW (Case A: web not welded yet, elongated access hole)

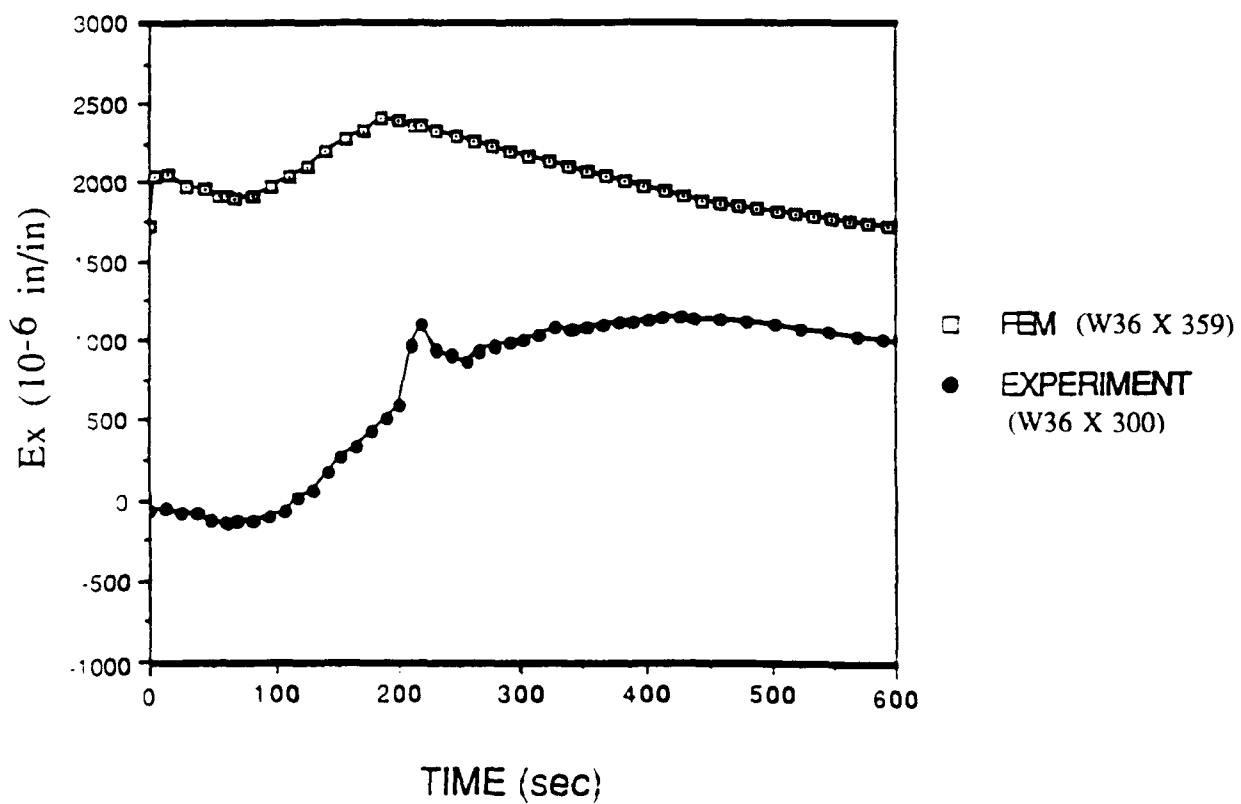
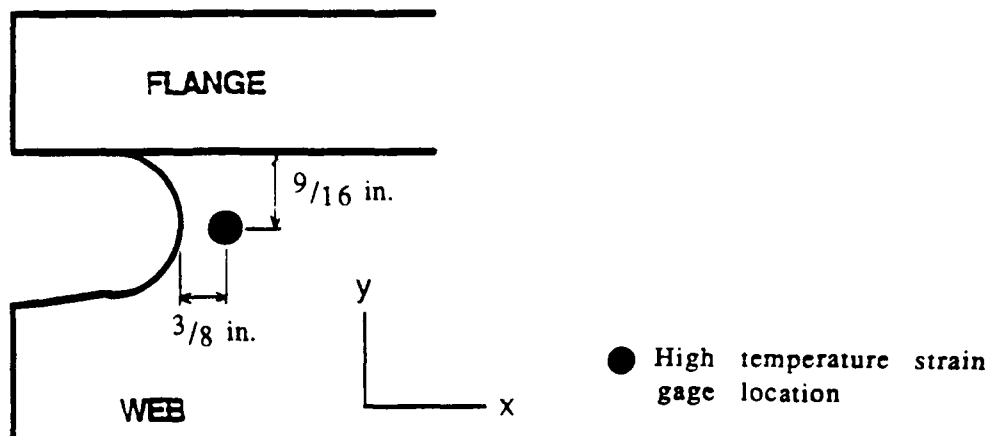


Figure 58. Thermal strains in x-direction during the flange weld with EGW (Case B: web not welded yet, elongated access hole)

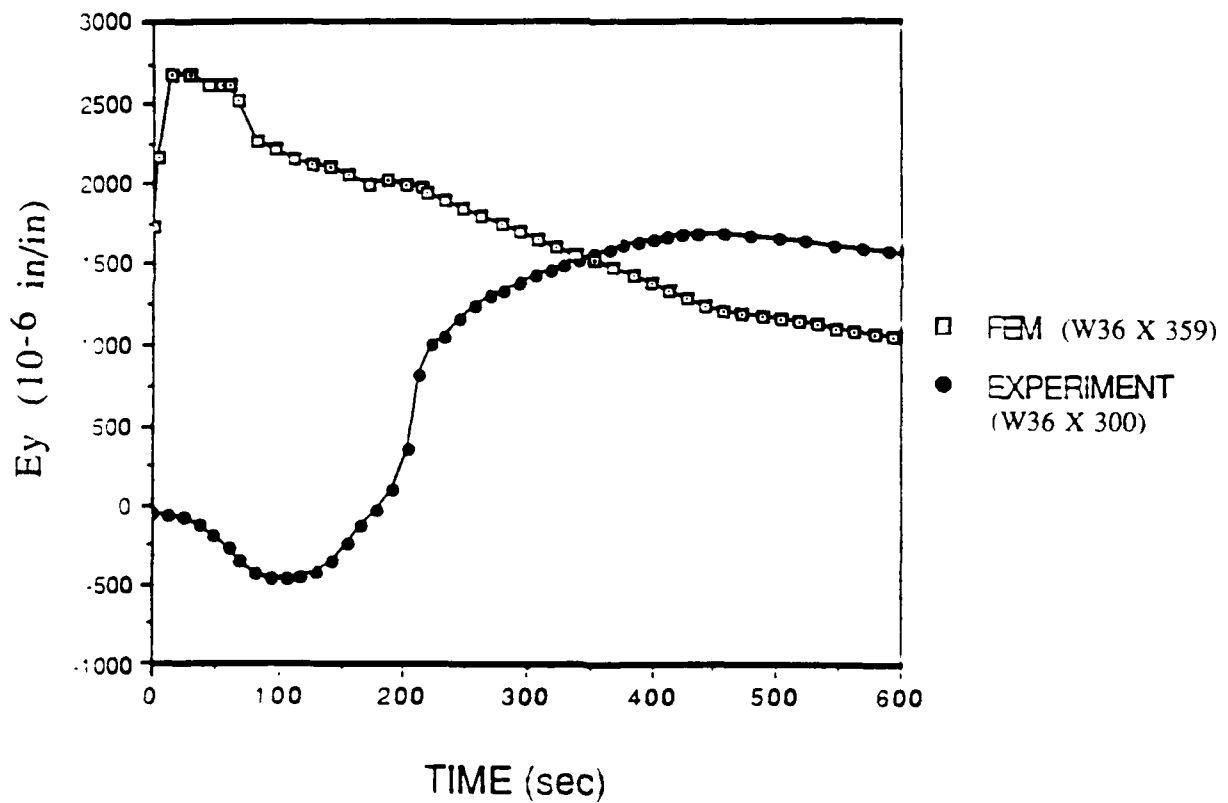
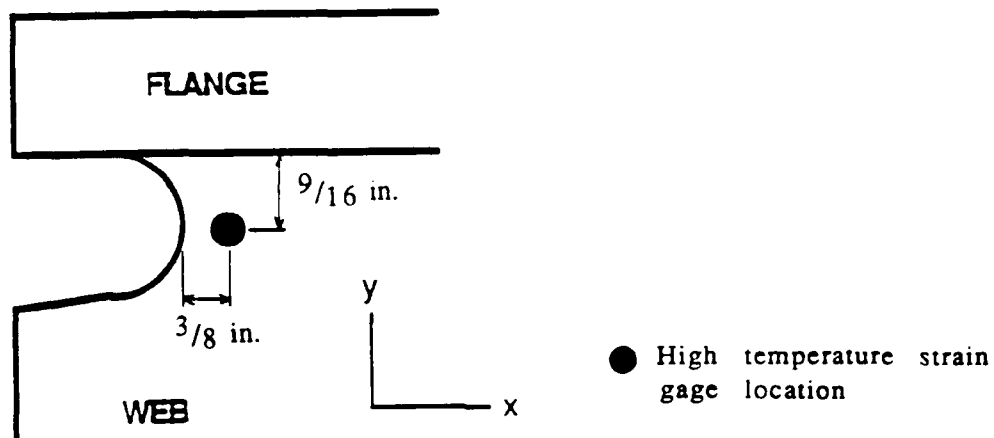


Figure 59. Thermal strains in y-direction during the flange weld with EGW (Case B: web not welded yet, elongated access hole)

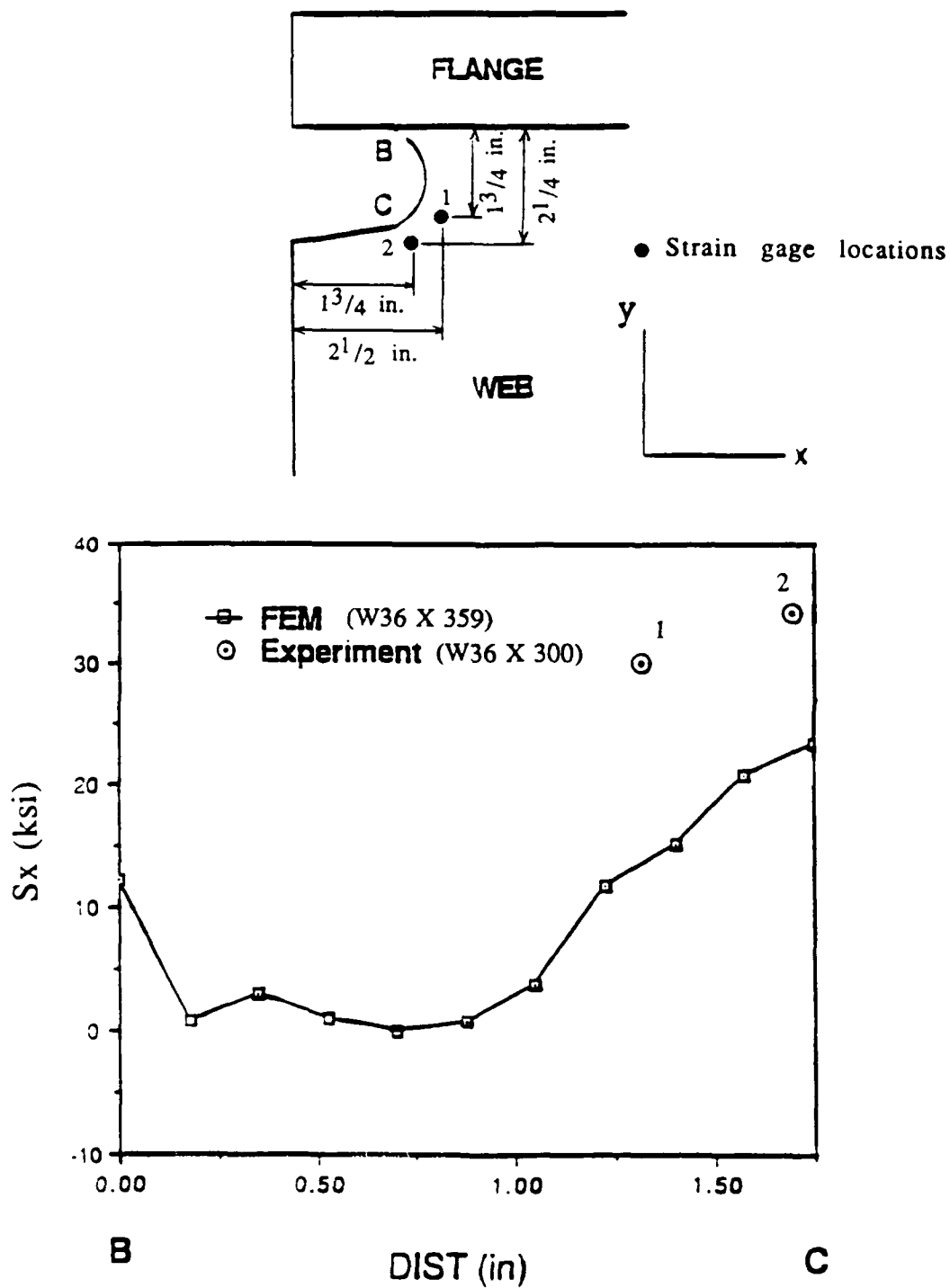


Figure 60. Comparison of final residual stress in the x-direction for Case A with EGW (elongated access hole)

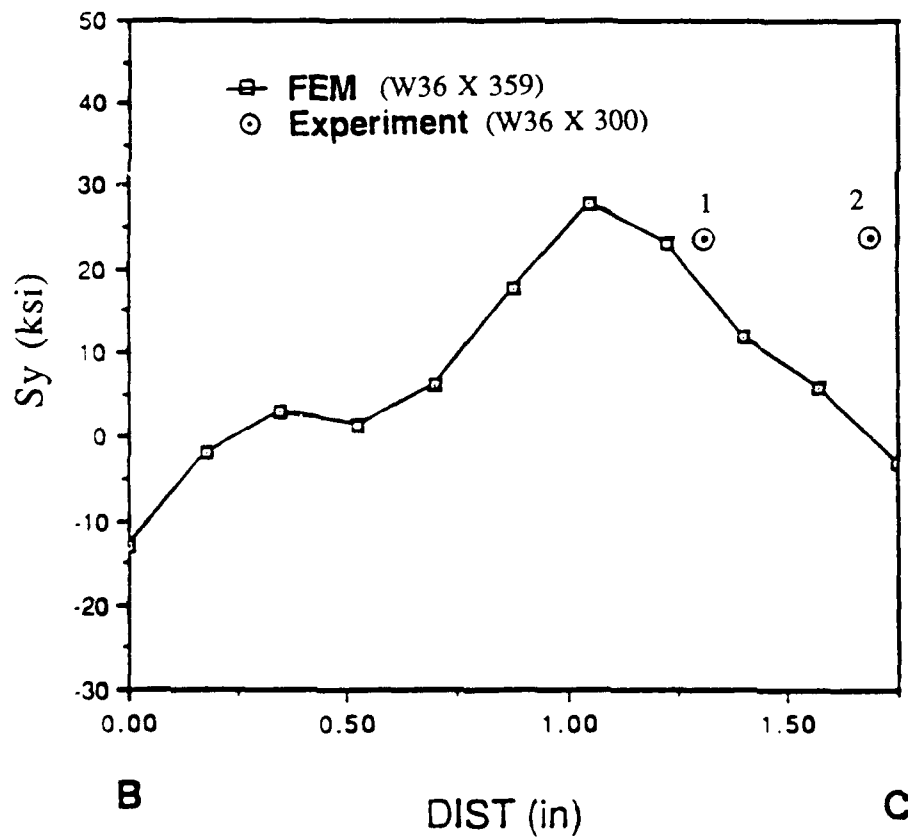
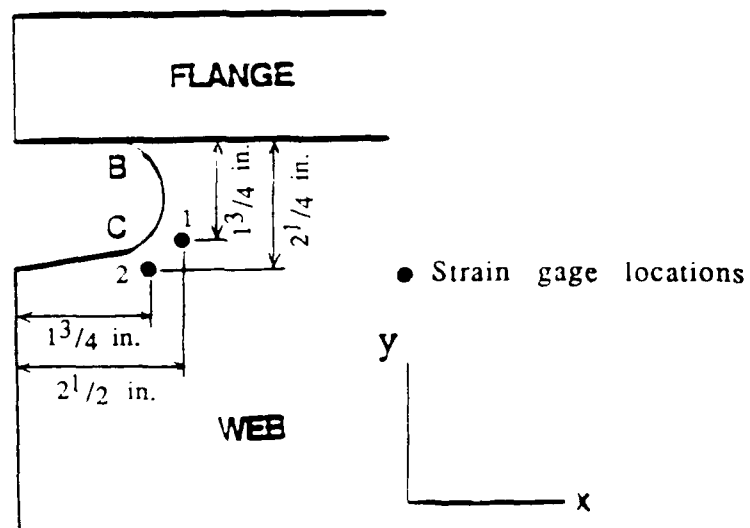


Figure 61. Comparison of final residual stress in the y-direction for Case A with EGW (elongated access hole)

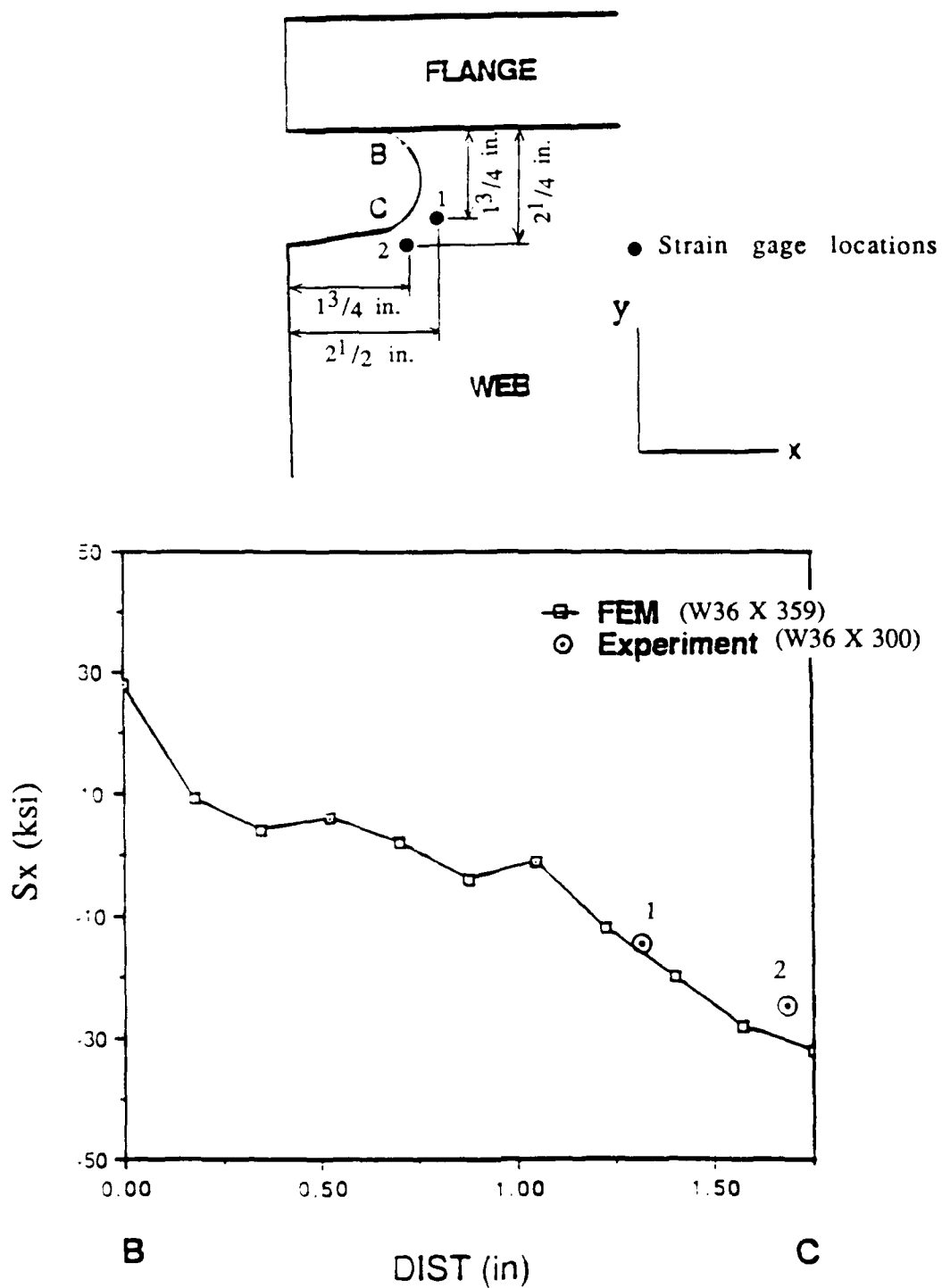


Figure 62. Comparison of final residual stress in the x-direction for Case B with EGW (elongated access hole)

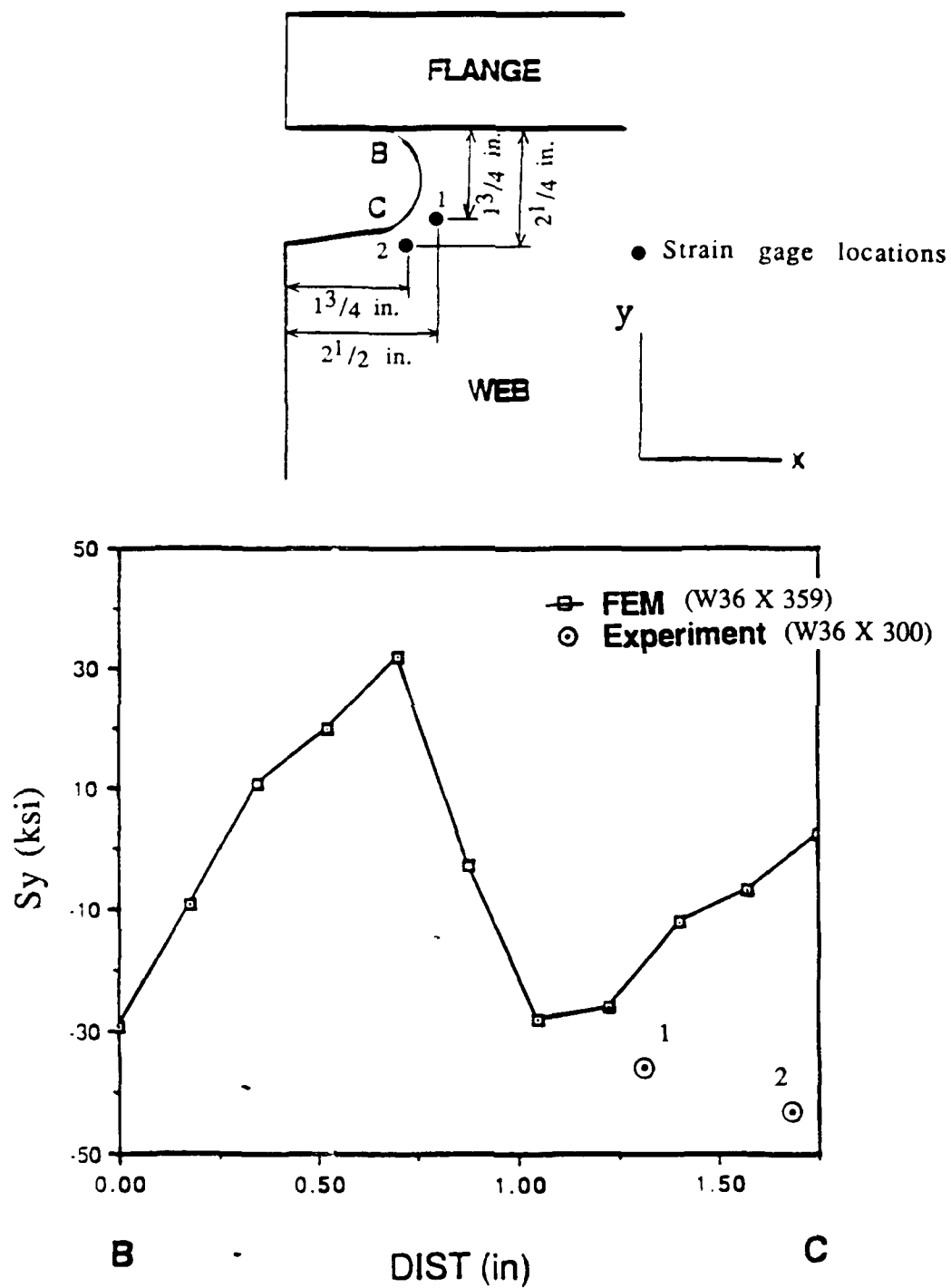


Figure 63. Comparison of final residual stress in the y-direction for Case B with EGW (elongated access hole)

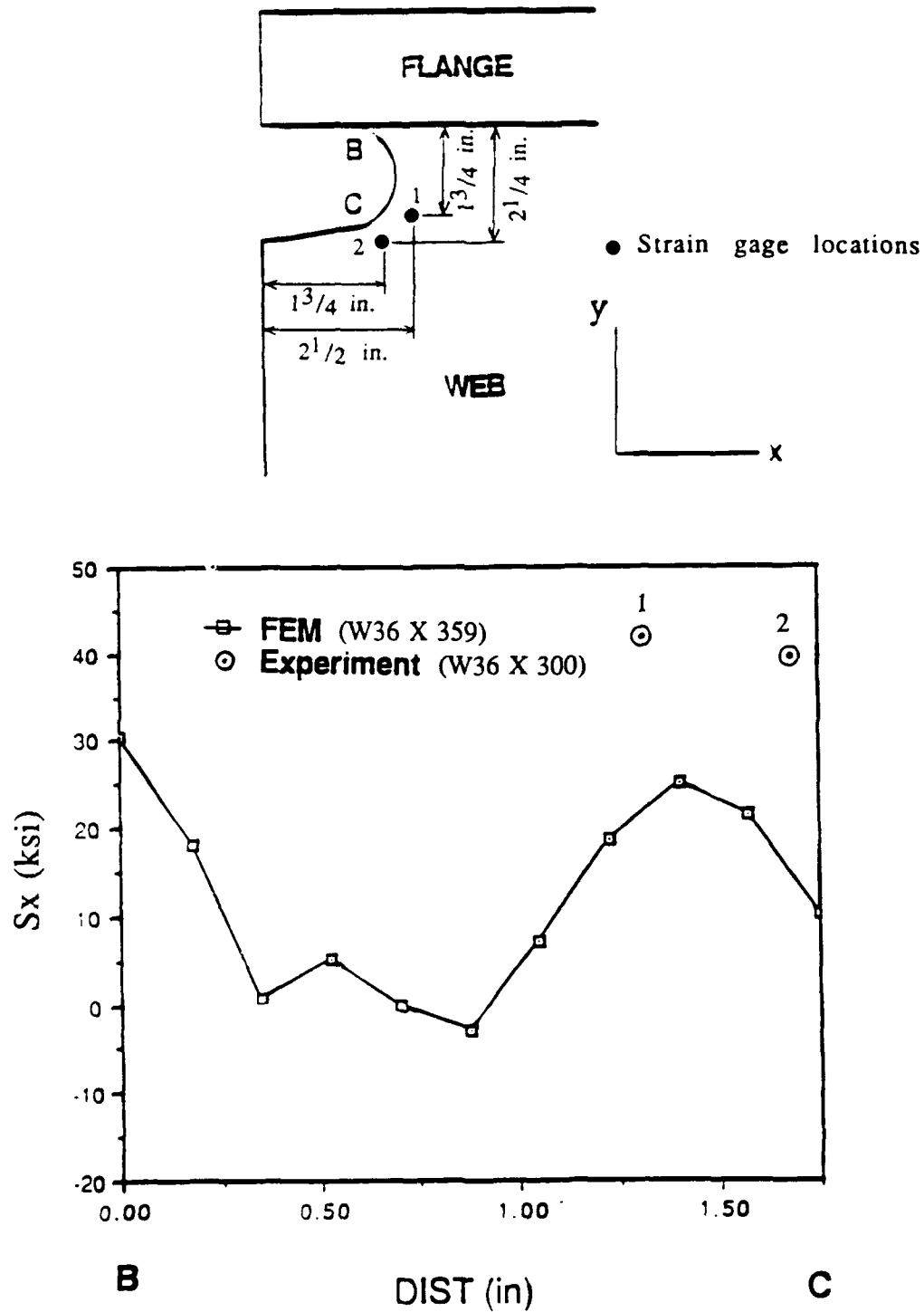


Figure 64. Comparison of final residual stress in the x-direction for Case A with SAW (elongated access hole)

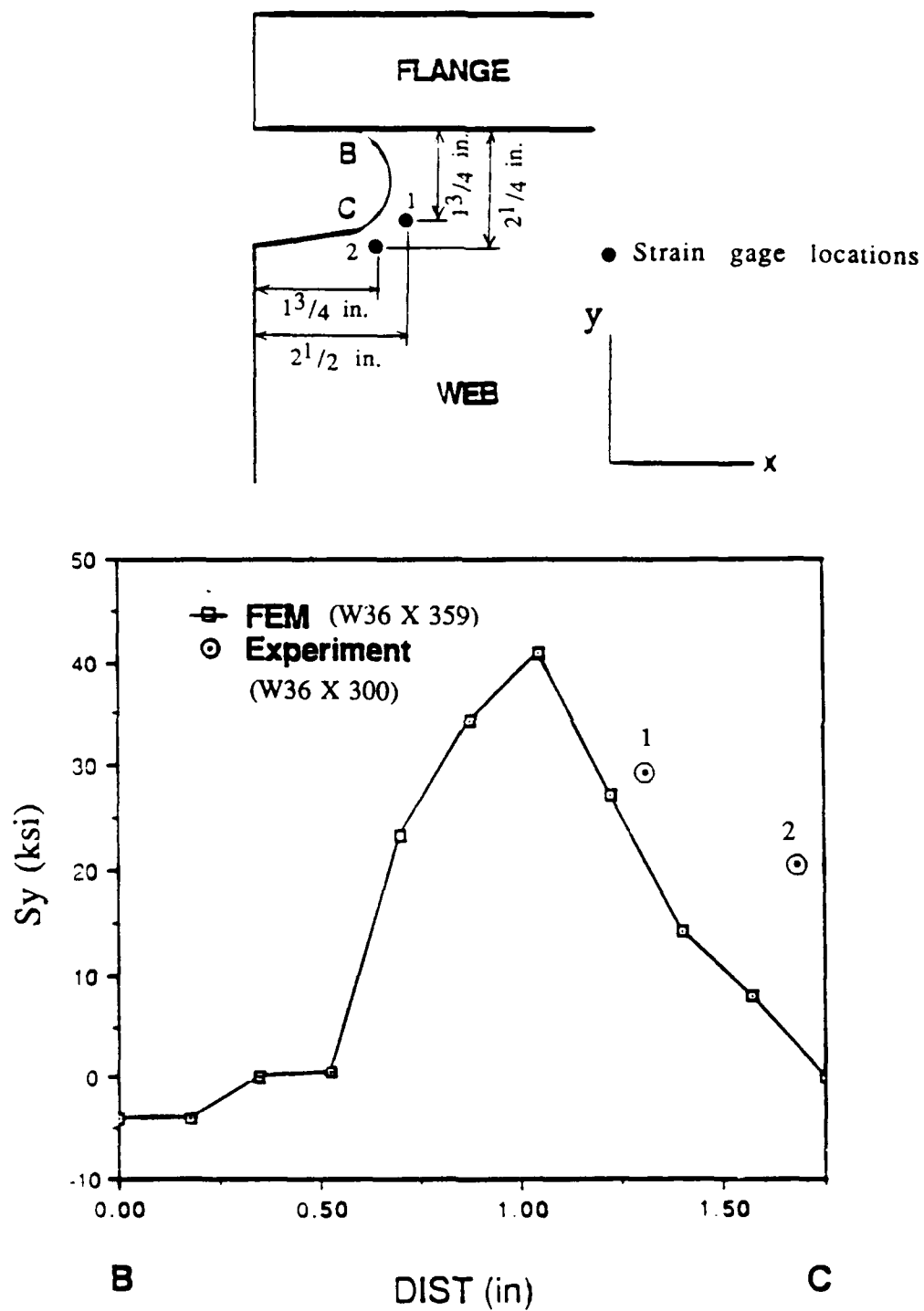


Figure 65. Comparison of final residual stress in the y-direction for Case A with SAW (elongated access hole)

PART V: CONCLUSIONS AND RECOMMENDATIONS

Conclusions

81. Field experience has shown that cracking in the flange or web of thick rolled shapes can occur when groove welded splices are used. The crack initiates from the interface between the flange and web plates at the weld access hole. The crack propagates through the web or flange material depending upon the welding sequence. Residual stress from welding and low toughness are suspected to be the causes for such cracking.

82. The residual stress normal to the splicing joint near the access hole interface was calculated for several conditions. Figure 66 summarizes the calculated results.

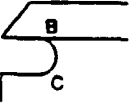
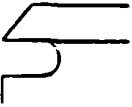
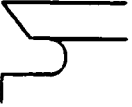
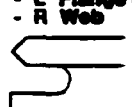






Sequence Process		Flange - Web 		Web - Flange 		Web - Flange 		U Flange - L Web - L Flange - R Web 
FCAW		30 mm Access hole	40 mm Access hole	30 mm Access hole	40 mm Access hole	30 mm Access hole	40 mm Access hole	30 mm Access hole
	B	-5.9	0	26.1	15.7	48.4	-21.3	31.0
	C	55.0	22.9	-44.2	2.0	-13.4	25.0	-7.0
SAW								
	B		30.3		37.9			
	C		25.1		-49.1			
EGW								
	B	16.7	12.2	30.3	27.9			
	C	46.1	23.4	-20.0	-32.3			

Figure 66. Comparison of residual stress (ksi) in x-direction at weld access hole

83. For minimizing the tensile residual stress at the crack initiation location, the FCAW process with a flange-then-web welding sequence appears to be most promising. The EGW process with the same flange-then-web welding sequence also produces low residual stress at the access hole interface due to

fast welding speed and minimum thermal interruption (i.e., single pass weld). The SAW process appears to be the least desirable welding process for joining the thick rolled shapes.

84. A groove joint with the root-opening at the outer surface of the flange produces high tensile residual stress, due to weld shrinkage, which causes large undesirable tensile strain at the inner surface of the plate.

85. Weld access holes that provide a longer opening in the web are more desirable from a residual stress vantage point because the longer opening makes the joint less restrictive in elongating and consequently terminates the hole in a compressive region of the flange. This compressive residual stress is transversed to the tensile residual stress in the web, and their combination results in larger shear stress, hence, a greater apparent ductility of the flange at the termination of the hole.

86. The angle of termination of the access hole also has some effect on the residual stress. The hole that terminates at a right angle with the flange has higher residual stress than a tangent transition termination.

87. The flange-then-web welding sequence produces the least residual stress in comparison to other sequences investigated. Alternating welding sequence with double-V-groove joints on the flanges did not show desirable results.

88. The cooling rate in the HAZ and its size were determined for FCAW and EGW processes from experimental measurements. The FCAW has a cooling rate of 372 °F/sec while the EGW is 19.4 °F/sec at 1,500 °F. Their respective HAZ size is 0.13 in. from fusion line for FCAW and 0.45 in. for EGW. This comparison indicates a significant difference in the heat input characteristics of these two welding processes. Low fracture toughness is anticipated for the EGW weldments.

Recommendations

89. The following recommendations are presented:

- a. For the three processes investigated, the FCAW process is recommended for splicing the thick rolled shapes. This process tended to produce weldments with good fracture toughness and low residual stress.
- b. The use of single-V-groove welds to join the flanges with a double-V-groove weld for the web is desirable. This joint design resulted in the least residual stress at the flange-web interface of the access hole.

- c. A flange-then-web welding sequence produced the least residual stress at the flange-web interface of the access hole, and hence, is the most desirable sequence.
- d. The longer access hole opening produces less tensile residual stress at the flange-web interface of the access hole. The interface with a tangent transition between the web and flange is most desirable.

PART VI: FUTURE WORK

Fracture Toughness of EGW Weldments

90. The EGW process is very promising for splicing the thick rolled shapes because of its high deposition rate and use of a single vertical up weld pass. This process uses a square-butt joint and requires almost no joint preparation.

91. However, the EGW weldment suffers from low toughness. This disadvantage currently outweighs the advantages of higher production rates and low residual stress.

92. Fracture toughness of the EGW weldments could be improved substantially by normalizing and stress relieving (Figure 67) (Masubucki 1970). To take full advantage of the EGW process, further studies to improve the weldment toughness are needed.

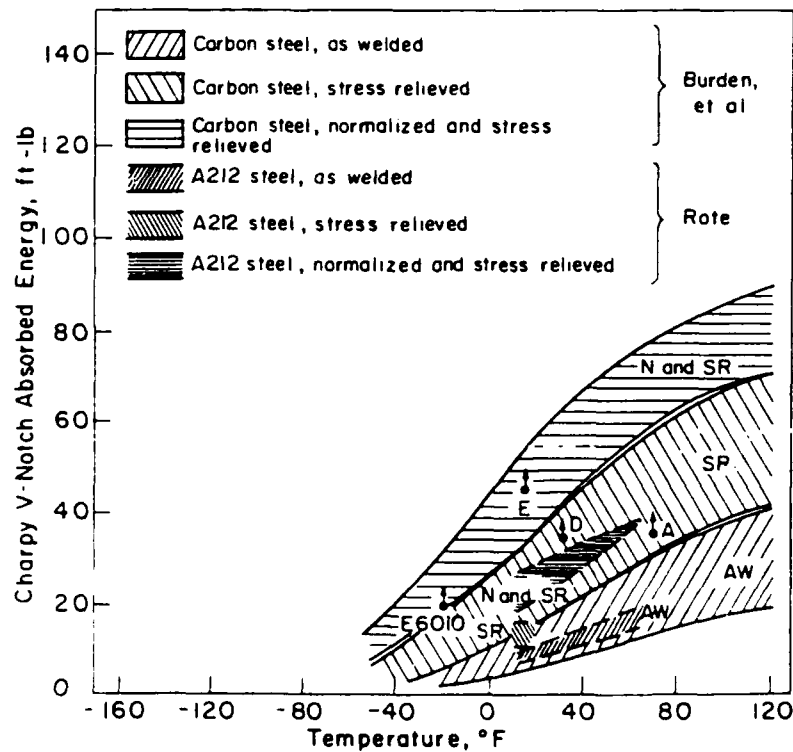


Figure 67. Improvement through heat treatment of notch-toughness of electroslog-deposited metals

Technology Transfer

93. The finite element model and analysis techniques need to be transferred to the US Army Corps of Engineers for their future applications. This transfer of technology could be made through workshops or onsite training of field engineers.

REFERENCES

- American Institute of Steel Construction. 1989. Proceedings, National Steel Construction Conference, Nashville, TN.
- Burden, C. A., Garstone, J., and Lacey, J. A. 1964. "Electro-Slag Welding of Relatively Thin Plate," British Welding Journal, Vol 11, No. 4, pp 148-155.
- Engineering News Record. 1988 (14 Apr 1988), p 8.
- Fisher, John W., and Pense, Alan W. 1987. "Experience with Use of Heavy W Shapes in Tension," American Institute Steel Construction Engineering Journal, Second Quarter, p 63.
- Jaeger, J. "Determination of Residual Stress and Effects in Thick Section Weldments for Hydraulic Structures," Technical Report in preparation, US Army Engineer Waterways Experiment Station, Vicksburg, MS.
- Masubuchi, Koichi. 1970. Materials for Ocean Engineering, The MIT Press, p 489.
- Rote, R. S. 1964. "Investigation of the Properties of Electrosag Welds," The Welding Journal, Vol 43, No. 5, pp 421-426.

Waterways Experiment Station Cataloging-In-Publication Data

Finite element modelling of welded thick plates for Bonneville Navigation Lock / by John J. Jaeger ... [et al.].

95 p. : ill. ; 28 cm. — (Technical report ; ITL-92-2)

Includes bibliographic references.

1. Welded joints — Testing. 2. Locks (Hydraulic engineering) — Columbia River — Design and construction. 3. Thermal stresses. 4. Finite element method. I. Title. II. Jaeger, John J. III. U.S. Army Engineer Waterways Experiment Station. III. Technical report (U.S. Army Engineer Waterways Experiment Station) ; ITL-92-2.
TA7 W34 no.ITL-92-2

WATERWAYS EXPERIMENT STATION REPORTS PUBLISHED UNDER THE COMPUTER-AIDED STRUCTURAL ENGINEERING (CASE) PROJECT

	Title	Date
Technical Report K-78-1	List of Computer Programs for Computer Aided Structural Engineering	Jan 1978
Instruction Report O-79-2	User's Guide: Computer Program with Interactive Graphics for Analysis of Plane Frame Structures (CFRAME)	Mar 1979
Technical Report K-80-1	Survey of Bridge-Oriented Design Software	Jan 1980
Technical Report K-80-2	Evaluation of Computer Programs for the Design/Analysis of Highway and Railway Bridges	Jan 1980
Instruction Report K-80-1	User's Guide: Computer Program for Design Review of Curvilinear Conduits/Culverts (CURCON)	Feb 1980
Instruction Report K-80-3	A Three-Dimensional Finite Element Data Edit Program	Mar 1980
Instruction Report K-80-4	A Three-Dimensional Stability Analysis/Design Program (3DSAD) Report 1: General Geometry Module Report 3: General Analysis Module (CGAM) Report 4: Special-Purpose Modules for Dams (CDAMS)	Jun 1980 Jun 1982 Aug 1983
Instruction Report K-80-6	Basic User's Guide: Computer Program for Design and Analysis of Inverted-T Retaining Walls and Floodwalls (TWDA)	Dec 1980
Instruction Report K-80-7	User's Reference Manual: Computer Program for Design and Analysis of Inverted-T Retaining Walls and Floodwalls (TWDA)	Dec 1980
Technical Report K-80-4	Documentation of Finite Element Analyses Report 1: Longview Outlet Works Conduit Report 2: Anchored Wall Monolith, Bay Springs Lock	Dec 1980 Dec 1980
Technical Report K-80-5	Basic Pile Group Behavior	Dec 1980
Instruction Report K-81-2	User's Guide: Computer Program for Design and Analysis of Sheet Pile Walls by Classical Methods (CSHTWAL) Report 1: Computational Processes Report 2: Interactive Graphics Options	Feb 1981 Mar 1981
Instruction Report K-81-3	Validation Report: Computer Program for Design and Analysis of Inverted-T Retaining Walls and Floodwalls (TWDA)	Feb 1981
Instruction Report K-81-4	User's Guide: Computer Program for Design and Analysis of Cast-in-Place Tunnel Linings (NEWTUN)	Mar 1981
Instruction Report K-81-6	User's Guide: Computer Program for Optimum Nonlinear Dynamic Design of Reinforced Concrete Slabs Under Blast Loading (CBARCS)	Mar 1981
Instruction Report K-81-7	User's Guide: Computer Program for Design Investigation of Orthogonal Culverts (CORTCUL)	Mar 1981
Instruction Report K-81-9	User's Guide: Computer Program for Three Dimensional Analysis of Building Systems (CTABSR9)	Aug 1981
Technical Report K-81-2	Theoretical Basis for CTABSR9: A Computer Program for Three Dimensional Analysis of Building Systems	Aug 1981
Instruction Report K-82-6	User's Guide: Computer Program for Analysis of Reinforced Structures with Nonlinear Support (CRAN)	Jan 1982

Continued

WATERWAYS EXPERIMENT STATION REPORTS PUBLISHED UNDER THE COMPUTER-AIDED STRUCTURAL ENGINEERING (CASE) PROJECT

(Continued)

	Title	Date
Instruction Report K-82-7	User's Guide: Computer Program for Bearing Capacity of Shallow Foundations (CBEAR)	Nov. 1982
Instruction Report K-83-1	User's Guide: Computer Program for Static and Dynamic Analysis of Plane Frame Structures (CFRAME)	Nov. 1983
Instruction Report K-83-2	User's Guide: Computer Program for Wireframe and Surface Geometry (SKETCH)	Nov. 1983
Instruction Report K-83-5	User's Guide: Computer Program to Calculate Stiffness, Mass, and Thrust (CSMT) from Stress Results of a Two Dimensional Finite Element Analysis	Nov. 1983
Technical Report K-83-1	Basic Pile Group Behavior	Nov. 1983
Technical Report K-83-3	Reference Manual: Computer Graphics Program for Generation of Engineering Geometry (SKETCH)	Nov. 1983
Technical Report K-83-4	Case Study of Six Major General Purpose Finite Element Programs	Nov. 1983
Instruction Report K-84-2	User's Guide: Computer Program for Optimum Dynamic Design of Nonlinear Metal Plates Under Blast Loading (OPTOBL)	Jan. 1984
Instruction Report K-84-7	User's Guide: Computer Program for Determining Interfacial Stresses and Consolidation Settlements (OSSTI)	Aug. 1984
Instruction Report K-84-8	Seepage Analysis of Confined Flow Problems by the Method of Fragments (CFRAG)	Jan. 1984
Instruction Report K-84-11	User's Guide for Computer Program (CFRAC) for General Flexure Analysis with Graphics	Nov. 1984
Technical Report K-84-3	Computer-Aided Drafting and Plotting for Civil Engineers and Engineers	Nov. 1984
Technical Report ATC-86-5	Decision Logic, Load Factors and Load Effects for Design Requirements for Reinforced Concrete and Steel Structures, Volume 1, Drafting, Volume 2, Form B	Nov. 1986
Technical Report TR-85-3	A Case Study of the Use of Finite Element Analysis in the Design of a Bridge	Nov. 1985
Instruction Report TR-87-1	Design of a Bridge Using the Finite Element Method	Nov. 1987
Instruction Report TR-87-2	Design of a Bridge Using the Finite Element Method (FEM) - A Case Study	Nov. 1987
Instruction Report TR-87-3	Design of a Bridge Using the Finite Element Method (FEM) - A Case Study	Nov. 1987
Instruction Report TR-87-4	Design of a Bridge Using the Finite Element Method (FEM) - A Case Study	Nov. 1987
Instruction Report TR-87-5	Design of a Bridge Using the Finite Element Method (FEM) - A Case Study	Nov. 1987
Instruction Report TR-87-6	Design of a Bridge Using the Finite Element Method (FEM) - A Case Study	Nov. 1987
Instruction Report TR-87-7	Design of a Bridge Using the Finite Element Method (FEM) - A Case Study	Nov. 1987
Instruction Report TR-87-8	Design of a Bridge Using the Finite Element Method (FEM) - A Case Study	Nov. 1987
Instruction Report TR-87-9	Design of a Bridge Using the Finite Element Method (FEM) - A Case Study	Nov. 1987
Instruction Report TR-87-10	Design of a Bridge Using the Finite Element Method (FEM) - A Case Study	Nov. 1987
Instruction Report TR-87-11	Design of a Bridge Using the Finite Element Method (FEM) - A Case Study	Nov. 1987
Instruction Report TR-87-12	Design of a Bridge Using the Finite Element Method (FEM) - A Case Study	Nov. 1987
Instruction Report TR-87-13	Design of a Bridge Using the Finite Element Method (FEM) - A Case Study	Nov. 1987
Instruction Report TR-87-14	Design of a Bridge Using the Finite Element Method (FEM) - A Case Study	Nov. 1987
Instruction Report TR-87-15	Design of a Bridge Using the Finite Element Method (FEM) - A Case Study	Nov. 1987
Instruction Report TR-87-16	Design of a Bridge Using the Finite Element Method (FEM) - A Case Study	Nov. 1987
Instruction Report TR-87-17	Design of a Bridge Using the Finite Element Method (FEM) - A Case Study	Nov. 1987
Instruction Report TR-87-18	Design of a Bridge Using the Finite Element Method (FEM) - A Case Study	Nov. 1987
Instruction Report TR-87-19	Design of a Bridge Using the Finite Element Method (FEM) - A Case Study	Nov. 1987
Instruction Report TR-87-20	Design of a Bridge Using the Finite Element Method (FEM) - A Case Study	Nov. 1987
Instruction Report TR-87-21	Design of a Bridge Using the Finite Element Method (FEM) - A Case Study	Nov. 1987
Instruction Report TR-87-22	Design of a Bridge Using the Finite Element Method (FEM) - A Case Study	Nov. 1987
Instruction Report TR-87-23	Design of a Bridge Using the Finite Element Method (FEM) - A Case Study	Nov. 1987
Instruction Report TR-87-24	Design of a Bridge Using the Finite Element Method (FEM) - A Case Study	Nov. 1987
Instruction Report TR-87-25	Design of a Bridge Using the Finite Element Method (FEM) - A Case Study	Nov. 1987
Instruction Report TR-87-26	Design of a Bridge Using the Finite Element Method (FEM) - A Case Study	Nov. 1987
Instruction Report TR-87-27	Design of a Bridge Using the Finite Element Method (FEM) - A Case Study	Nov. 1987
Instruction Report TR-87-28	Design of a Bridge Using the Finite Element Method (FEM) - A Case Study	Nov. 1987
Instruction Report TR-87-29	Design of a Bridge Using the Finite Element Method (FEM) - A Case Study	Nov. 1987
Instruction Report TR-87-30	Design of a Bridge Using the Finite Element Method (FEM) - A Case Study	Nov. 1987
Instruction Report TR-87-31	Design of a Bridge Using the Finite Element Method (FEM) - A Case Study	Nov. 1987
Instruction Report TR-87-32	Design of a Bridge Using the Finite Element Method (FEM) - A Case Study	Nov. 1987
Instruction Report TR-87-33	Design of a Bridge Using the Finite Element Method (FEM) - A Case Study	Nov. 1987
Instruction Report TR-87-34	Design of a Bridge Using the Finite Element Method (FEM) - A Case Study	Nov. 1987
Instruction Report TR-87-35	Design of a Bridge Using the Finite Element Method (FEM) - A Case Study	Nov. 1987
Instruction Report TR-87-36	Design of a Bridge Using the Finite Element Method (FEM) - A Case Study	Nov. 1987
Instruction Report TR-87-37	Design of a Bridge Using the Finite Element Method (FEM) - A Case Study	Nov. 1987
Instruction Report TR-87-38	Design of a Bridge Using the Finite Element Method (FEM) - A Case Study	Nov. 1987
Instruction Report TR-87-39	Design of a Bridge Using the Finite Element Method (FEM) - A Case Study	Nov. 1987
Instruction Report TR-87-40	Design of a Bridge Using the Finite Element Method (FEM) - A Case Study	Nov. 1987
Instruction Report TR-87-41	Design of a Bridge Using the Finite Element Method (FEM) - A Case Study	Nov. 1987
Instruction Report TR-87-42	Design of a Bridge Using the Finite Element Method (FEM) - A Case Study	Nov. 1987
Instruction Report TR-87-43	Design of a Bridge Using the Finite Element Method (FEM) - A Case Study	Nov. 1987
Instruction Report TR-87-44	Design of a Bridge Using the Finite Element Method (FEM) - A Case Study	Nov. 1987
Instruction Report TR-87-45	Design of a Bridge Using the Finite Element Method (FEM) - A Case Study	Nov. 1987
Instruction Report TR-87-46	Design of a Bridge Using the Finite Element Method (FEM) - A Case Study	Nov. 1987
Instruction Report TR-87-47	Design of a Bridge Using the Finite Element Method (FEM) - A Case Study	Nov. 1987
Instruction Report TR-87-48	Design of a Bridge Using the Finite Element Method (FEM) - A Case Study	Nov. 1987
Instruction Report TR-87-49	Design of a Bridge Using the Finite Element Method (FEM) - A Case Study	Nov. 1987
Instruction Report TR-87-50	Design of a Bridge Using the Finite Element Method (FEM) - A Case Study	Nov. 1987

WATERWAYS EXPERIMENT STATION REPORTS PUBLISHED UNDER THE COMPUTER-AIDED STRUCTURAL ENGINEERING (CASE) PROJECT

(Continued)

	Title	Date
Instruction Report ITL-87-4	User's Guide: 2-D Frame Analysis Link Program (LINK2D)	Jun 1987
Technical Report ITL-87-4	Finite Element Studies of a Horizontally Framed Miter Gate Report 1: Initial and Refined Finite Element Models (Phases A, B, and C), Volumes I and II Report 2: Simplified Frame Model (Phase D) Report 3: Alternate Configuration Miter Gate Finite Element Studies--Open Section Report 4: Alternate Configuration Miter Gate Finite Element Studies--Closed Sections Report 5: Alternate Configuration Miter Gate Finite Element Studies--Additional Closed Sections Report 6: Elastic Buckling of Girders in Horizontally Framed Miter Gates Report 7: Application and Summary	Aug 1987
Instruction Report GL-87-1	User's Guide: UTEXAS2 Slope-Stability Package; Volume I, User's Manual	Aug 1987
Instruction Report ITL-87-5	Sliding Stability of Concrete Structures (CSLIDE)	Oct 1987
Instruction Report ITL-87-6	Criteria Specifications for and Validation of a Computer Program for the Design or Investigation of Horizontally Framed Miter Gates (CMITER)	Dec 1987
Technical Report ITL-87-8	Procedure for Static Analysis of Gravity Dams Using the Finite Element Method - Phase 1a	Jan 1988
Instruction Report ITL-88-1	User's Guide: Computer Program for Analysis of Planar Grid Structures (CGRID)	Feb 1988
Technical Report ITL-88-1	Development of Design Formulas for Ribbed Mat Foundations on Expansive Soils	Apr 1988
Technical Report ITL-88-2	User's Guide: Pile Group Graphics Display (CPGG) Post-processor to CPGA Program	Apr 1988
Instruction Report ITL-88-2	User's Guide for Design and Investigation of Horizontally Framed Miter Gates (CMITER)	Jun 1988
Instruction Report ITL-88-4	User's Guide for Revised Computer Program to Calculate Shear, Moment, and Thrust (CSMT)	Sep 1988
Instruction Report GL-87-1	User's Guide: UTEXAS2 Slope-Stability Package; Volume II Theory	Feb 1989
Technical Report ITL-89-3	User's Guide: Pile Group Analysis (CPGA) Computer Group	Jul 1989
Technical Report ITL-89-4	CBASIN--Structural Design of Saint Anthony Falls Stilling Basins According to Corps of Engineers Criteria for Hydraulic Structures; Computer Program X009a	Aug 1989

(Continued)

**WATERWAYS EXPERIMENT STATION REPORTS
PUBLISHED UNDER THE COMPUTER-AIDED
STRUCTURAL ENGINEERING (CASE) PROJECT**

(Concluded)

	Title	Date
Technical Report ITL-89-5	CCHAN—Structural Design of Rectangular Channels According to Corps of Engineers Criteria for Hydraulic Structures; Computer Program X0097	Aug 1989
Technical Report ITL-89-6	The Response-Spectrum Dynamic Analysis of Gravity Dams Using the Finite Element Method; Phase II	Aug 1989
Contract Report ITL-89-1	State of the Art on Expert Systems Applications in Design, Construction, and Maintenance of Structures	Sep 1989
Instruction Report ITL-90-1	User's Guide: Computer Program for Design and Analysis of Sheet Pile Walls by Classical Methods (CWALSHT)	Feb 1990
Technical Report ITL-90-3	Investigation and Design of U-Frame Structures Using Program CUFRBC Volume A: Program Criteria and Documentation Volume B: User's Guide for Basins Volume C: User's Guide for Channels	May 1990
Instruction Report ITL-90-6	User's Guide: Computer Program for Two-Dimensional Analysis of U-Frame or W-Frame Structures (CWFRAM)	Sep 1990
Instruction Report ITL-90-2	User's Guide: Pile Group—Concrete Pile Analysis Program (CPGC) Preprocessor to CPGA Program	Jun 1990
Technical Report ITL-91-3	Application of Finite Element, Grid Generation, and Scientific Visualization Techniques to 2-D and 3-D Seepage and Groundwater Modeling	Sep 1990
Instruction Report ITL-91-1	User's Guide: Computer Program for Design and Analysis of Sheet-Pile Walls by Classical Methods (CWALSHT) Including Rowe's Moment Reduction	Oct 1991
Instruction Report ITL-87-2 (Revised)	User's Guide for Concrete Strength Investigation and Design (CASTR) in Accordance with ACI 318-89	Mar 1992
Technical Report ITL-92-2	Finite Element Modeling of Welded Thick Plates for Bonneville Navigation Lock	May 1992